DEFORMATION BANDS RECORD OBLIQUE-SLIP FAULTING IN THE CAÑON CITY EMBAYMENT, COLORADO

by

EDWARD QUENTIN ANLIAN

(Under the Direction of Christian Klimczak)

ABSTRACT

The Cañon City Embayment (CCE) in south-central Colorado is a large-scale syncline comprised of Ordovician to Tertiary sedimentary rocks overlying Proterozoic basement that was affected by several major faults during the Laramide orogeny. Such faulting may be accompanied by a damage zone that, when within highly porous rocks, manifests itself as arrays of deformation bands that increase in density towards the fault. As such, the deformation bands are precursors to the faults, with geometric and kinematic properties related to the fault that they are associated with. Three field areas were studied and measurements were collected on 1131 deformation bands. The orientation and kinematics of the deformation bands indicate that they are part of oblique-slip fault damage zones. The field area with the highest deformation band density describes a contractional horsetail splay that may have developed from pre-existing weaknesses from older faults attributed to the Ancestral Rocky Mountain orogeny.

INDEX WORDS: Cañon City Embayment, deformation bands, oblique-slip, contractional horsetail splay, Laramide orogeny, Ancestral Rocky Mountain orogeny

DEFORMATION BANDS RECORD OBLIQUE-SLIP FAULTING IN THE CAÑON CITY EMBAYMENT, COLORADO

by

EDWARD QUENTIN ANLIAN

B.S., University of Arizona, 2015

A Thesis Submitted to the Graduate Faculty of The University of Georgia in Partial Fulfillment of the Requirements for the Degree

MASTER OF SCIENCE

ATHENS, GEORGIA

2017

DEFORMATION BANDS RECORD OBLIQUE-SLIP FAULTING IN THE CAÑON CITY EMBAYMENT, COLORADO

by

EDWARD QUENTIN ANLIAN

Major Professor:	Christian Klimczak
Committee:	Douglas E. Crowe
	Steven M. Holland

Electronic Version Approved:

Suzanne Barbour
Dean of the Graduate School
The University of Georgia
May 2017

ACKNOWLEDGEMENTS

I would like to thank my advisor, Christian Klimczak. I am grateful to have an advisor who was willing to help and give me guidance during my time here at UGA. This thesis would not have been possible without the logistical support, knowledge, and advice given to me from Doug Crowe, Steve Holland, Dave Barbeau, Chris Fleisher, and all the other faculty members who came out to Cañon City.

I also want to thank those who supported me throughout these two years. These individuals are Hudson Farren, Jake Lee, Corbin Kling, Julianna Jeffers, Kelsey Crane, and Melanie Callihan. I would also like to thank my fellow graduate students here in the department.

Finally, I want to thank my family. Your unwavering support over the past two years has been vital to the completion of this project and degree. Thank you.

TABLE OF CONTENTS

Page

LIST OF TABLES

Page

LIST OF FIGURES

Page

CHAPTER 1

Introduction

1.1 Regional Geology of the Cañon City Embayment (CCE)

The Cañon City Embayment (CCE) includes outcrops of Proterozoic crystalline rock found mainly in the topographic highs and Ordovician to Cenozoic sediments exposed in the topographic lows. The rock units within this area, especially porous Ordovician to Cretaceous sandstones, host well-defined deformation band structures that indicate past faulting, which are likely tied to orogenic processes in the CCE. Deformation bands are tabular structural discontinuities that represent brittle deformation in porous sandstones, so they are suitable indicators for identifying kinematics of large-scale tectonics (Aydin and Johnson, 1978; Fisher and Knipe, 2001). The CCE marks one of the easternmost expressions of the Rocky Mountain extent. The embayment is approximately 397 square kilometers in area, and three areas within the CCE were examined in detail: the Mixing Bowl, South Twin Mountain, and Sheep Mountain (Fig. 1).

The embayment is characterized by Proterozoic basement rock in contact with younger sedimentary units (Fig. 1). The elevated ridges of the Wet Mountains and Front Range constrain the boundaries of the embayment. Ordovician to Cenozoic rock units form in a broad, gently folded, sedimentary basin above the Proterozoic basement rock. Faulting is pervasive through the Proterozoic basement and penetrates the overlying younger sedimentary units (Taylor et al., 1975; Wobus et al., 1979; Wobus et al., 1985; Scott et al. 1977).

The geologic history of the CCE began with the formation of the Proterozoic basement that is exposed in both the Wet Mountains to the south-southwest and the Front Range to the north-northeast (Scott et al., 1978). The Proterozoic basement is an 1800 Ma gneissic complex composed of meta-granitic intrusions (1700 Ma, 1400 Ma, and 1000 Ma) and various metasedimentary and metavolcanic rocks (1720–1460 Ma, 1400 Ma, and 1000 Ma) (Tweto 1977, 1980a). The oldest Paleozoic sediments were deposited in the Ordovician, and include the Early Ordovician Manitou Formation, the Middle Ordovician Harding Sandstone, and the Late Ordovician Fremont Formation. Mapping focused on the Harding Sandstone, which is host to many deformation bands. It was deposited in a microtidal coastal environment during the Turinian to Chatfieldian stages of the Ordovician some 456 to 449 Ma ago. It is found in the northeast to northwest portions of the CCE (Sweet, 1984; Allulee and Holland, 2005; Fig. 1).

Two deformation events contributed to the formation of the CCE. During the Pennsylvanian, the Ancestral Rocky Mountain orogeny resulted from the complex tectonic interaction between the North American plate and the South American-African plate that formed Pangea (Kluth and Coney, 1981). In the CCE, the Ancestral Rocky Mountain orogeny was characterized by northwest–southeast crustal shortening and resulting intra-cratonic block uplift (DeVoto, 1980; Tweto, 1980; Kluth and Coney, 1981). This block uplift formed the Wet Mountains and Front Range (Tweto 1980; Fig. 1). During the Pennsylvanian, topographic relief of the Ancestral Rocky Mountains is thought to be approximately 3,000 m (DeVoto, 1980). The erosion of the Ancestral Rocky Mountains led to the thick and aerially extensive deposition of the Pennsylvanian Fountain Formation. The Fountain Formation is a prominent geologic unit commonly used by geologists to constrain the timing of the exhumation of the Ancestral Rocky Mountain orogenic block uplifts (Hubert, 1960; Mallory, 1972, Rascoe and Baars, 1972; Wilson,

1975, DeVoto, 1980; Tweto, 1980; Kluth and Coney, 1981). The Ancestral Rocky Mountains further eroded and deposition of sediments in the Jurassic and Cretaceous occurred (Erslev et al., 2004). Jurassic sediments such as the Middle Jurassic Ralston Creek Formation and the Late Jurassic Morrison Formation were deposited throughout CCE (Frederickson et al., 1956).

During the Early Cretaceous, the Dakota Group was deposited. The Dakota Group consists of the Purgatoire Formation and the Dakota Sandstone. The older Purgatoire Formation is composed of the Lytle Sandstone Member and the Glencairn Shale Member. The Lytle Sandstone is Aptian to Albian (Weimer 1990). The Glencairn Shale is late Albian (Weimer, 1990). The Dakota Sandstone is Cenomanian, overlies the Purgatoire Formation, and is the primary unit to form topographic highs in the CCE that are resistant to erosion. Together with the Jurassic units and Upper Cretaceous sedimentary rocks, the Dakota Group forms the Dakota Hogback (Taylor et al., 1975, Wobus et al., 1979; Wobus et al., 1985; Scott et al., 1977; Fig. 1). These rock units along the Dakota Hogback encompasses Cañon City from the southwest to north to northeast. The northwest extent of the Dakota Hogback is part of the southeast-plunging, asymmetrical Chandler Syncline (Jurista, 1996; Taylor et al., 1975, Wobus et al., 1979; Wobus et al., 1985; Scott et al., 1977). The exhumed fold limbs of the Chandler Syncline define the morphology and expanse of the Dakota Hogback within the CCE.

In the northern quadrants of the CCE, faulting is pervasive within Proterozoic basement rock and Ordovician sedimentary rocks, and is less pervasive towards the south (Fig. 1). However, within the southern extent of the embayment, Jurassic and Cretaceous sedimentary units come into fault contact with the Proterozoic basement rocks. Temporally, faulting during the Ancestral Rocky Mountain orogeny could only deform the Pennsylvanian Fountain Formation syn-depositionally and deform pre-Pennsylvanian units post-depositionally (DeVoto,

1980; Tweto, 1980; Kluth and Coney, 1981, Taylor et al., 1975; Wobus et al., 1979; Wobus et al., 1985; Scott et al. 1977; Fig. 1). Faults seen within Jurassic to Paleocene rocks must have been deformed as part of a later large-scale orogenic event.

During the Late Cretaceous to late Paleocene, the oblique, northeast-trending, shallow subduction of the Farallon Plate (Lipman et al., 1971; Lowell, 1974; Dickinson and Snyder, 1978) produced the second main deformation event, the Laramide orogeny. The Laramide orogeny exhibited a northeast-trending crustal shortening direction, and generated an anastomosing system of basement-cored arches, bounding the northern and eastern margins of the Colorado Plateau (Erslev, 2004; Hamilton, 1981; Fig. 2). These basement-cored arches form en-echelon steps towards the northeast of topographic highs of Proterozoic crystalline rock (Kluth and Nelson, 1988; Erslev et al., 1988; Erlsev 1993; Hamilton, 1981; Fig. 2). The Laramide orogeny is found to account for the en-echelon formation of northwest–southeast oriented ridges in the CCE: The Wet Mountains, bounding the CCE to the south-southwest, and the Front Range, bounding the embayment to the north-northeast (Fig. 1). As a result of the crustal shortening, these northwest–southeast ridges were exhumed by thrust faulting initiated in the Late Cretaceous as indicated by syn-orogenic sediments deposited along the flanks through thrust faulting (Tweto 1975; Kluth and Nelson, 1988; Erslev et al., 1988; Erslev, 1993). Uplift from the Laramide orogeny ended in the Paleogene and a late Eocene erosional surface formed in the CCE, truncating Laramide structures from younger Cenozoic sediments (Epis and Chapin 1975; Leonard and Langford 1994).

1.2 Oblique-Slip Tectonics and Previous Structural Analyses

Strike-slip faults are kinematic consequences of large-scale plate motion on a sphere (Wilson, 1965). They are well known for developing in continental and oceanic transform plate boundaries but can also form in intraplate settings as a continental interior reaction to plate collision as well as manifest as transfer zones of deformation between normal faults in rift systems, and thrust faults in fold-thrust belts (Woodcock 1986; Sylvester 1988; Yeats et al., 1997; Marshak et al., 2003). Strike-slip faults are prevalent in obliquely convergent subduction zones where inter-plate strain is partitioned into arc-parallel strike-slip zones in the fore-arc, arc, and back-arc regions (Beck 1983, Jarrard 1986; Sieh and Natawidjaja 2000). Wrench faulting (Moody and Hill, 1956) is the formation of vertical or near-vertical faults displaying strike-slip movement with a component of dip-slip. Transpressional or transtensional tectonic environments can also form by wrench faults. Structures classified as transpressional or transtensional are described as strike-slip structures that differ from simple shear because of an element of extension or compression orthogonal to the zone of deformation (Dewey et al., 1998). In general, the combination of a strike-slip component and a dip-slip component of slip along a fault indicates oblique-slip fault movement. When described in the field, right-lateral reverse oblique-slip motion along a fault surface can be referred to as right-lateral reverse-slip. Likewise, right-lateral normal oblique-slip movement can be described as a right-lateral normal-slip. During the initiation of faults containing a component of strike-slip, they form en-echelon sets of fault and fold segments (Cloos, 1928; Riedel, 1929; Tchalenko, 1970; Wilcox et al., 1973), forming fault bends. Such fault bends are described as divergent bends and convergent bends. Usually, divergent and convergent bends are described as having offset where bounding strike-slip faults are continuously linked and curved across the area of deformation. In contrast, stepover

structures are zones of slip transfer by sharply stepping over laterally, containing oblique-slip faults in the overlap region between the fault segments (Wilcox et al., 1973; Crowell 1974; Aydin and Nur 1982,1985). Over time, fault-segmented faults coalesce at the stepover regions (Zhang et al., 1989; Peacock and Sanderson, 1991; McClay and Bonora 2001). Consequently, fault bends and stepovers are complementary to each other (Cunningham and Mann, 2007). Fault bends that accommodate contraction and extension are described as restraining and releasing bends, respectively (Crowell 1974; Christie-Blick and Biddle 1985). Restraining bends and releasing bends may form in single and en-echelon sequences of fault planes that describe unique geologic structures with lateral components of movement (Cunningham and Mann, 2007; Fig. 3).

Jurista (1996) conducted a structural analysis in the CCE using orientations of small faults. The goal of this study was to test different tectonic models within the area, including strike-slip, rotational, and multi-stage origins for the CCE. The findings of this study recognized that the Laramide maximum principal orientation of tectonic stress in the general area of the CCE trends around N75ºE and plunged nearly horizontally. There is no evidence within the CCE for multiple maximum orientations of tectonic stress, furthermore, this northeastward direction lines up with Laramide stress trends observed in the Front Range. Regional slip directions observed along slip surfaces in the CCE were previously reported to trend toward ~N76Eº, plunging gently (around ~7º), and matching the recognized principal stress direction of Laramide deformation in the area (Jurista, 1996). Cross sections constructed across the embayment indicate different directions of thrust movement. Jurista (1996) states the southern extent of the CCE as containing eastward thrusting and the northern segment of the CCE having eastward and westward thrusting. Jurista (1996) further hypothesizes that the en-echelon geometry of the Rocky Mountain front in Colorado and the formation of embayments arises from accumulation

of slip and relay of slip along north to south oriented faults. Jurista (1996) further states that the coaxial relationship between stress and strain seen in this area indicates a pure shear environment that is not consistent with large-scale wrench faulting.

1.3 Structural Characteristics of Deformation Bands

Deformation bands are key indicators for interpreting oblique-slip, strike-slip, and dip-slip kinematics in porous sandstones. Their spectacular exposures in the CCE allow for a detailed study of fault damage zone evolution originating from large-scale orogenic processes. Deformation bands are localized, tabular structural discontinuities accommodating porosity reduction indicating that they are diagnostic structures of strain-localized zones within particulate materials, such as sandstones (Aydin and Johnson, 1978; Fisher and Knipe, 2001). Deformation bands show mm- or cm-scale shear offset, dilation or compaction, and involve various micro-mechanisms of deformation, such as grain rearrangement, cataclasis and cataclastic flow, or pressure-solution (Aydin et al., 2006; Fossen et al., 2007). Cataclastic deformation bands reduce porosity and permeability of otherwise highly porous sandstones (e.g., Fowles and Burley, 1994; Fisher and Knipe, 1998; Ogilvie and Glover, 2001; Fossen and Bale, 2007; Torabi et al., 2013). Reduction of porosity and permeability is driven by the concentration of cataclasis present in the bands (Pittman, 1981; Crawford, 1998; Ballas et al., 2012). Therefore, cataclastic bands are able to baffle, channelize, or trap fluid flow in reservoir settings (Harper and Moftah, 1985; Antonellini et al., 1999; Sternlof et al., 2006; Rotevatn et al., 2009; Tueckmantel et al., 2012). These bands are present in the CCE (Gibson, 1998). Cataclastic bands displaying components of shear and compaction are the most common deformation bands in zones of localized strain (Fowles and Burley, 1994; Fisher and Knipe, 1998; Ogilvie and Glover, 2001; Fossen and Bale, 2007; Torabi et al., 2013).

Cataclastic deformation bands can be seen in single strands, in an assemblage of multiple strands forming band clusters, or as arrays of single strands and clusters forming a damage zone within fault cores with up to hundreds or thousands of individual bands. Structural characteristics of deformation bands in fault zones include increases in band density with proximity to a major fault. Deformation bands are precursors of larger faults, so their presence and geometric properties are indicative of the geometry and kinematics of the parent-faulting event. As precursors to faulting, deformation bands allow different tectonic regimes to be discerned. For example, deformation bands share the same sense of slip as the major fault with which they are associated, allowing the kinematics of faulting to be deduced. Faults form in conjugate sets where a single homogenous stress state forms two simultaneous fault planes (Anderson, 1905; Fig. 4). In this fault model, the maximum compressive stress is described by the acute bisector between the two planes. The minimum compressive stress is marked by the obtuse angle that forms between the planes, and the intermediary compressive stress lies parallel to the point of intersection (Fig. 4). Deformation bands also form conjugate sets (Cruikshank et al., 1991; Olsson et al. 2004). The two fault planes that form are described as the master and antithetic (Tchalenko, 1970; Tchalenko and Ambraseys, 1970; Davis et al., 2000), where the master deformation band plane shares the same orientation with the master fault plane (Fig. 4). Ladder structures, which consist of longer bounding bands accommodating offset from smaller linking bands, describe larger assemblages of conjugate deformation bands (Davis, 1999). The assemblage of ladder structures gives insight on kinematics associated with large networks of observed slipped deformation bands. Deformation bands also manifest in larger sets of simultaneously forming planes known as quadrimodal and polymodal faulting (Fig. 4). A quadrimodal fault set describes four clusters of poles representing the master and antithetic

bimodal conjugate faults as well as nested conjugate faults coincident to both master and antithetic (Fig. 4). Polymodal faulting, which includes quadrimodal faulting, displays a seemingly continuous orientation distribution of poles spanning finite arcs of strike and dip (Peacock and Sanderson 1992; Healy, 2015; Fig. 4). Deformation bands can express polymodal fault sets and were first observed in the Entrada and Navajo sandstones found in southeast Utah, and in the Wingate Sandstone in Colorado (Aydin and Reches, 1982; Jamison and Stearns, 1982).

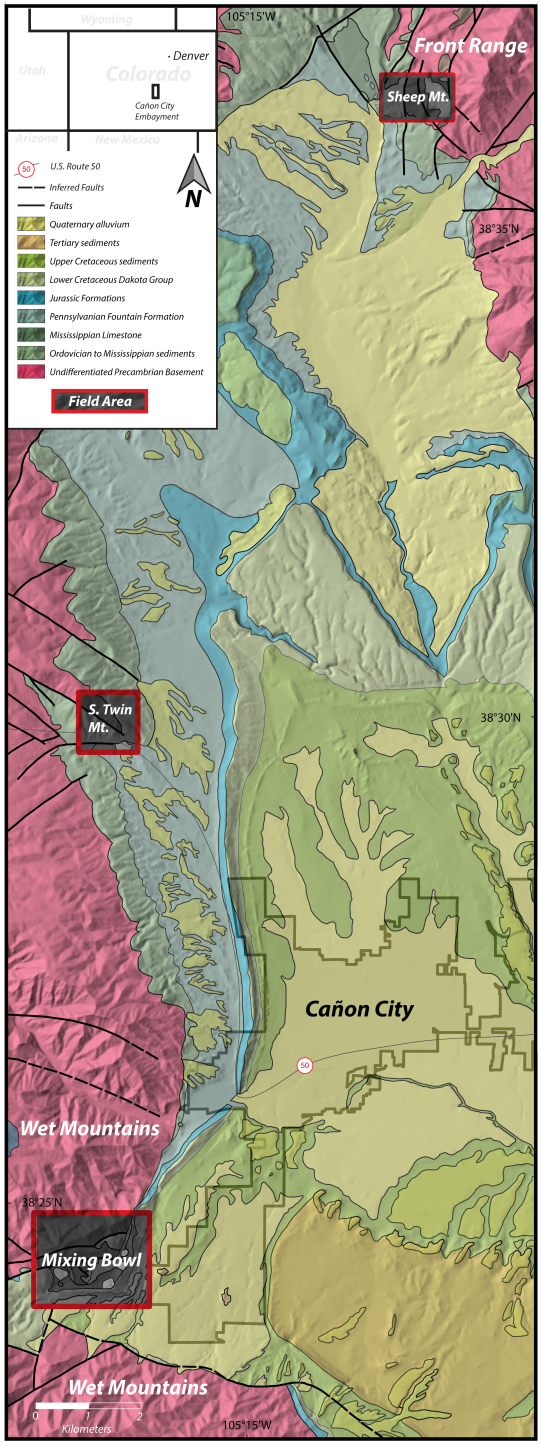

Figure 1. Geologic map of the Cañon City Embayment (CCE), Colorado. Proterozoic basement rocks are overlain by Ordovician to Cenozoic sedimentary units that form a broad syncline between the Wet Mountains and the Front Range. Modified from Taylor et al. (1975), Wobus et al. (1979), Wobus et al. (1985), and Scott et al. (1977).

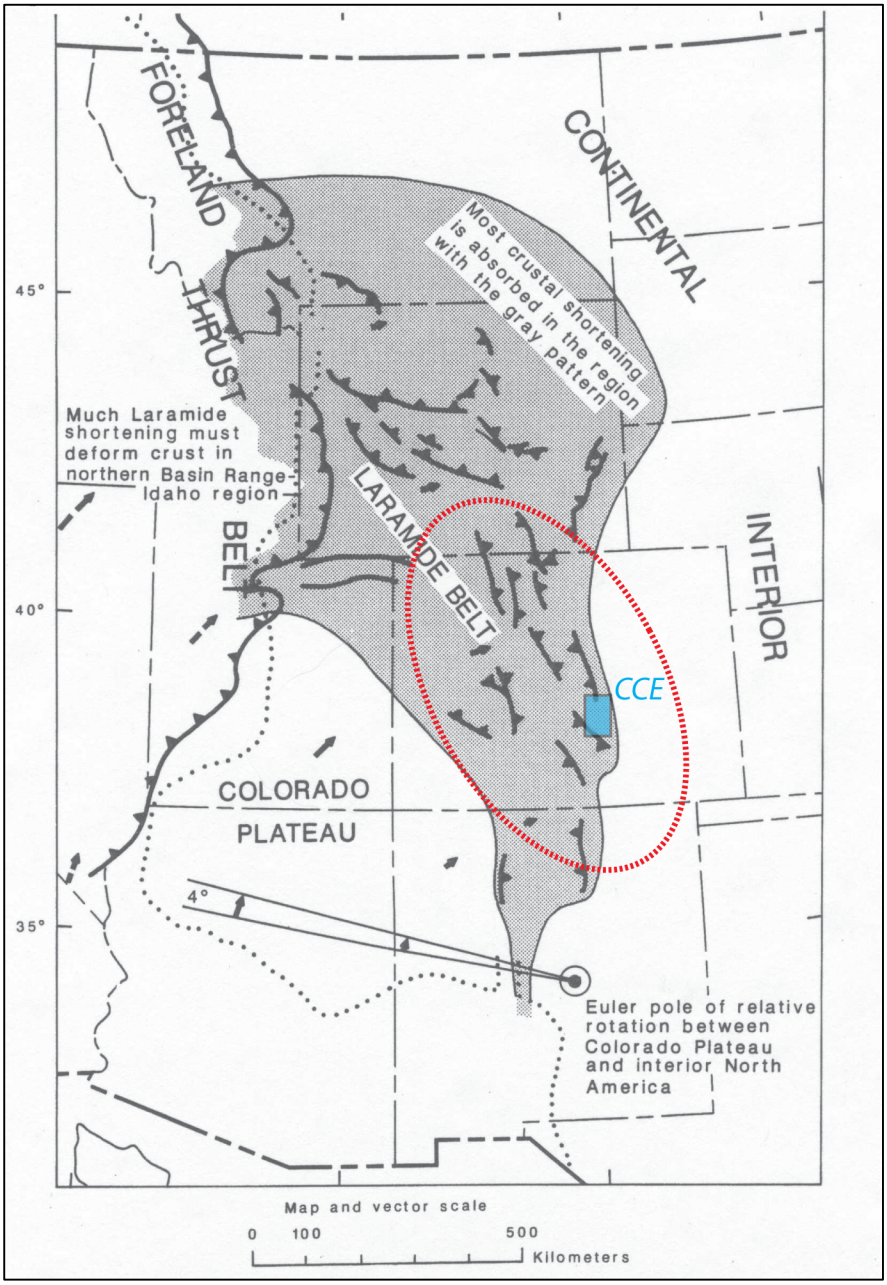

Figure 2. Geographical extent of the Laramide orogeny (Modified from Hamilton, 1981). During the Late Cretaceous to late Paleocene, the oblique, northeast-trending, shallow subduction of the Farallon Plate (Lipman et al., 1971; Lowell, 1974; Dickinson and Snyder, 1978) produced the Laramide orogeny. The Laramide orogeny exhibited a northeast-trending crustal shortening direction. Noted within the red ellipse, this crustal deformation event generated an anastomosing system of northwest–southeast oriented basement-cored arches. The arches were exhumed through thrust faulting (Erslev, 2004) The CCE is located within this region, and is noted in blue.

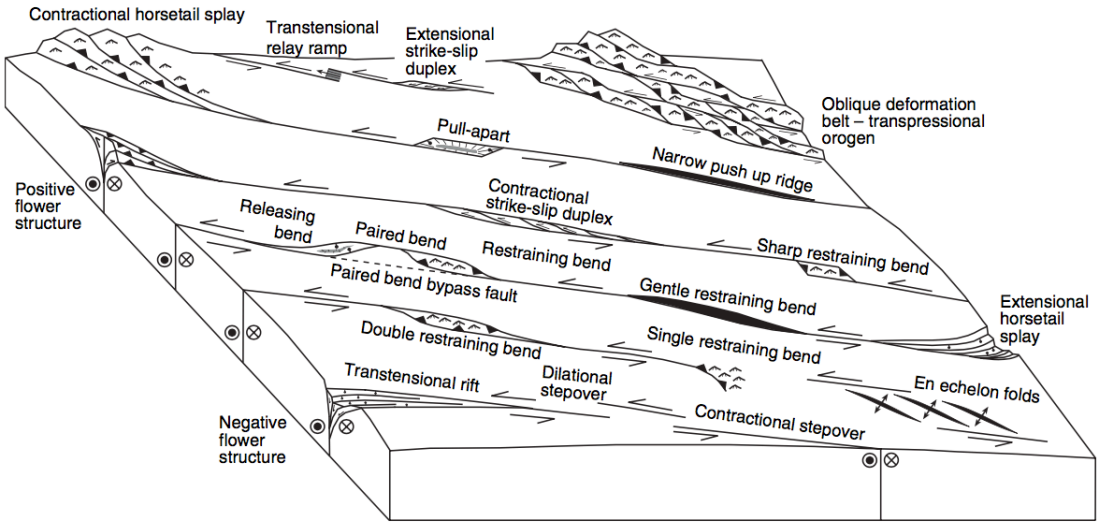

Figure 3. Oblique-slip geologic structures.
Tectonic structures affiliated with strike-slip restraining and releasing bends (after Cunningham and Mann, 2007).

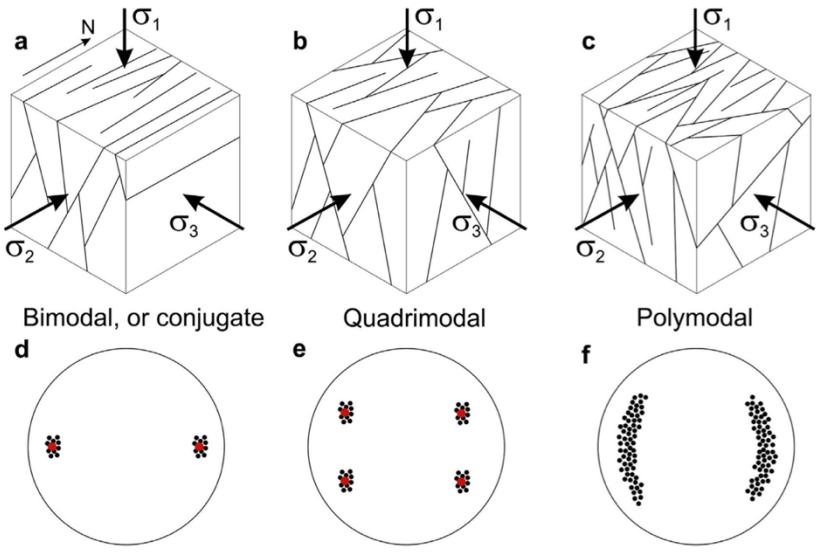

Figure 4. Conjugate, quadrimodal, and polymodal faulting (Modified from Healy et al., 2015). **(a)** Conjugate set of faults where the master and antithetic planes form under a single homogenous stress (Anderson, 1905). The acute angle between the master and antithetic fault plane describe the acute bisector. The acute bisector describes the orientation of the maximum compressive stress. The poles to the fault planes are observed beneath the block diagram. **(b, c)** Faults may display multiple sets of planes when they develop. Quadrimodal and polymodal faulting describe multiple clusters of poles representing the master and antithetic bimodal conjugate faults as well as nested conjugate faults coincident to both the master and antithetic faults (Peacock and Sanderson 1992).

CHAPTER 2

Methods

This thesis focuses on the collection of field data through detailed structural mapping of faults and deformation bands within porous sandstones. The field data were used for a fault-kinematic analysis that allowed for a comprehensive interpretation of the tectonic evolution of the field sites in the CCE via construction of geologic cross sections in the Mixing Bowl field area. Samples collected from the fault zones were used to evaluate and describe the micro-scale deformation.

Data collection for this project concentrated on three separate field areas within the CCE: the Mixing Bowl, South Twin Mountain, and Sheep Mountain (Fig. 1). The Mixing Bowl shows deformation in the southwestern extent of the CCE directly bordering the Wet Mountains. The South Twin Mountain field area, about 8 km north of the Mixing Bowl, characterizes deformation in the western extent of the embayment. The Sheep Mountain field area, 12 km northeast of South Twin Mountain field area, represents the interface between the basin of the embayment and deformation along the southwestern extent of the Front Range. Mapped lithologic units were described in this thesis from observations in these field areas (see Chapter 3).

The collection of field data focused on the detailed structural characterization and geologic mapping of each of these three field areas. A total of 688 bedding orientations of Ordovician to Cretaceous sediments were recorded. A total of 1131 deformation band orientations and the lithologies they were found in were also recorded. Each deformation band

measurement was recorded as being either an individual deformation band, part of an assemblage of bands in a band cluster, or a fault core. Deformation band length was measured and grouped into <1 m, 1 − 3 m, 3 − 10 m, and 10+ m. Strand thickness of deformation bands as well as cluster thicknesses were collected and assembled in values from 0 − 2 mm, 2 − 5 mm, 5 mm − 2 cm, 2 − 10 cm, and 10+ cm. Where present, conjugate sets of deformation bands were noted. If the offset between deformation bands was apparent, it was also recorded. If there was no apparent offset, deformation band orientations were used as an approximation of the stress field, especially when multiple band orientations were present in the outcrop. This was described only if there was no indication of rotation of bedding units from a subsequent deformation event. The attitudes of 112 slickenlines were recorded from well-developed deformation band slip surfaces. Slip direction was recorded if clearly visible from slickenline formation along the slip surface or deformation band offset. Slickenlines display grooves that display a millimeter-high topography on their surface, or ridges, which indicate slip direction of the fault plane or, in this case, deformation bands (Brown and Scholz, 1985; Petit 1987; Power et al., 1987; Lee and Bruhn, 1996; Doblas 1998; Renard et al., 2006; Sagy et al., 2007; Sagy and Brodsky, 2009; Candela et al., 2009; Candela et al., 2012; Foundriest et al., 2013; Siman-Tov et al., 2013).

Bedding orientations, deformation band orientations, and slickenline measurements were recorded using Midland Valley's FieldMove Clino application through a portable tablet device. Midland Valley is a structural geology software company that employs techniques to reduce structural uncertainty in the field. FieldMove Clino is the Midland Valley proprietary field application that can be used as a traditional hand-held bearing compass and clinometer measuring and recording the orientation of planar and linear features in the field. The device captures the longitude and latitude of each measurement through automatic positioning from the

device GPS. All recorded measurements were identified, validated, and recorded, with a physical field map. FieldMove Clino files were exported as .csv files for kinematic analyses through stereonet construction.

Kinematic analyses of recorded deformation bands were described in equal area stereonet constructions. A total of 69 stereonets were constructed using the coding package, Graphics for Spherical and Earthquake Focal Mechanisms (RFOC; Lees, 2017), in the statistical computing programming language R (R Core Team, 2015). Refer to Appendix B for a template of the R code. Stereonets were annotated after the construction process. These stereonets represent 23 stations of collected deformation band measurements. Four stereonets contained more than 45 deformation band planes and were plotted as poles in a density plot. The density plots were generated using Stereo32, a stereonet construction program created at the Ruhr-Universitat, Bochum, Germany. Each one of these stations describes the kinematics along observed deformation band damage zones. Within these stereonets, deformation band orientations, attitudes of associated slickenline data, and, if applicable, slip direction of those slickenlines are displayed. Slip direction along a corresponding deformation band slip surface is a direct indication of fault kinematics related to that deformation band. Stereonets were annotated to describe and illustrate deformation band kinematics. Geologic cross sections were manually constructed through each of the three field areas, as well.

Fault rocks were also described on the microscopic scale. The fault rock thin sections were studied under a Zeiss AXIO Scope.A1 microscope. Microscope imaging was collected through an Axiocam 506 color camera attachment. Three fault rock samples were examined microscopically from the Mixing Bowl field area.

CHAPTER 3

Description of Mapped Lithologic Units

3.1 Proterozoic Basement Rock

In this thesis, the Proterozoic basement is mapped as undifferentiated. The topographic highs seen in the Front Range and Wet Mountains around the CCE are composed of this unit (Figure 1). Within the Mixing Bowl and South Twin Mountain field areas, this rock unit was identified by pink, red, and gray crystalline exposures of a porphyritic, quartz monzonite defined as the San Isabel Granite (Boyer, 1962). Outcrops of black to gray, metamorphic crystalline rock, first described as a migmatitic biotite gneiss (Taylor and Scott, 1973) was also mapped as Proterozoic basement. Both of these Proterozoic units form the most prominent exposures in the Wet Mountains (Boyer, 1962; Taylor and Scott, 1973). In the Sheep Mountain field area, the Proterozoic basement rock is predominantly black to gray, massive to foliated hornblende and biotite quartz diorite is found in the southwestern extent of the Front Range (Jurista, 1996). Modern erosion of the Proterozoic basement generates an extensive cover of pebble-size fragments over other rock units that it juxtaposes, including Ordovician to Jurassic units.

3.2. Lower Ordovician Manitou Formation

The Manitou Formation is a massive gray dolomitic limestone with thin interbedded red to white shale layers. The unit has distinguishing white chert nodules and ribbons near its base. The formation is pink to purple where weathered. The Manitou Formation is observable in the Sheep Mountain and South Twin Mountain field areas. It can be thoroughly studied in the northern portion of the CCE, outcropping as a cliff-former, but is commonly covered by younger

units towards the south to southwest limits of the embayment. The maximum unit thickness is 15 meters (Erslev, 1996). The Manitou Formation lies nonconformably on the Proterozoic basement.

3.3 Middle Ordovician Harding Formation

The Harding Formation consists of red, white, and green, moderately cemented, fine- to coarse-grained, well-rounded, moderately sorted, porous, quartz arenite sandstones with interbedded subsets of sandstone and variegated shale. A white, quartz-pebble conglomerate marks the bottom of the Harding Formation, and the top is marked by a less than a meter-thick yellow sandstone layer. Where weathered, the Harding Formation is dark gray. Like the Manitou Formation, it is well-exposed near the northern part of the CCE as a cliff-former, but is less exposed towards the south to southwest. It is exposed in the Sheep Mountain, South Twin Mountain, and Mixing Bowl field sites. The thickness of the unit is approximately 20 meters, and it pinches out towards the south (Erslev and Selvig, 1996). The Harding Sandstone lies unconformably on the Manitou Formation or nonconformably on the Proterozoic basement.

3.4 Upper Ordovician Fremont Formation

The Fremont Formation is composed of white to gray, fossiliferous dolomite. Where weathered, the Fremont Formation is red to gray. The Fremont Formation is a cliff-former and predominantly crops out in the northern segment of the CCE in conjunction with both the Manitou Formation and Harding Sandstone. Though it becomes less extensive in the south to southwestern limits of the CCE, it still forms cliffs. It is exposed in the Sheep Mountain, South Twin Mountain, and Mixing Bowl field sites. The formation has a maximum thickness of 10 meters (Erslev and Selvig, 1996). The Fremont Formation lies unconformably on the Harding Sandstone.

3.5 Pennsylvanian Fountain Formation

The Fountain Formation includes purple to red, poorly cemented, coarse-grained, sub-rounded, poorly sorted, porous, arkosic sandstone with interbedded, feldspathic pebble to cobble conglomerates derived from Proterozoic rocks. The Fountain Formation is extensive across the CCE as a slope-former. It can be found within all three field areas. It is the thickest of all rock units in the CCE, with a maximum thickness of up to 600 meters (Erslev and Selvig, 1996). The Fountain Formation unconformably overlies the Fremont Formation.

3.6 Middle Jurassic Ralston Creek Formation

The Ralston Creek Formation consists of white, pink, and green, poorly cemented, coarse-grained, sub-angular to sub-rounded, poorly sorted, porous, subarkosic sandstones with interbedded pink, feldspathic conglomerates. The conglomerate clasts range from pebble- to cobble-size, with their provenance likely from Proterozoic rocks. The Ralston Creek Formation is seen throughout the CCE, in particular, in the Mixing Bowl field area and outcrops as a slope-former. The formation has a maximum thickness of approximately 20 meters (Erslev and Selvig, 1996). The Ralston Creek Formation unconformably overlies the Pennsylvanian Fountain Formation.

3.7 Upper Jurassic Morrison Formation

The Morrison Formation is composed of white, pink, and green fine-grained siltstone. The thickness of the formation averages approximately 90 meters (Erslev and Selvig, 1996). The Morrison Formation is observed only in the Mixing Bowl field area, where it is a slope-former that is extensively covered by vegetation. The Morrison Formation lies unconformably on the Ralston Creek Formation.

3.8 Lower Cretaceous Lytle Sandstone

The Lytle Sandstone is a white to gray, well-cemented, fine- to coarse-grained, porous, quartz arenite sandstone with sub-angular to sub-rounded, moderately sorted grains. The sandstone layers are locally interbedded with pebble-sized, chert conglomerates. Where weathered, the unit is red to orange. This unit is exposed in the Mixing Bowl as a cliff-former. The sandstone has a thickness ranging from 10 to 30 meters (Erslev and Selvig, 1996).

3.9 Lower Cretaceous Glencairn Shale

The Glencairn Shale is a white to blue to gray, fissile shale. It is exposed in the Mixing Bowl. The shale layer is approximately 20 meters thick (Erslev and Selvig, 1996). The Glencairn Shale forms a conformable contact with the underlying Lytle Sandstone.

3.10 Lower Cretaceous Dakota Sandstone

The Dakota Sandstone is a white to gray, well-cemented, fine- to medium-grained, sub-rounded, well-sorted, porous, quartz arenite sandstone. Where weathered, the unit is red to maroon. The Dakota Sandstone is exposed along the top of the ridges, as a cliff-former, surrounding the Mixing Bowl to the west, south, and east. The sandstone is 35 to 50 meters thick (Erslev and Selvig, 1996).

3.11 Upper Cretaceous Graneros Shale

The Graneros Shale is blue to black and is exposed on the west, south, and east side of the Mixing Bowl map area. The unit is approximately 30 meters thick (Logan, 1966). It conformably overlies the Dakota Sandstone and is part of the Cretaceous Benton Group (Mateer, 1987).

CHAPTER 4

Structural Styles of Faulting in the CCE

4.1. Expressions of Fault Rocks in Mapped Lithologic Units

Deformation bands, heavily cemented sandstones, and incohesive brecciated fault rocks are observable in the CCE (Fig. 5). Prominent across each field area (Fig. 1) are the presence of deformation bands. Deformation bands are white, gray, pink to brown, very fine-grained, angular, poorly sorted, discontinuous bands hosted in porous sandstone (Fig. 6). Deformation bands are highly resistant to erosion relative to its host sandstone (Fig. 5b). Deformation bands are visible in the Fountain Formation (Fig. 7), Ralston Creek Formation (Fig. 7), Lytle Sandstone (Fig. 6), and the Dakota Sandstone (Fig. 8). They are also present in the Harding Formation in all three field areas (Fig. 9). Bands are commonly observed as single strands of varying thickness ranging from <2 mm to 1 cm (Fig. 6). Single strands are also viewed in larger accumulations, such as band clusters (Fig. 10). Strand accumulations range from two to three, and in certain locations include hundreds to thousands of strands to form a fault core with a deformation band damage zone (Fig. 11). Strand clusters and fault cores range from 2 cm to over 10 cm in thickness (Fig. 11). Deformation band lengths of thinner, single strands range from <1 m to 3 m long (Fig. 11). Deformation band clusters are 3 to 10 meters long, and the thickest band clusters are more than 10 meters long (Fig. 11). These arrays of deformation bands form en-echelon sets with similar orientations (Fig. 8). Frequently, multiple sets of deformation band orientations are present in a single location (Fig. 12), and offset between two bands may occur along a slipped band (Fig. 13). Offset can also be observed from slickenlines along slipped band surfaces (Fig.

14). In zones of higher intensity of deformation, ladder structures show bounding and linking bands (Fig. 8; Fig. 12).

Heavily cemented sandstones and incohesive fault breccias are visible in the middle of the Mixing Bowl field area (Fig. 16; Fig. 17). The middle of the Mixing Bowl field area consists of Proterozoic basement rock that is in structural contact with the Harding, Fremont, Fountain, and Ralston Creek Formations (Fig. 15). Smaller outcrops of the Harding Formation within the extent of the Proterozoic basement rock outcrop occur (Fig. 15). A horizontal structural contact is expressed solely in the Harding Formation at four different locations on the map (Fig. 15). The location of sample S2 indicates where these heavily cemented sandstones appear within the Harding Formation (Fig. 18). These sandstones consist of white, dense, firmly compacted grains (Fig. 16). The compacted sandstones form abruptly adjacent to the porous Harding Sandstones (Fig. 16), and are only observable when in proximity to the structural contact between the Harding Formation and the Proterozoic basement rock.

Incohesive brecciated fault rocks are visible in the Mixing Bowl and Sheep Mountain field area (Fig. 19). Within both field areas, brecciated fault rocks mark the boundaries between the Harding Sandstone and Proterozoic rock (Fig. 5d; Fig. 17). Like the heavily cemented Harding Sandstone, the brecciated fault rock is also only found in the middle of the Mixing Bowl field area (Fig. 15). The location of sample S24 indicates where these brecciated fault rocks appear in the middle of the Mixing Bowl (Fig. 18). The brecciated fault rock consists of purple, and green to white incohesive rock fragments directly below outcrops of the Harding Sandstone (Fig. 5e; Fig. 17) The purple brecciated layer overlies the white to green brecciated layer. Grain size between the two layers differs, with the purple layer being very fine, whereas the white to green brecciated layer displays medium to coarse-grained sized brecciated fragments (Fig. 20).

The fault breccia located in the Sheep Mountain field area is visible throughout the easternmost structural contact between the Harding Formation and the Proterozoic basement rock (Fig. 19). The fault rock consists of white brecciated clasts (Fig. 5d).

4.2. Mixing Bowl Field Area

4.2a. General Geologic Observations of the Field Area

The Mixing Bowl field area is located southwest of Cañon City (Fig. 1). It marks one the westernmost points where Paleozoic to Cenozoic rocks crop out in the CCE (Taylor et al., 1975; Wobus et al., 1979; Wobus et al., 1985; Scott et al., 1977). The Wet Mountains surround the field area to the south, west, and north. The field area is approximately four square kilometers. Throughout the field area, 527 bedding measurements were collected (Fig. 18). Cretaceous sedimentary units bound the field area to the east, south, and west. Proterozoic basement rock bounds the Mixing Bowl to the north. Within the Mixing Bowl, the Proterozoic basement comes into structural or fault contact with younger Ordovician, Pennsylvanian, Jurassic, and Cretaceous units. In the northern portion of the mapped area, the Harding Formation lies nonconformably above the Proterozoic basement rock. In the central Mixing Bowl area, the Proterozoic basement is in fault contact with the Harding Formation (Fig. 17). Observed between the Proterozoic basement rock and the Harding Formation are purple, and white to green layers of sheared brecciated rock fragments (Fig. 20). The Proterozoic basement rock is inferred to be in structural contact with the Fremont Formation, Fountain Formation, and Ralston Creek Formation (Fig. 15). The bedding orientations of Ordovician to Cretaceous rock units are consistent across depositional contacts, but increase in dip magnitude when in proximity to a structural contact (Fig. 15).

The Manitou Formation is not present in the Mixing Bowl. The Harding Formation is present in the middle of the Mixing Bowl as well as in the northeastern section. The Fremont Formation lies unconformably on the Harding Formation, and bedding orientations are the same above and below the contact. In the middle portion of the field area, the orientations along the contact dip towards the south-southeast between 0º and 10º (Fig. 18). Likewise, in the northeastern section, the orientations along the contact display dip directions towards the south-southeast with dips of 5º to 15º (Fig. 18). The Fountain Formation lies unconformably above the Fremont Formation and bedding attitudes dip towards the south-southeast between 10º and 20º along the contact.

The Fountain Formation extends from the northeastern quadrant of the mapped area, forming an arcuate map pattern, towards the western portion of the map (Fig. 18). The Fountain Formation is in structural contact with both the Fremont Formation and the Harding Formation in the northeast quadrant of the map (Fig. 15). The Ralston Creek Formation lies unconformably above the Fountain Formation. Along the unconformable contact in the east, orientations between the two units dip approximately 20º to the south. In the west, dip magnitudes are between 20º and 30º with dip direction towards the southeast (Fig. 18). The Ralston Creek Formation mimics the arcuate map pattern of the Fountain Formation (Fig. 18) The Morrison Formation lies unconformably above the Ralston Creek Formation with like bedding attitudes above and below the unconformity. Dip magnitudes along this contact are between 20º and 30º towards the southeast (Fig. 18).

The Cretaceous Dakota Group Formation lies unconformably above the Morrison Formation. Bedding attitudes above and below the contact are consistent throughout the field area. In the west, bedding orientations dip towards the south-southwest at approximately 15º. In

the east, dips above and below the contact dip between 20º and 30º toward the east-southeast. The Cretaceous Dakota Group consist of the Lytle Sandstone Member, Glencairn Shale Member, and Dakota Sandstone, and dip shallowly in the west and transition to a moderate dip towards the northeast section of the area (Fig. 18). Unrestricted structural contacts are apparent along the Cretaceous Dakota Group Ridge. For example, two major faults trend east-west and southwest-northeast along the ridge and are continuous through each of the three units (Fig. 15). The Cretaceous Benton Group is conformably above the Cretaceous Dakota Group. The Cretaceous Benton Group is represented in the field area by the stratigraphically lowermost unit, the Graneros Shale. The Graneros Shale marks the boundary of the mapped region of the Mixing Bowl to the south and the east (Fig. 18). Bedding planes in the Graneros Shale are shallowly to steeply dipping and follow the dip magnitudes in the Cretaceous Dakota Group. All observed unconformities in the field area display little to no difference in strata orientation above and below the contacts (Fig. 15). Refer to Table 1 for a summary of the results presented below. Refer to Appendix A for field photos of the Mixing Bowl field area.

4.2b. Station Observations of Deformation Bands

4.2b.i. Cretaceous Dakota Group Ridge

The Cretaceous Dakota Group Ridge bounds the Mixing Bowl to the west, south, and east (Fig. 15). The topographically raised landform contains the Lytle Sandstone Member, Glencairn Shale Member, and Dakota Sandstone. These sandstones host well-deformed deformation band damage zones correlating to major and minor faulting seen along the ridge (Fig. 15). Deformation bands located along the ridge are hosted in both the Dakota Sandstone and Lytle Sandstone. The Cretaceous Dakota Group Ridge is a well-developed representation of these arrays of pervasive brittle deformation structures. Across the Cretaceous Dakota Group

Ridge, 626 deformation band measurements and 64 slickenline measurements from deformation band slip surfaces were collected. There are eight stations that these measurements are compiled into.

Station 1 is located along the northern segment of the Cretaceous Dakota Group Ridge (Fig. 15). Stereonet locations are represented by numbered white circles (Fig. 15). Stereonets 1a, 1b, and 1c are substations of station 1. The stereonet locations are numerically arranged north to south. At this station location, 30 deformation bands were measured along with 16 slickenline measurements from their correlated deformation band slip surfaces.

Stereonet substation 1a displays 14 deformation band orientations and 8 slickenline measurements (Fig. 15; Fig. 21.1a). Five sets of band orientations are present. Deformation bands dip in all directions. Deformation bands dip from moderate to steep with a maximum dip of 75º and a minimum dip of 34º. Observable slickenlines along band surfaces show trends toward the northwest, east-northeast, and southeast. Plunges are steeply dipping with three measurements dipping moderately. The maximum plunge of slickenlines is 74º and minimum plunge is 32º. Deformation bands show left-lateral reverse-slip, right-lateral reverse-slip, and thrust dip-slip offset.

Stereonet substation 1b shows 11 deformation band attitudes and 7 slickenline measurements (Fig. 15; Fig. 21.1b). Five sets of deformation band orientations are observable. Deformation bands vary in dip direction from the northeast to northwest to southwest. Deformation bands have steep dip magnitudes. Dip magnitudes have a maximum of 88º and a minimum at 51º. A cluster of deformation bands dip towards the northeast and southwest. Slickenlines trend toward the northeast and southwest. Plunges range from shallow to

predominantly moderate with a maximum plunge of 52º and a minimum plunge of 18º. Deformation bands display left-lateral reverse-slip and right-lateral reverse-slip offset.

Stereonet substation 1c contains 5 deformation bands and 1 slickenline (Fig. 15; Fig. 21.1c). The single set of deformation bands are uniformly dipping to the northeast. Deformation bands have steep dip magnitudes. The maximum dip magnitude is 71º and the minimum is 53º. The single slickenline trends towards the east-southeast with a plunge of 35º. Deformation bands show right-lateral reverse-slip offset.

Station 2 covers areas including a low elevation topographic gap between the north and south ridges as well as the deformation bands located along the northwestern face of the south ridge of Cretaceous Dakota Group Sandstones (Fig. 15). The stereonet locations for each substation are situated west through the low elevation topographic gap at the bottom of the ridge, and established east at the top of the ridge towards substation 2d. Within this area, a total of 393 deformation band measurements and 9 slickenline measurements were recorded. Substations that contained more than 45 deformation band measurements were displayed as poles in density plots. Stereonet substations 2a, 2b, and 2d were expressed in this manner. For each plot, maximum density is in black and minimum to zero density is in white. Each stereonet contains different density maximums and minimums due to the differing amount of deformation bands in each substation. The extensive amount of recorded data from deformation band orientations is due to outcrop exposure through the low elevation topographic gap and on top of the ridge (Fig. 15).

Stereonet substation 2a, includes 280 deformation band orientations and 4 slickenline measurements (Fig. 15; 21.2a). At least four sets of deformation band orientations represented by pole accumulations in the density plot (Fig. 22.2a). These sets are defined by the dark region in

the center and the lighter gray regions in the southwest and southeast quadrants. Deformation bands dip in all directions and have shallow to steep dip magnitudes. The maximum dip is 89º and the minimum dip is 2º. Slickenlines in this substation trend towards the northeast and southwest. Plunge measurements in this substation are 7º, 8º, 35º, and 38º. In the center of the stereonet, the maximum density of deformation band poles is located in the black region (Fig. 22.2a). The black region has a maximum density of 53 poles. To emphasize the amount of poles located in that single area, a red circle highlights the maximum density contour (Fig. 22.2a). Deformation bands show low-angle dip-slip, right- and left-lateral strike-slip as well as right- and left-lateral reverse-slip offset.

Stereonet substation 2b consists of 47 deformation band measurements (Fig. 15; Fig. 21.2b). At least four sets of deformation bands are present (Fig. 22.2b). Deformation bands dip in every direction. Dip magnitudes for deformation bands range from shallow to steep. The maximum dip is 89º and the minimum dip is 11º. There were no slickenlines visible in this substation. The maximum density of poles is located in the southeastern quadrant (Fig. 22.2b). The black region has a maximum density contour of 9 poles. The red circle in the middle of the black region indicates the maximum density of poles (Fig. 22.2b). Deformation bands exhibit right-lateral strike-slip, left-lateral strike-slip, right-lateral reverse-slip, left-lateral strike-slip, and low-angle dip-slip.

Stereonet substation 2c displays 13 deformation band orientations and 4 slickenline measurements (Fig. 15; 21.2c). At least five sets of deformation bands are observable. Dip direction of deformation bands are oriented in each direction besides the northeast. Dip magnitudes range from shallow to steep. The maximum dip is 87º and the minimum dip is 6º. Slickenlines in this area trend towards the northeast. The plunges of these slickenlines are 9º, 12º,

and 31º. Deformation bands show right and pure, left-lateral strike-slip offset. These bands also display right-lateral reverse-slip offset.

Stereonet substation 2d, includes 53 deformation band orientations and 5 slickenline measurements (Fig. 15; Fig. 21.2d). At least four sets of deformation bands are present. Deformation bands dip in every direction. Dip magnitudes of deformation bands range from shallow to steep. The maximum dip is 89º and the minimum dip is 15º. The trends of the slickenline orientations are towards the northeast, and their plunge magnitudes are 22º, 28º, 32º, 39º, and 59º. The greatest concentration of poles, marking the maximum density contour for substation 2d, is located in the southwestern quadrant (Fig. 22.2d). The maximum density contour, describing the black extent of the density plot, is 16 poles. The red circle in the middle of the black region characterizes the highest density of poles to deformation band planes (Fig. 22.2d). Deformation bands show right-lateral and left-lateral reverse-slip offset.

Stations 3 and 4 are a continuation of observed deformation bands along the southern portion of the Cretaceous Dakota Group Ridge that constitute the southeastern segment of the map (Fig. 15). For station 3, substations are arranged east to west. At this station, 34 deformation bands along with 5 slickenlines from slip surfaces were recorded.

Stereonet substation 3a displays 22 deformation band orientations and two slickenline lineations (Fig. 15; Fig. 21.3a). Six sets of deformation bands are present. Deformation bands largely dip towards the southeast and south-southwest. A small accumulation of deformation bands dip to both the northwest and northeast. Deformation bands range in dip magnitudes from moderate to steep with a maximum dip of 88º and a minimum dip of 33º. Noticeable slickenlines along deformation band slip surfaces display trends toward the north-northeast. Plunges of the

slickenlines are 41º and 15º. Deformation bands exhibit right-lateral reverse-slip and left-lateral strike-slip offset.

Stereonet substation 3b shows 8 deformation band orientations (Fig. 15; Fig. 21.3b). There are two sets of deformation bands visible. Deformation bands from this substation dip towards the northeast and northwest. Dip magnitudes from these measurements are steep with a maximum dip of 63º and minimum dip of 47º. Deformation bands display right-lateral reverse-slip and left-lateral strike-slip offset.

Stereonet substation 3c indicates the presence of 4 deformation band and three slickenline measurements (Fig. 15; Fig. 21.3c). Four sets of deformation bands are observable. Dip direction of deformation bands are towards the northeast, northwest, and southeast. The magnitude of dip of these deformation bands range from moderate to steep. The maximum dip measurement recorded is 89º and the minimum dip measurement recorded is 43º. Slickenlines display trends from the east-northeast and east-southeast. Plunges of slickenlines range from 29º and 28º to 6º. Deformation bands show right-lateral reverse-slip, left-lateral reverse-slip, and left-lateral strike-slip offset.

Station 4 contains substations arranged from north to south (Fig. 15). This station includes 31 deformation bands and 7 slickenline measurements. Stereonet substation 4a displays 18 deformation band measurements and 3 slickenline measurements (Fig. 15; Fig. 21.4a). There are six sets of deformation band orientations. Deformation bands dip in all directions besides the southwest. The dips vary from moderate to steep. The maximum dip is 81º and the minimum dip is 44º. Slickenlines in substation 4a are trending toward the southeast and northeast. Plunges of slickenlines are shallow. These plunges are 15º, 1º, and 2º. Deformation bands express right-lateral strike-slip, right-lateral reverse-slip, and left-lateral strike-slip offset.

Stereonet substation 4b displays 8 deformation bands and 4 slickenline orientations (Fig. 15; Fig. 21.4b). Three sets of deformation bands are present. Deformation bands dip towards the northwest and northeast. Dip magnitudes of these deformation bands are steep. The maximum dip is 83º and the minimum dip is 59º. Slickenlines in this area are trending towards the northeast. Plunges of the slickenlines are shallow. The plunge magnitudes range from 19º to 0º. Deformation bands display right-lateral reverse-slip, and both left-lateral reverse-slip and strike-slip offset.

Stereonet substation 4c exhibits 5 deformation bands. There are three sets of deformation band orientations present. The deformation bands in this substation reflect dips toward the northeast, southwest, and northwest (Fig. 15; Fig. 21.4c). The dip magnitudes of these deformation bands are steep. The maximum dip is 76º and the minimum dip is 49º. There were no observed slickenlines. Offset between deformation bands show left-lateral strike-slip motion.

Station 5 marks the bend in the Cretaceous Dakota Group Ridge (Fig. 15). This station designates the change between the eastern segment of the ridge and western segment of the ridge. Within this area, substations record the transition from deformation band orientations in the eastern segment to deformation bands observed in the western segment of the ridge. Station 5 includes 22 deformation band measurements and 13 slickenline measurements.

Stereonet substation 5a displays 7 deformation band and 2 slickenline measurements (Fig. 15; Fig. 23.5a). Three sets of deformation bands are present in this substation. Deformation bands dip towards the northwest and the northeast. Dip magnitudes are steep. The maximum dip is 82º and the minimum dip is 59º. The slickenlines trend towards the northeast. The plunges of the two observed slickenlines are 23º and 22º. Deformation bands show left-lateral reverse-slip and right-lateral reverse-slip offset.

Stereonet substation 5b includes 13 deformation bands and 9 slickenlines (Fig. 15; Fig. 23.5b). Three sets of deformation band orientations are in this substation. Deformation bands dip toward the north, northwest, and southeast. Deformation band dip magnitudes range from moderate to steep. The maximum dip is 86º and the minimum dip is 32º. The slickenlines observed in this area trend towards the northeast and southwest. The plunges associated with these slickenlines are shallow. The maximum plunge is 29º and the minimum plunge is 4º. Deformation bands express left-lateral strike-slip, left-lateral reverse-slip, and right-lateral strike-slip offset.

Stereonet substation 5c includes 2 deformation bands and 2 slickenline measurements (Fig. 15; Fig. 23.5c). Dip magnitudes of the deformation bands are 85º and 89º. Slickenlines show trends toward the northeast and southwest and plunge 12º and 24º. Deformation bands show right- and left-lateral reverse-slip offset.

Station 6 is the first cluster of substations along the western ridge. The substations are aligned east to west. Station 6 includes 40 deformation band measurements and 7 slickenline measurements. Stereonet substation 6a displays 11 deformation bands and 4 slickenline measurements (Fig. 15; Fig. 23.6a). Five sets of deformation band orientations are present. Bands dip towards the northwest, northeast, and southwest. Dip magnitudes of these deformation bands range from shallow to steep. The maximum dip is 85º and the minimum dip is 15º. The slickenlines observed in this substation trend to the northeast and east. Plunges of these slickenlines are shallow. The maximum plunge is 22º and the minimum plunge is 7º. Deformation bands display left- and right-lateral strike-slip, and left-lateral reverse-slip offset.

Stereonet substation 6b, involves 16 deformation bands and 2 slickenlines (Fig. 15; Fig. 23.6b). There are four sets of deformation band orientations present. Deformation bands in this

area dip toward the northwest, northeast, and southwest. The dip magnitudes range from moderate to steep. The maximum dip is 88º and the minimum dip is 33º. The slickenlines consist of trends toward the northeast and southwest. The slickenline plunges are shallow at 12º and 23º. Deformation bands exhibit left-lateral reverse-slip and right-lateral reverse-slip offset.

Stereonet substation 6c consists of 4 deformation bands (Fig. 15; Fig. 23.6c). Three sets of deformation band orientations are present. Deformation bands have dip directions towards the northwest and southwest. Dip magnitudes of these deformation bands are 64º, 81º, 81º, and 83º. There were no observed slickenlines in this substation. Deformation bands show left-lateral strike-slip and right-lateral strike-slip offset between bands.

Stereonet substation 6d encompasses 10 deformation band measurements and one slickenline measurement (Fig. 15; Fig. 23.6d). There are two sets of deformations observed in this substation. Dip directions of recorded deformation bands are toward the northwest and the northeast. The dip magnitudes range from moderate to steep. The maximum dip is 73 and the minimum dip is 41º. The one slickenline measurement exhibits trends to the southwest and plunges 15º. Deformation bands display right-lateral reverse-slip offset along slipped deformation bands.

Station 7 marks the end of the western segment of the Cretaceous Dakota Group Ridge (Fig. 15). The substations are aligned east to west. Within this area, 72 deformation bands were measured along with 3 slickenlines. Stereonet 7c displays 48 deformation bands and was plotted in a density plot of poles to deformation band planes.

Stereonet substation 7a includes 17 deformation bands and 4 slickenline measurements (Fig. 15; Fig. 23.7a). Substation 7a includes five sets of deformation bands. Deformation bands dip toward the northwest, northeast, southwest, and southeast. The dip magnitudes range from

moderate to steep. The maximum dip is 87º and the minimum dip is 41º. Slickenlines trend to the northeast and southwest. Plunges of the three recorded slickenlines are 0º, 26º, and 28º. Deformation bands express right- and left-lateral reverse-slip, and left-lateral strike-slip offset.

Stereonet substation 7b exhibits 7 deformation bands (Fig. 15; Fig. 23.7b). This substation contains only one set of deformation band orientations. The dip direction of these deformation bands is towards the northwest. The dip magnitudes of these deformation bands are steep. The maximum dip is 83º and the minimum dip is 59º. There were no slickenlines recorded in this area. Right-lateral strike-slip offset was observed between bands.

Stereonet substation 7c, displays 48 deformation bands and no slickenlines (Fig. 15; Fig. 23.7c). At least two sets of deformation band orientations are present. Dip direction of deformation bands dip in every direction except towards the northeast. Dip magnitudes range from shallow to steep. The maximum dip is 89º and the minimum dip is 21º. The gray spot in the southeast quadrant of the stereonet describes the maximum density of poles to deformation band planes (Fig. 24.7c). Highlighted in red, the maximum density contour is 18 poles. Deformation bands display left-lateral strike-slip offset.

Station 8 is the farthest west that the Cretaceous Dakota Group outcrops in the Mixing Bowl field area (Fig. 15). This area does not contain pervasive arrays of deformation bands. Station 8 contains two substations. Stereonet substations 8a and 8b are arranged from the south to the north. Between these two substations, there are 4 deformation band measurements. Fig. 15; Fig. 23.8a; Fig. 23.8b). Dip directions of these deformation bands are towards the northwest and south. The dip magnitudes are 81º, 62º, 77º, and 73º. There are no recorded slickenline measurements. Left-lateral strike-slip motion is observable between band offset.

4.2b.ii. Central Mixing Bowl

The Central Mixing Bowl describes the deformation band kinematics as well as deformation structures associated with the outcrop of Proterozoic basement rock (Fig. 15). The porous sandstone units that host deformation bands in this area are the Harding Formation and Ralston Creek Formation. These stations represent deformation recorded by 104 deformation band measurements and 10 slickenline measurements recorded from slipped deformation bands.

Station 9 characterizes the zone of deformation encompassing a fault through the Ralston Creek Formation (Fig. 15). The substations within station 9 are arranged south to north. Along this fault zone, there are 35 deformation band measurements and 4 slickenline measurements. Stereonet substation 9a displays 24 deformation band measurements and 3 slickenline measurements (Fig. 15; Fig. 25.9a). Nine sets of deformation band orientations are present in substation 9a. Deformation bands dip in every direction besides the east. The dip magnitudes of these deformation bands are mainly steep. The maximum dip magnitude is 89º and the minimum dip magnitude is 44º. Slickenlines in this zone are trending towards the north and west. The plunge magnitudes of the three slip surfaces are 63º, 3º, and 3º. Deformation bands in substation 9a show right- and left-lateral strike-slip, and reverse dip-slip offset.

Stereonet substation 9b contains 7 deformation bands and one slickenline measurement (Fig. 15; Fig. 25.9b). There are three sets of deformation band orientations. Deformation bands dip towards the northwest and are steeply dipping. The maximum dip is 89º and the minimum dip is 78º. The slickenline measurement is trending to the southwest with a plunge of 4º. Deformation bands show right- and left-lateral strike-slip offset.

Stereonet substation 9c includes 4 deformation bands that dip towards the northwest and southeast Fig. 15; Fig. 25.9c). Two deformation band orientations are present in this substation.

The dip magnitudes of these deformation bands are 82º, 84º, 84º, and 85º. There was no offset seen in this substation.

Station 10 includes deformation band damage zones that directly describe the horizontal fault zone between the Harding Formation and Proterozoic basement rock (Fig. 15). At this station, deformation bands associated with the heavily cemented sandstones are observed and recorded. Substations 10a, 10b, 10c, and 10d record deformation band orientations from this structural contact that is observed in the middle of the Mixing Bowl field area. The substations in Station 10 are arranged from south to north. This zone of deformation within the Mixing Bowl is characterized by 74 deformation band measurements and 5 slickenline measurements.

Stereonet substation 10a, includes 26 deformation band measurements (Fig. 15; Fig. 25.10a). There are approximately seven deformation band orientations visible in this area. The deformation bands within this substation dip in each direction besides the southwest. The dip magnitudes of the observed deformation bands range from shallow to steep. The maximum dip magnitude is 88º and the minimum dip magnitude is 3º. There were no visible slickenlines in the area nor offset seen between bands. The prominent horizontal brecciated fault zone between the Harding Formation and the Proterozoic basement rock was identified in this substation and is dipping approximately 10º to the north (Fig. 17).

Stereonet substation 10b, displays 15 deformation band measurements (Fig. 15; Fig. 25.10b). There are approximately six deformation band orientations observable. The dip magnitudes of the deformation band orientations range from steep to shallow. The maximum dip is 86º and the minimum dip is 8º. There was no observable offset in the area.

Stereonet substation 10c, characterizes 25 deformation bands and 3 slickenlines (Fig. 15; Fig. 25.10c). There are approximately eight deformation band orientations observed in this

substation. Deformation bands dip in every direction. The dip magnitudes of these deformation bands are largely steep with a single shallow deformation band. The maximum dip is 89º and the minimum dip is 3º. Trend directions of the lineations are towards the southwest and the northeast. Slip direction along these slipped deformation bands were ambiguous to identify in the field, and there was no offset observed between deformation bands.

Stereonet substation 10d, includes 8 deformation band and 2 slickenline measurements (Fig. 15; Fig. 25.10d). There are six deformation band orientations observed in this area. The dip angles seen in this zone of deformation are steep. The maximum dip is 89º and the minimum dip is 59º. Slickenline measurements trend towards the northeast and the south. In this area, slickenline slip directions are ambiguous in the field. No offset between deformation bands were observed.

4.2b.iii East Mixing Bowl

The East Mixing Bowl consists of deformation bands in the Ralston Creek Formation located west of the Cretaceous Dakota Group Ridge (Fig. 15). Station 11 describes these deformation band damage zones. Station 11 is broken up into two substations, 11a and 11b. These stations are arranged southwest to northeast. There are 18 measured deformation bands between the two stations. No slickenline data was collected at station 11.

Stereonet substation 11a, contains 4 deformation bands (Fig. 15; Fig. 25.11a). There are four deformation band orientations present. Deformation bands dip towards the northeast, northwest, and southeast. The dips of the deformation bands are 38º, 57º, 61º, and 74º. No offset was observed. Deformation band orientations describe high-angle faulting.

Stereonet substation 11b, includes 14 measured deformation band orientations (Fig. 15; Fig. 25.11b). Five deformation band orientations are observable. Deformation bands dip towards

the northwest, northeast, and southwest. The dips within this zone are mainly steep with a single sub-horizontal deformation band. The maximum dip is 86º and the minimum dip is 7º. No offset was observed. The deformation bands show high-angle faulting with one band exhibiting low-angle faulting.

4.2b.iv. North Fault Zone

The North Fault Zone segment of the Mixing Bowl field area represents deformation band orientations along the northern most structural contact between the Harding Formation and the Proterozoic basement (Fig. 15). Deformation bands observed in the North Fault Zone are compiled into station 12. There are three substations of station 12. Substations within this segment are ordered from east to west. There are 17 measured deformation bands and 7 slickenline measurements in station 12.

Stereonet substation 12a, characterizes 6 deformation bands and 3 slickenline measurements (Fig. 15; Fig. 25.12a). Four deformation band orientations are present. Deformation bands dip towards the northwest and southeast. Deformation bands dip steeply. The maximum dip magnitude is 76º and the minimum is 64º. The slickenlines in this area trend towards the southeast. The plunge of the slickenlines are 57º, 68º, and 72º. Deformation bands show left-lateral reverse-slip offset.

Stereonet substation 12b, consists of 9 deformation bands and 3 slickenlines (Fig. 15; Fig. 25.12b). There are three deformation band orientations. Deformation bands dip towards the northwest and the southeast. Dips of deformation bands are steep. The maximum dip angle is 84º and the minimum dip angle is 64º. Slickenline data trends toward the northeast. The plunges of these lineations are shallow. Deformation band orientations exhibit left-lateral strike-slip offset.

Stereonet substation 12c, contains 2 deformation bands and 1 slickenline (Fig. 15; Fig. 25.12c). Two deformation band orientations are observable. Deformation band dips toward the north and the southeast. The dips of the deformation bands are 30º and 25º. The slickenlines in this area trend toward the northeast. The plunge of this deformation band is 1º. Deformation bands show right-lateral strike-slip offset.

4.2b.v. Ordovician Plateau

The Ordovician Plateau describes the deformation that occurs in the topographically high Ordovician sedimentary units in the northeastern quadrant of the map (Fig. 15). Within this area, the Harding Formation comes into structural contact with the Proterozoic basement and the Fountain Formation. The Fremont Formation also comes into structural contact with the Fountain Formation. Substations in this area are arranged west to east. This segment of the map includes 58 deformation bands and 17 slickenlines described in station 13.

Stereonet substation 13a displays 26 deformation bands and 8 slickenline orientations (Fig. 15; Fig. 26.13a). Four deformation band orientations are observable. Deformation bands dip mainly towards the northwest and southeast, with one deformation band dipping towards the northeast. Deformation band dips are steep. The maximum dip magnitude is 88º and the minimum dip magnitude is 50º. Observable slickenlines trend in all directions. Slickenline plunge magnitudes are shallow to steep. The maximum plunge magnitude is 61º and the minimum dip magnitude is 8º. Deformation bands show right and left-lateral normal-slip as well as normal dip-slip offset.

Stereonet substation 13b includes 31 deformation band and 8 slickenline measurements (Fig. 15; Fig. 26.13b). There are approximately four deformation band orientations. Like substation 13a, deformation bands dip towards the northwest and to the southeast. Deformation

band dip magnitudes are steep. The maximum dip magnitude is 89º and the minimum dip magnitude is 48º. Slickenlines in substation 13b trend in every direction. Slickenline plunge magnitudes range from shallow to steep. The maximum plunge recorded is 74º and the minimum plunge is 13º. Deformation bands display right and left-lateral normal-slip offset.

Stereonet substation 13c consists of 1 deformation band and 1 slickenline (Fig. 15; Fig. 26.13c). The singular deformation band dips toward the southwest and has a dip magnitude of 77º. The slickenline measurement associated with this deformation band trends to the south. The slickenline has a plunge of 77º. The slip observed along this deformation band indicates right-lateral reverse-slip offset.

4.2b.vi. Central Fault Zone

The Central Fault Zone section of the field area describes deformation band assemblage along the structural contact between the Proterozoic basement and the Ordovician, Pennsylvanian, and Jurassic units (Fig. 15). This structural contact is located in the central portion of the Mixing Bowl field area. The Central Fault Zone area is described by deformation bands hosted in the Harding, Fountain, and the Ralston Creek. Across the Central Fault Zone, 126 deformation bands and 5 slickenlines were measured.

Station 14 describes deformation bands from four substations along the Central Fault Zone (Fig 15). Substations 14a, 14b, and 14c are oriented from west to east. Substation 14d is located southwest of substation 14a. Station 14 describes 46 deformation band measurements and 5 slickenline measurements. Stereonet substation 14a consists of 8 deformation bands and 3 slickenlines (Fig. 15; Fig. 26.14a). Five sets of deformation bands are present. Deformation bands dip in all directions besides the southeast. Dip magnitudes range from moderate to steep with a maximum dip of 85º and a minimum dip of 35º. Slickenlines trend towards the northwest

with plunges of 32º, 37º, and 80º. Deformation bands show left-lateral reverse-slip as well as reverse dip-slip offset.

Stereonet substation 14b includes 13 deformations bands and 1 slickenline (Fig. 15; Fig. 26.14b). Five sets of deformation bands are observable. Deformation bands dip in all directions except the northeast. Dip magnitudes are steep. The maximum dip is 88º and the minimum dip is 59º. The slickenline in substation 14b trends toward the southwest and plunges at 88º. Deformation bands show left-lateral normal-slip offset.

Stereonet substation 14c characterizes 7 deformation bands and 1 slickenline (Fig. 15; Fig. 26.14c). Four sets of deformation band orientations are observable. Deformation bands dip in all directions. Deformation band dip magnitudes are steep. The maximum dip measurement is 86º and the minimum dip magnitude is 68º. The slickenline associated with this substation trends toward the northwest and has a plunge of 32º. Deformation bands exhibit left-lateral reverse-slip offset.

Stereonet substation 14d describes 18 deformation bands (Fig. 15; Fig. 26.14d). Seven sets of deformation band orientations are present. Deformation bands dip in each direction. Deformation band dip magnitudes are steep and range from 89º to 59º. There was no offset observed in substation 14d. Near vertical to vertical deformation bands describe faulting developing at high-angles.

Stations 15 and 16 both characterize the western portion of the Central Fault Zone (Fig. 15). Both stations are arranged west to east. Between the two stations, 80 deformation bands were recorded. No offset was recorded. Station 15 characterizes 47 deformation bands (Fig. 15; Fig. 26.15a-d). There are approximately seven deformation band orientations present. Station 15 largely describes deformation bands dipping to the northwest and southeast. The maximum dip

magnitude is 89º and the minimum is 39º. Station 16 characterizes 33 deformation bands (Fig. 15; 26.16a-d). There are approximately seven deformation band orientations observable. Deformation bands dip in every direction. Dip magnitudes range from a maximum of 89º to a minimum of 58º. In both stations, deformation band orientations mainly describe faulting occurring at high-angles.

4.2c. Microstructural Expressions of Fault Rocks in the Mixing Bowl Field Area

Fault rocks contained in the Mixing Bowl field area display different grain-scale microstructural deformation mechanisms. The fault rocks observed in the Mixing Bowl field area consist of numerous low-temperature deformation processes ranging from grain reorganization and mechanical grain size reduction to recrystallization. Certain internal and external factors control these deformation processes, such as mineralogy, grain size, porosity and permeability, presence and composition of intergranular fluid, lattice-preferred orientations, temperature, lithostatic pressure, differential stress, fluid pressure, and imposed strain rate (Passchier et al., 2005). Deformation mechanisms are observed in sampled fault rocks of the Proterozoic basement rock, Harding Formation, and Dakota Sandstone (Fig. 18).

4.2c.i. Recrystallization of the Middle Ordovician Harding Sandstone (S2)

Sample S2 was collected in the Harding Sandstone in the central portion of the Mixing Bowl field area (Fig. 15), where the unit sits directly above a nearly horizontal fault contact with the Proterozoic basement. Microscopically, generally undeformed Harding Sandstone contains an intense amount of poorly sorted quartz grains ranging from 200 to 1000 μm in diameter (Fig. 27.1). Grain shape is sub-rounded to rounded with medium to low sphericity (Wadell, 1932), which describes how well the grain shape matches a perfect sphere. Porosity is evident throughout the section with epoxy filling the void spaces (Fig. 27.1). Although this is considered

generally undeformed, quartz grains show intragranular fractures or microcracks where deformation affects only single grains throughout the section (Fig. 27.1). Sample S2 consists overwhelmingly of quartz crystals with almost no porosity (Fig. 27.2). A small portion of the thin section shows brown minerals that are identified as hematite. In cross-polarized light, the quartz grain shape is subhedral, or partially bounded by well-defined faces, with largely anhedral shapes, or not well-defined faces, throughout the section. Grains show undulose extinction with variable extinction angles. The aggregation of quartz grains displays a bimodal (inequigranular) distribution of grain sizes (Moore, 1970), where grain sizes vary between exclusively very fine-grained, with an average diameter of 50 μm, to coarse-grained material, with an average diameter of 600 μm (Fig. 27.2a). The darkening of grains toward the edges of the coarse grains as well as the occurrence of fine-grained quartz fragments around the edges of larger grains (Fig. 27.2a) are an indication that this sandstone underwent low-temperature recrystallization involving a grain boundary migration process referred to as bulging (BLG) (Baily and Hirsch 1962; Drury et al. 1985; Shigematsu 1999; Stripp et al. 2002). At low temperatures, the ability of the grain boundary to move may be limited, and the grain boundary may be forced into the grain with the greater dislocation density, or the grain that can accommodate movement, and form new, singular, smaller grains. Moreover, these large grains continue to bulge and create subgrain boundaries, which evolve into new grain boundaries or show a migration of older grain boundaries (Means 1981; Urai 1986; Tungatt and Humphries 1984; Stipp et al. 2002). Undulose extinction occurs in these smaller grains at different angles in relation to the larger quartz grains they surround (Fig. 27.2b).

The inequigranular distribution of quartz grains is observed throughout the entire thin section but there is a greater occurrence of fine quartz grains to one side of the thin section (Fig.

27b), showing a gradual transition from coarse grains to fine grains. BLG typically occurs in low temperature but high strain rate environments (Tullis, 1990) so the increasing abundance of fine-grained, recrystallized quartz indicates an increasing strain rate and thus increasing proximity to a fault surface. The characteristics and microscale deformation revealed in this sample indicate that faulting heavily modified the otherwise porous Harding Sandstone via recrystallization and grain boundary migration, changing grain shapes and grain sizes and reducing its porosity. These observations indicate low temperature environments at burial depths between approximately 3.5 km and 5 km in depth (Darton, 1920). Collectively, these processes have led to a pronounced structural diagenesis (Laubach et al., 2010) of the Harding Sandstone in this region producing a structural quartzite. Although the Harding Sandstone is present throughout the CCE and all three field areas, this structural quartzitic Harding Sandstone is only observed in the central segment of the Mixing Bowl field area.

4.2c.ii. Horizontal Fault Zone in the Central Mixing Bowl (S24)

Sample S24 was collected from the brecciated fault zone between the Proterozoic basement rock and the Harding Formation in the central portion of the Mixing Bowl field area (Fig. 17; Fig. 18). Within the fault zone, the sample was taken from the white to green brecciated rock layer (Fig. 20b). The thin section contains an amalgamation of quartz, muscovite and biotite mica (Fig. 28). The thin section largely consists of granular quartz, ribbon quartz, and ribbon biotite throughout. Quartz grains here vary in size from about 100 μm to more than 1000 μm. The quartz grains are sub-rounded and display undulose extinction. Ribbon quartz, biotite, and muscovite are apparent in spaces between the larger quartz grains (Fig. 28). The continuity of the ribbon quartz and biotite are interrupted by the larger quartz grains (Fig. 28). The muscovite mica displays a distinct type of deformation, known as bookshelf sliding (Fig. 28a). Bookshelf

sliding indicates a sense of shear applied to the minerals with subsequent rotation of the minerals (Lovering, 1928). Bookshelf sliding of muscovite micas (Fig. 28a) indicates a top-to-right sense of shear, where mica crystals have detached along crystal boundaries and rotated clockwise in response to an applied stress. The presence of the bookshelf sliding micro mechanism as well as the interruption of ribbon quartz and biotite around the larger quartz crystals indicate that the deformation observed in this section is indicative of a pronounced horizontal fault zone between the Harding Formation and the Proterozoic basement rock.

4.2b.iii. Cataclastic Deformation Bands in Dakota Sandstone (S32)

Sample S32 was collected along the Cretaceous Dakota Group ridge from a deformation band damage zone within the Dakota Sandstone (Fig. 29). The section shows quartz grains and pore space (black space), which is filled with epoxy (Fig. 29). The void space seen throughout the section is characteristic of the porous Dakota Sandstone. The grain size distribution is inequigranular with the larger grains ranging in size from 150 μm to approximately 500 μm in diameter (Fig. 29). Smaller grains that make up the banded regions, highlighted by white dashed lines, show a very fine-grained texture with grains less than 50 μm. The larger grains seen in this section are sub-rounded to rounded and display medium to low sphericity. A portion of the larger quartz grains display undulose extinction as well as intragranular fractures and microcracks.

Grain size within this section abruptly changes between larger quartz grains and the smaller quartz grains (Fig. 29). The boundary between the larger quartz grains and the smaller quartz grains marks the change between less deformed porous sandstone and intense cataclasis (Fig. 29a). The boundary between the two shows evidence for the microstructural mechanism known as cataclastic flow, which occurs when grains begin to break into smaller particles as they slide and rotate past each other (Sibson 1977b; Evans 1988; Blenkinsop 1991b; Rutter and

Hazidah 1991; Lin 2001). As void space begins to open during cataclastic flow, the mechanically reduced quartz particulates begin to fill the open space (Passchier et al., 2005). This infill of smaller quartz particulates marks the bands seen in the sample from the Dakota Sandstone (Fig. 29). Furthermore, cataclastic flow decreases porosity as well as permeability through the porous sandstone (Pittman, 1981; Crawford, 1998; Ballas et al. 2012). From the top and bottom of Figure 29a, porosity and permeability decreases towards the cataclastic deformation band. Overall, deformation micro mechanisms observed in fault rocks show numerous low-temperature deformation processes. These micro-scale deformation processes vary from grain reorganization and mechanical grain size reduction to the recrystallization of grains. The accretion of these processes over time allow for a larger-scale observance of fault rocks in the field area.

4.2d. Fault Kinematics and Cross Sections through the Mixing Bowl Field Area

Integrating expressions of fault rocks in mapped lithologic units (*Section 4.1*), station observations of deformation bands (*Section 4.2b*), microstructural expressions of fault rocks (*Section 4.2c)* and field photos of deformation band orientations and kinematic offset indicators (*Section 4.1*) illustrate the larger fault kinematics in the Mixing Bowl field area. Deformation bands dip in all directions and contain horizontal to vertical dips, but vertical and sub-vertical oriented deformation band sets are predominant throughout zones of major and minor faulting (Fig. 15). In these zones where deformation bands were well-exposed, such as the Cretaceous Dakota Group Ridge (Fig. 15), up to eight sets of deformation band orientations were observed, where four individually striking sets were composed of conjugate deformation band pairs (Fig. 21-24). These sets strike north-northeast to south-southwest (blue and purple), east-northeast to west-southwest (green and pink), north-northwest to south-southeast (orange), and west-northwest to east-southeast (brown) (Fig. 21-24). At a given station along the ridge, the

conjugate deformation band pairs may display the master fault (solid line), antithetic fault (dashed line), or both. Stereonets that display more than two sets of these color-coded deformation bands express polymodal faulting (Fig. 4). Deformation bands that strike north-northeast to south-southwest and north-northwest to south-southeast consistently show right-lateral reverse-slip or right-lateral, pure strike-slip offset (Fig. 30). Deformation bands that strike east-northeast to west-southwest as well as west-northwest to east-southeast constantly exhibit left-lateral reverse-slip or left-lateral pure strike-slip offset (Fig. 30). Vertical to sub-vertical deformation bands along the North Fault Zone and Central Fault Zone show various amounts of offset present, but do not show consistent patterns of deformation band orientations, rather, their orientations display the undulating trend of the mapped fault (Fig. 30). These two fault zones share the same trend of the east-northeast to west-southwest fault zone seen along the western segment of the Cretaceous Dakota Group Ridge (Fig. 30).

Horizontally to sub-horizontally dipping deformation bands are mainly concentrated in the topographically low gap between the north and south portions of the Cretaceous Dakota Group Ridge (station 2) as well as in the Central Mixing Bowl (station 10) (Fig. 30). These bands offset sub-vertical to vertical bands. For example, horizontal and sub-horizontal deformation bands offset the vertical to sub-vertical deformation bands in station 2 (Fig. 31**).**

Moderate to sub-vertical deformation bands that display pure dip-slip offset and oblique-slip offset are largely observable along the northern segment of the Cretaceous Dakota Group Ridge (station 1) as well as the Ordovician Plateau (station 13) (Fig. 30). Deformation bands that show pure dip-slip along the northern segment of the Cretaceous Dakota Group are offset by vertical and sub-vertical deformation bands that have a component of strike-slip movement (Fig. 30). Pure normal dip-slip, and right and left-lateral normal-slip fault zones that trend northeast-

southwest offset deformation bands related to the Central Fault Zone, where the two intersect at substations 14a and 14b (Fig. 30).

Cross sections A-A' and B-B' (Fig. 32), C-C' and D-D' (Fig. 33), E-E' and F-F' (Fig. 34) interpret the subsurface architecture and inferred kinematics of the fault structure in the Mixing Bowl. Inferred kinematics of the fault structure were derived from observed deformation band kinematics at the surface. Bedding orientations were projected above the surface to display what the layers may have resembled before erosion. The constructed cross sections describe vertical and sub-vertical fault zones as they project into the subsurface of the Mixing Bowl, and display the relatively low magnitude of vertical slip along these faults when compared to the overall strike-slip movement accommodated along these slipped planes.

Cross section A-A' (Fig. 15; Fig. 32) includes the inferred, reverse fault in the northeast quadrant of the map where the Proterozoic basement rock is observed to come into contact with the Cretaceous Dakota Group. The Proterozoic basement is in the hanging wall and Ordovician to Cretaceous sedimentary units are in the footwall dipping towards the east-northeast.

Cross section B-B' (Fig. 15; Fig. 32) includes left-lateral reverse-slip faults associated with the North Fault Zone and the Central Fault Zone, and the thrust fault in the northern segment of the Cretaceous Dakota Group. Also visible are the two normal faults that offset the Harding and Fremont Formation through the Ordovician Plateau. Bedding orientations at the surface change and display minor folding as they become proximal to the reverse and thrust faults (Fig. 15). Bedding is sub-horizontal along the Ordovician Plateau then takes a monoclinal dip to the southeast where bedding becomes moderately tilted.

Cross section C-C' (Fig. 15; Fig. 33) includes the two left-lateral reverse-slip faults from the North Fault Zone and the Central Fault Zone as well as the right-lateral reverse-slip fault

along the Cretaceous Dakota Group Ridge. The two normal faults appear but are restricted to just faulting the Proterozoic basement rock. Bedding orientations increase in dip magnitude to the southeast across the right-lateral reverse-slip fault, indicating gentle drag folding along the fault plane.

Cross Section D-D' (Fig. 15; Fig. 33) consists of the two left-lateral reverse-slip faults from the North Fault Zone and the Central Fault Zone, as well as the two reverse-slip faults intersecting at the bend in the Cretaceous Dakota Group Ridge. These two faults display left-lateral reverse-slip and right-lateral reverse slip and form a complex zone of deformation where they intersect (Fig. 12). Dip magnitudes of bedding orientations increase across the intersection zone of the two faults, indicating gentle drag folding similar to cross section C-C'.

Cross section E-E' (Fig. 15; Fig. 34) includes the two left-lateral reverse-slip faults from the North Fault Zone and the Central Fault Zone, as well as a continuous fault plane where the fault orientation translates from vertical to horizontal to sub-vertical. Along this fault plane inferred faults are dashed in black where the fault plane is unknown. The inferred fault is exhumed at the surface as the left-lateral reverse-slip fault expressed along the Cretaceous Dakota Group Ridge. Bedding measurements (Fig. 18) are constant across this fault. The uniformity of dips indicates little to no drag folding, and a minimal amount of dip-slip accommodated along the fault. The horizontal fault zone expressed in this cross section is evident through multiple observations. First, the contact between the Proterozoic basement rock and the Harding Formation is observed as a fault breccia at both the outcrop scale and the micro-scale (Fig. 17; Fig. 28). Second, there is microstructural evidence for heavily cemented sandstones forming abruptly in the Harding Formation directly above the contact with the Proterozoic basement (Fig. 16; Fig. 27.2). Lastly, horizontal deformation bands in the central

portion of the Mixing Bowl, and in the field area as a whole, describe the existence of a horizontal fault zone. Despite all of this evidence, it is hard to explain how the presence of a horizontal fault zone fits into the tectonic setting of the Mixing Bowl field area.

Cross Section F-F' (Fig. 15; Fig. 34) consists of the left-lateral reverse slip fault of the Central Fault Zone and the inferred segment of the left-lateral reverse slip fault of the North Fault Zone. Though questionable along the surface due to erosion and cover (Fig. 15), the left-lateral reverse-slip fault is inferred to be present in the subsurface.

4.3 South Twin Mountain Field Area

4.3a General Geologic Observations of the Field Area

The South Twin Mountain field area is located west of Cañon City along U.S. Route 50 (Fig. 1). This field site is approximately 1 square kilometer in area (Fig. 35). Throughout the area, 27 bedding measurements were collected (Fig. 35). Proterozoic basement rock is present in the higher elevations of South Twin Mountain, bounding the map towards the north (Fig. 35). Towards the south, the mapped area is bounded by U.S. Route 50 (Fig. 35). The Proterozoic basement comes into structural contact with the Manitou Formation, Harding Formation, and Fremont Formation near the middle of the map along a fault plane oriented northwest-southeast (Fig. 35). The Proterozoic basement also outcrops near the dirt roads (4WD) at the southern portion of the map as a nonconformable contact with the Manitou Formation (Fig. 35). The Manitou Formation is present throughout the western segment of the map (Fig. 35). Bedding orientations of the Manitou Formation contain dip directions toward the southeast and southwest (Fig. 35). Dip magnitudes of the unit are shallow unless in structural contact with the Proterozoic basement where they increase to a moderate degree (Fig. 35). The Manitou Formation lies unconformably below the Harding Formation. Both units have a similar bedding orientation

along the unconformable contact (Fig. 35). The Harding Formation outcrops along U.S. Route 50 and its expanse include the west, south, and east sections of the map (Fig. 35). Bedding orientations display dip magnitudes from shallow to moderate throughout the area (Fig. 35). The Harding Formation shows dip directions ranging from the north-northeast, south-southeast, and south-southwest (Fig. 35). The change in dip directions indicate the occurrence of en echelon anticlinal and synclinal folding (Fig. 35). When the unit is in proximity to the structural contact with the Proterozoic basement, it displays a moderate degree of dip (Fig. 35).

The Fremont Formation is unconformably above the Harding Formation. Dip attitudes above and below the unconformable contact are comparable to one another (Fig. 35). The Fremont Formation crops out throughout the central area of the map (Fig. 35). The bedding orientation of the unit is shallow but is inferred to become steeper near the structural contact with the Proterozoic basement (Fig. 35). The dip direction of the Fremont Formation varies between south-southeast and south-southwest (Fig. 35).

All observed unconformities in the South Twin Mountain field area display little to no difference in strata orientation above and below the contacts (Fig. 35). The en-echelon anticlinal and synclinal folding of the Ordovician units parallel the orientation of the structural contact with the Proterozoic basement (Fig. 35). Refer to Table 2 for a summary of the results presented below. Refer to Appendix A for field photos of the South Twin Mountain field area.

4.3b Station Observations of Deformation Bands

4.3b.i. Southern Portion of South Twin Mountain Field Area

The southern portion of the South Twin Mountain Field area includes measurements topographically below and south of the Fremont Formation (Fig. 35). This portion of the map bounds the field area to the south. Across this segment of the map, deformation bands may

describe the en-echelon sets of anticlinal and synclinal folding. Bands may be representing deformation occurring within the fold limbs of the anticlines and synclines. In the field area, deformation bands that occur in the southwest limb of either synclines or anticlines are colored blue in the substation stereonets (Fig. 36). Deformation bands that occur in the northeast limb of the synclines and anticlines are colored pink (Fig. 36). Deformation bands that are generally oriented orthogonally to northeast- and southwest-dipping bands have vertical to sub-vertical dips, and are colored orange (Fig. 9a; Fig. 36). These bands are observed to be bounding bands between the northeast and southwest dipping deformation bands, which are acting as linking bands in a ladder structure. The lack of slickenlines in the areas of folding do not permit the identification of a slip direction along these bands but, in station 20b (Fig. 35; Fig. 36.20b) there is one deformation band that describes right-lateral, reverse-slip from a slickenline measurement. Though north of the en-echelon folding, the deformation band orientation matches that of the bounding bands and does not match the orientation of the thrust fault. Applying this slip direction to the bounding bands would indicate a right-lateral component to the reverse faulting associated with the folding.

Three stations describe the southern portion of the South Twin Mountain field area with 100 deformation band orientations and one slickenline measurement collected. Station 17 exhibits deformation band orientations in the far southern extent of the map (Fig. 35). Substations 17a, 17b, and 17c are oriented south to north. These substation locations describe 34 deformation band orientations. Stereonet substation 17a includes 12 deformation band orientations (Fig. 35; Fig. 36.17a). Deformation bands dip in all directions except towards the southwest. These bands have moderate to steep dips. The maximum dip is 80º and the minimum dip is 21º. There were no slickenlines observed in the area. Deformation bands that describe slip

in the southwest limb of the anticline are present. Bounding bands, dipping sub-vertically towards the northwest are apparent, as well. There is an anomalous deformation band that dips towards the southwest shallowly at 21º.

Stereonet substation 17b describes 14 deformation band orientations (Fig. 35; Fig. 36.17b). Deformation bands dip towards the southeast and northeast. Deformation bands in substation 17b have steep dips. The maximum dip is 89º and the minimum dip is 66º. No slickenlines were seen in substation 17b. Vertical and sub-vertical bounding bands largely describe the deformation seen in substation 17b.

Stereonet substation 17c exhibits 8 deformation band orientations (Fig. 35; Fig. 36.17c). Deformation bands dip towards the northeast, southeast, and northwest. The dips of these deformation bands are steep. The maximum dip is 89º and the minimum dip is 69º. There were no slickenlines observed in this substation. Consistent with substations 17a and 17b, this substation contains deformation bands in the southwest limb of the anticline as well as vertical to sub-vertical bounding bands between deformation bands. Deformation bands dipping approximately towards the south are inferred to be indicative of deformation bands contained in the northeast limb of the anticlinal fold. Station 17 characterizes the accommodation of anticlinal folding through slip along deformation bands, which act as a linking band to a sub-vertical to vertical set of bounding deformation bands within an expansive system of ladder structures.

Station 18 describes deformation band orientations in the central part of the map (Fig. 35). Substations 18a and 18b are arranged on the map southeast to northwest. The two substations describe 7 deformation bands (Fig. 35; Fig. 36.18a; Fig. 36.18b). Deformation bands dip towards the northwest, northeast, and southeast. Deformation band dips are steep. The maximum dip magnitude is 87º and the minimum dip magnitude is 68º. There were no

slickenlines observed in this substation. Deformation bands have sub-vertical to vertical dip magnitudes with one deformation band describing movement along slipped bands in the southwest limb of the syncline (Fig. 35) The sub-vertical to vertical deformation bands in 18a and 18b are indicative of the bounding bands present in station 17. The interconnection of linking bands–the deformation bands common in fold limbs, and bounding bands (Fig. 9a)– sub-vertical to vertical deformation bands connecting the linking bands, show the connectivity of deformation bands across both synclinal and anticlinal structures.

Station 19 encompasses deformation band orientations observed further northwest of station 18 (Fig. 35). Three substations describe station 19 and are arranged east to west. There are 59 deformation band orientations and 1 slickenline measurement in station 19. Stereonet substation 19a contains 17 deformation band measurements (Fig. 35; Fig. 36.19a). Deformation bands dip in all directions. The dips of these deformation bands are steep. The maximum and minimum dips in substation 19a are 89º and 66º. There were no slickenlines observed in substation 19a. Bands in this substation describe deformation in both the northeast and southwest limbs of the syncline (Fig. 35). Consistent with the sub-vertical to vertical bounding bands seen in stations 17 and 18, substation 19a predominantly displays the same orientation of deformation bands.

Stereonet substation 19b includes 22 deformation band and 1 slickenline measurement (Fig. 35; Fig. 36.19b). Dip directions of deformation bands are toward the southwest, northwest, and northeast. Dips of deformation bands are steep besides one anomalous measurement dipping shallowly at 20º. This measurement is analogous to the shallow dipping deformation band in substation 17a. Of the steep dip magnitudes, the maximum dip is 87º and the minimum dip is 60º. One slickenline was recorded trending 006º and plunging 3º. Direction of slip along this

slickenline is ambiguous but describes pure, strike-slip movement along a shallow fault plane. Substation 19b includes bands characterizing deformation in the northeast limb of the syncline. Sub-vertical to vertical bounding bands are apparent in this substation.

Stereonet substation 19c encompasses 20 deformation band measurements (Fig. 35; Fig. 36.19c). Deformation bands dip towards the northeast, southeast, and northwest. Dip magnitudes of these deformation bands are steep. The maximum dip is 89º and the minimum dip is 59º. There were no apparent slickenlines observed in this area. Deformation bands in this area represent deformation localized in the northeast limb of the syncline. Sub-vertical to vertical bounding bands are widely observable in this area. Station 19 contains deformation bands in both the southwest and northeast limbs of the fold. Bounding bands connect these deformation bands and include sub-vertical to vertical dip magnitudes.

4.3b.ii. Northern Portion of Twin Mountain Field Area

The northern portion of the Twin Mountain field area includes the topographically high deformation band measurements collected in the Harding Formation north of the well-defined, cliff-forming Fremont Formation. This segment of the map includes the interaction, as described by the deformation bands, between Ordovician sedimentary units and the overthrusted Proterozoic basement rock.

Station 20 describes the northern portion of the South Twin Mountain field area (Fig. 35). There were 9 deformation band orientations and 6 slickenline measurements recorded. Substations 20a, 20b, and 20c are arranged northwest to southeast. Stereonet substation 20a contains 4 deformation band and 2 slickenline measurements (Fig. 35; Fig. 36.20a). Dip direction of deformation bands are towards the southwest. Dip magnitudes range from moderate to steep. The dips of these deformation bands are 14º, 36º, and 88º. There were two observed

slickenline measurements. These slickenlines trend towards the southwest. Deformation band orientations mimic the orientation of the structural contact between Ordovician sedimentary units and the Proterozoic basement rock. Deformation bands display master and antithetic orientations in proximity to the structural contact between the Harding Formation and the Proterozoic basement rock. Observed slickenlines along these deformation bands show a pure, thrust dip-slip and right-lateral reverse-slip motion.

Stereonet substation 20b includes 3 deformation band and 3 slickenline measurements (Fig. 35; Fig. 36.20b). Dip direction of deformation bands are toward the northeast and northwest. Dips of these deformation bands are 44º, 46º, and 63º. The slickenlines observed in this station trend towards the northeast and northwest. Plunges of these slickenlines are 41º, 42º, and 58º. Deformation bands and their corresponding slickenlines in substation 20b show right-lateral reverse-slip motion.

Stereonet substation 20c comprises of two deformations band measurements (Fig. 35; Fig. 36.20c). Deformation bands dip to the southwest and northeast. Dips of these deformation bands are 74º and 84º. There were no slickenlines observed in this substation. Deformation bands in this substation do not describe the fault contact but may describe fold-related deformation seen in stations 17 to 19 as they share the same deformation band orientations.

4.3c. Fault Kinematics and Cross Section through South Twin Mountain Field Area

In summary, the South Twin Mountain field area describes en-echelon synclinal and anticlinal folding in the footwall of a fold-and-thrust zone (Fig. 37). Deformation bands in the southern portion of the map indicate the damage zone associated with the folding. Deformation bands in the northern portion of the map may describe a right-lateral, thrust fault zone.

4.4 Sheep Mountain Field Area

4.4a General Geologic Observations of the Field Area

The Sheep Mountain field area is located northeast of Cañon City (Figure 1). The field area marks a portion of the southwest extent of the Front Range. It is approximately 1.6 square kilometers in size (Fig. 19). Throughout the field site, 86 bedding measurements were collected (Fig. 19). Proterozoic basement is present in the topographically higher elevations of Sheep Mountain, bounding the map towards the east (Fig. 19). The University of Kansas Field Camp, located at Garden Park Road, marks the confines of the map to the west (Fig. 19). The Proterozoic basement comes into structural contact with the Manitou Formation, Harding Formation, and Fremont Formation along two en-echelon planes oriented north-south (Fig. 19). The Manitou Formation lies nonconformably above the Proterozoic basement in the eastern portion of the map. The Manitou Formation is present in two segments that mirror orientations of the two parallel structural contacts (Fig. 19). The dip of the bedding unit ranges from shallow to steep to overturned in the western portion, whereas, in the eastern portion of the mapping area, the dips of the bedding are exclusively shallow (Fig. 19). Steep to overturned beds are seen in proximity to the western structural contact (Fig. 19). Along the unconformable Manitou/Harding Formations contact, the bedding measurements are comparable between both formations (Fig. 19). The Harding Formation crops out in both the eastern and western portions of the Sheep Mountain field area (Fig. 19). Similar to the Manitou Formation, the Harding Formation also comes into structural contact with the Proterozoic basement along the two parallel fault contacts (Fig. 19). The Harding Formation displays dip degrees that are moderate to high in the western portion of the field area (Fig. 19). The increase in steepness seen in the western segment of the field area represents the increasing proximity to the structural contact with the Proterozoic

basement (Fig. 19). In the eastern portion of the field area, the Harding Formation dips shallowly to moderately (Fig. 19). Again, when proximal to the structural contact with the Proterozoic basement in the eastern section of the map, the dips of the Harding Formation become more moderate (Fig. 19). The upper portion also includes minor anticlines and synclines that parallel en-echelon fault orientations (Fig. 19).

The Fremont Formation lies unconformably above the Harding Formation and the two units have comparable bedding measurements at the point of contact (Fig. 19). The extent of the Fremont Formation is sparse in both the western and eastern segments of the Sheep Mountain field area (Fig. 19). In the western portion, the unit outcrops as a cliff-former whereas in the eastern portion of the map the unit is not as topographically prevalent. The Fremont Formation comes into structural contact with the Proterozoic basement in the eastern segment of the map (Fig. 19).

Overall, observed unconformities in the field area show little to no difference in strata orientation above and below the contacts (Fig. 19). The dip magnitude of the Ordovician units increases when in proximity to structural contacts (Fig. 19). The inclusion of the two parallel fault planes between Proterozoic basement rock and Ordovician sedimentary units, the overturned beds near the western fault contact, and the presence of horizontal to sub-horizontal bedding units describe a monoclinal structure. Deformation bands form in zones near these fault contacts and display moderate to high-angle orientations. The small amount of slickenlines throughout the area creates ambiguity in slip direction. Refer to Table 3 for a summary of the results presented below. Refer to Appendix A for field photos of the Sheep Mountain field area.

4.4b Station Observations of Deformation Bands

4.4b.i. Western Portion of Sheep Mountain Field Area

The western portion of Sheep Mountain describes deformation bands hosted in the Harding Formation along the western fault contact with the Proterozoic basement rock (Fig. 19). Deformation seen in the western portion of Sheep Mountain is characterized through stations 21 and 22. Deformation bands in this area detail the orientation of the fault contact, colored in blue on the stereonets (Fig. 38), between the Harding Formation and Proterozoic basement rock. In this portion of the map, 50 deformation bands and two slickenlines were recorded.

Station 21 describes the northern segment of the western fault contact. Stereonet substations are oriented north to south. In this station, 35 deformation bands and one slickenline measurement were recorded. Substation 21a includes 32 deformation band measurements (Fig. 19; Fig. 38.21a). Deformation bands dip in all directions, but bands predominantly dip towards the northeast. Dips of these deformation bands are generally steep. The maximum dip is 86º and the minimum dip is 46º. There were no slickenlines observed in this substation. Deformation band orientations mimic the trend of the fault contact and indicate a reverse fault orientation. This substation also displays a second orientation of deformation bands that dip towards the north and south. This set of deformation bands may describe a separate deformation event. This is due to the fact that the bands are orthogonal to the structural contact (Fig. 19) and dip around 60º, possibly expressing normal dip-slip motion. The absence of slickenline data does not permit the ability to determine if any lateral or vertical slip is present. Substation 21b describes 3 deformation bands (Fig. 19; Fig. 38.21b). Dip directions of deformation bands are towards the northeast and southeast. The dip magnitudes of these bands are 82º and 49º. One slickenline measurement was recorded. The trend of the slickenline is towards the southwest and plunges

13º. Deformation band orientations follow the curvature along the fault plane and the slickenline observed may describe a strike-slip component of movement along the fault plane. The slickenline and deformation band measurement show left-lateral reverse-slip offset. Overall, deformation bands in this station display high-angle fault orientations with one slickenline describing left-lateral reverse-slip movement along the fault.

Towards the south, station 22 includes deformation bands that further detail the deformation associated with the fault contact between the Ordovician sedimentary units and the Proterozoic basement rock (Fig. 19). Along this part of the fault contact, 15 deformation bands were analyzed along with one slickenline measurement. Substation 22a characterizes 6 deformation bands and one slickenline (Fig. 19; Fig. 38.22a). Deformation bands dip towards the southeast. The dips are steep ranging between 52º and 70º. One slickenline was identified in this area and trends towards the northeast with a plunge of 7º. The deformation bands observed in this area mimic the undulating behavior of the fault.

In stations 21 and 22, the fault changes slip direction (Fig. 19). The deformation bands are indicative of this change in fault orientation. The slickenline seen in this area describes pure strike-slip movement along these bands. The direction of slip is right-lateral, described by the grooves along the slip surface. This right-lateral slip indicates that the southern segment of the fault has an opposite direction of shear movement in comparison to the northern segment. Between these two measurements, there is ambiguity in the direction of the lateral movement. The identification of horizontal and sub-horizontal slickenlines from slip surfaces indicate that there is at least the presence of lateral movement along the fault plane. Substation 22b exhibits 9 deformation band measurements (Fig. 19; Fig. 38.22b). Deformation bands in this substation dip towards the southeast and southwest. The dips of these deformation bands are steep. The

maximum dip measurement observed in the field is 89º and the minimum dip is 68º. There were no apparent slickenlines observed in this substation. Two of the observed deformation bands are interpreted to describe the fault contact. The other deformation bands may be displaying orientations of the fault contact as it undulates from north to south. Station 22 is consistent with station 21 through a general indication of the fault contact orientation. Station 22 includes slickenline data that indicates a component of shear movement along the fault plane, but the near lack of slickenline data limits the ability to determine slip direction along the plane.

4.4b.ii. Eastern Portion of Sheep Mountain Field Area

The eastern portion of Sheep Mountain characterizes deformation related to the eastern fault contact between Ordovician sedimentary units and the Proterozoic basement (Fig. 19). Deformation bands along this fault contact are hosted in the Harding Formation. The eastern fault contact includes station 23. In this area, 23 deformation band measurements were collected with two of those deformation band displaying slip surfaces with slickenlines (Fig. 19; Fig. 38.23a-23d). Station 23 indicates the kinematics along the eastern fault contact seen in the mapped area. Deformation bands dip in all direction and the dip magnitudes of these deformation bands range from moderate to steep. The slickenlines observed in this area indicate pure dip-slip movement along the upper fault contact. The dip magnitudes of these deformation bands indicate that this fault contact is a pure thrust fault. The vertical to sub-vertical deformation bands may indicate a secondary set of bands that accommodate lateral slip near the fault zone. These deformation bands may also be related to the minor anticlinal and synclinal folds that are also present in the Harding Formation.

4.4c Fault Kinematics and Cross Section through Sheep Mountain Field Area

In summary, deformation bands in the Sheep Mountain field area describe two parallel, en-echelon thrust faults (Figure 39). The lower fault indicates oblique-slip, but with limited slickenline data, it is unclear on whether the slip is right- or left-lateral. The eastern fault is indicative of a pure dip-slip thrust fault regime where Proterozoic basement rock is overthrusting on top of Ordovician sedimentary units. Deformation band orientations with corresponding slickenlines as well as bedding orientations indicate the formation of a southwest-northeast oriented monocline with an anticlinal bend (Fig. 39).

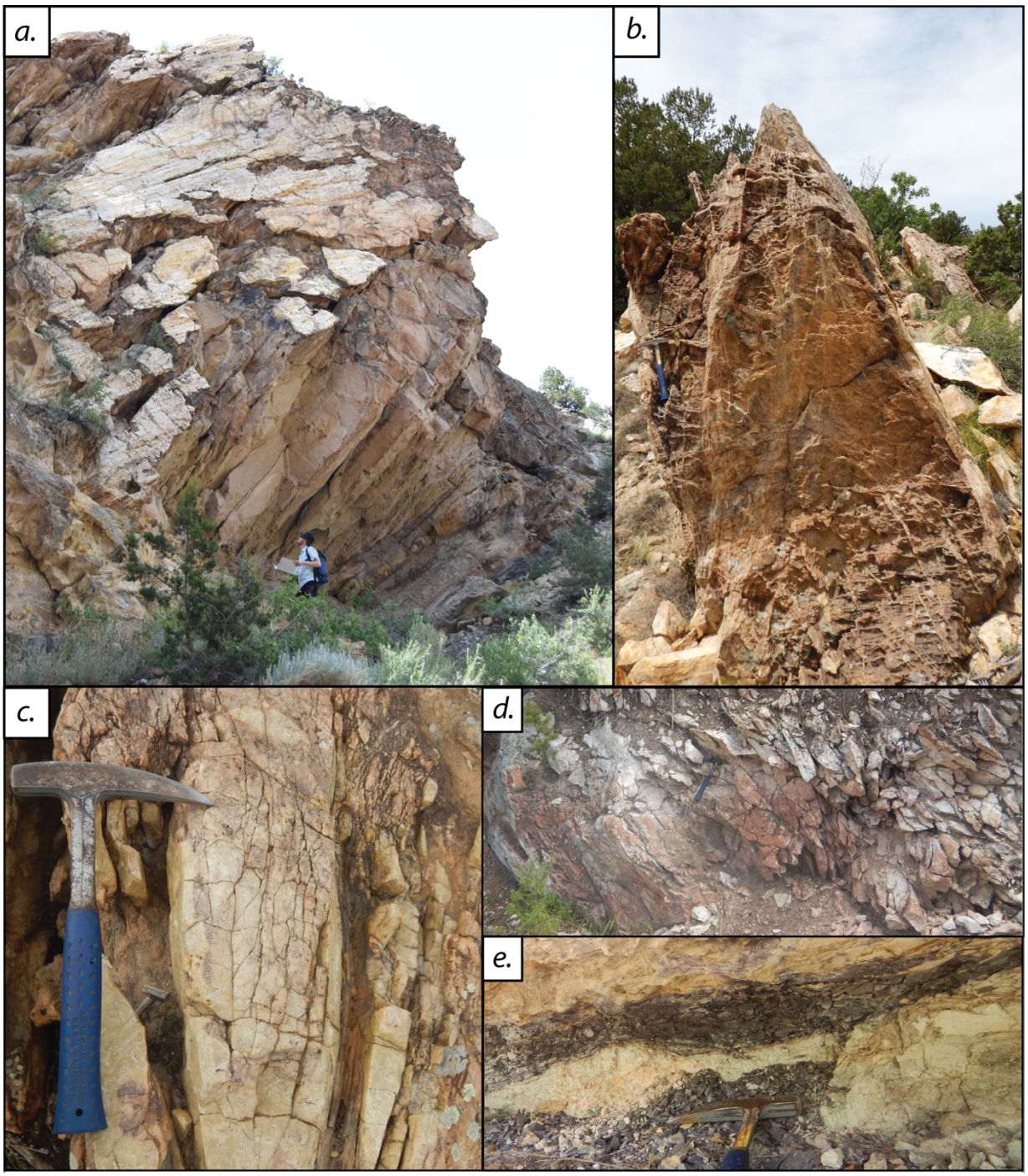

Figure 5. Fault rocks observed in the CCE.
(a) A slip surface observed through the Cretaceous Dakota Group Sandstones with a man for scale. **(b)** A non-erosional, vertically protruding fault core in a deformation band damage zone along the Cretaceous Dakota Group Ridge. **(c)** Heavily cemented sandstones found in the central portion of the Mixing Bowl field area. **(d)** An incohesive fault breccia located along the eastern fault within the Sheep Mountain field area. **(e)** Inchohesive brecciated fault rocks between the Proterozoic basement rock and Harding Formation in the central portion of the Mixing Bowl field area**.**

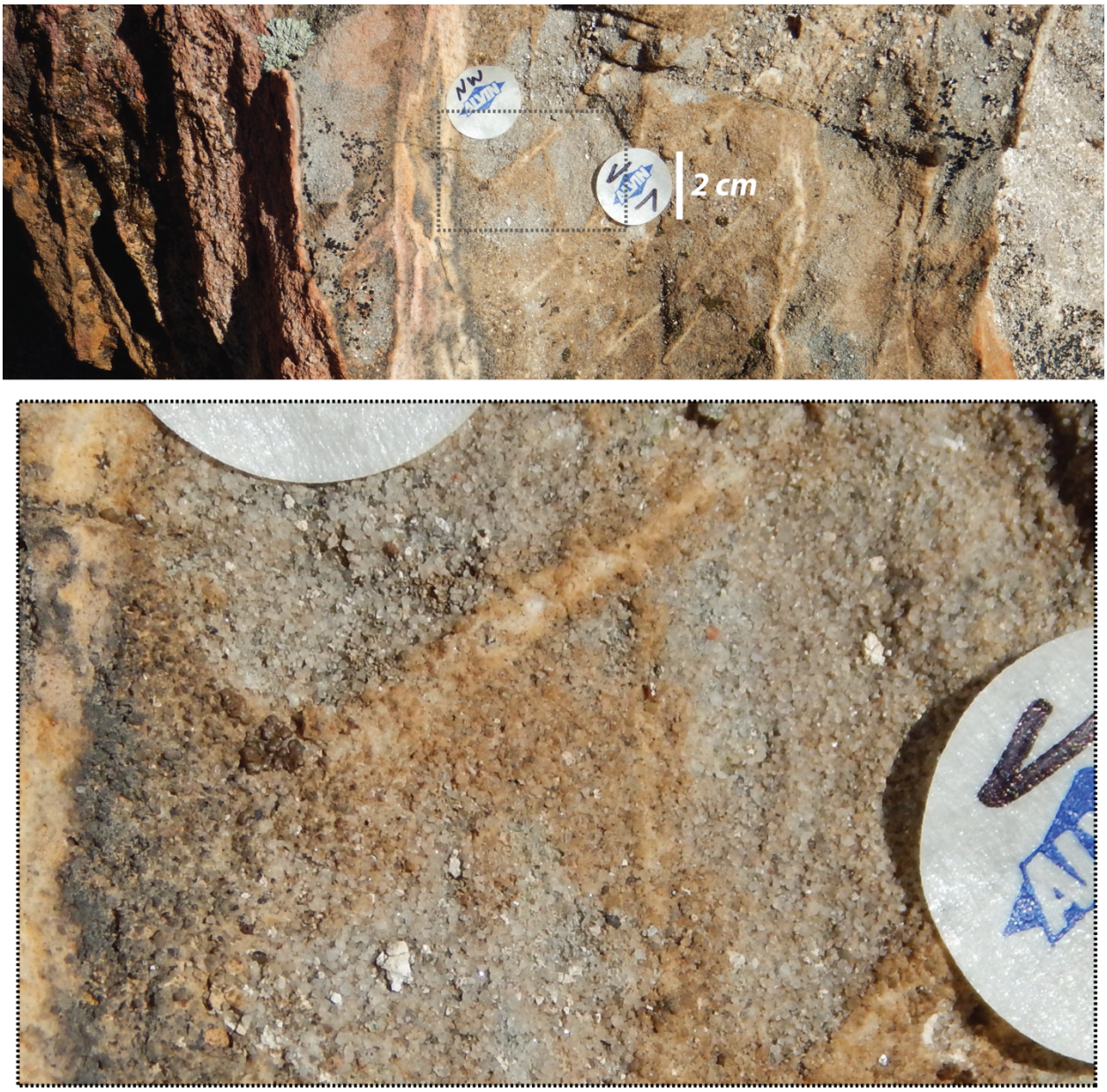

Figure 6. Deformation bands hosted in the Lytle Sandstone in the Mixing Bowl field area. Notice the change in grain size between the deformation bands and the porous Lytle Sandstone.

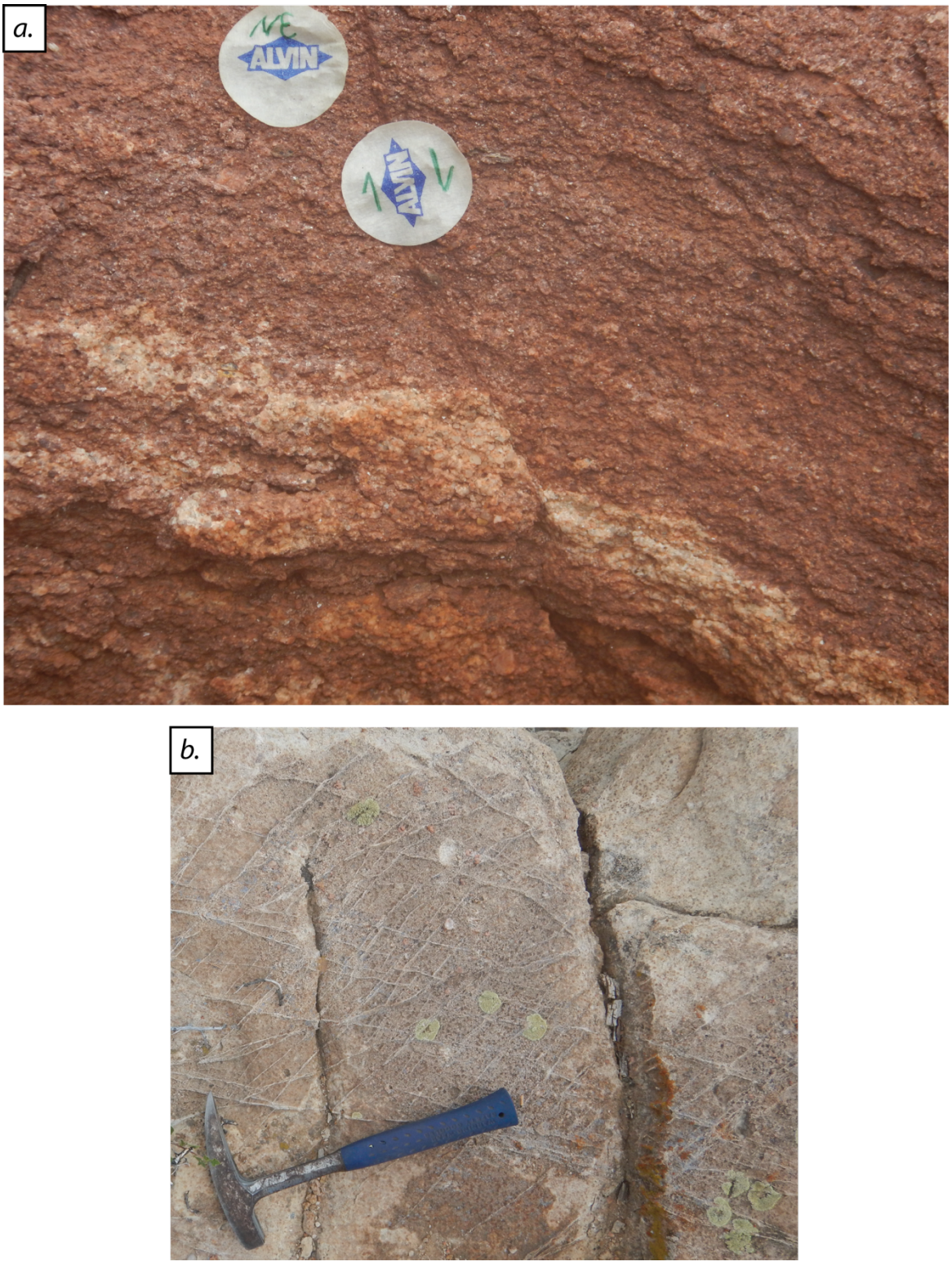

Figure 7. Deformation bands in Fountain **(a)** and Jurassic Ralston Creek **(b)** Formations.

Figure 8. Deformation bands observed as ladder structures in the Dakota Sandstone.
In zones of higher intensity of deformation, ladder structures form. Ladder structures are composed of linking and bounding bands. The bands oriented horizontally in this figure are bounding bands, and the bands oriented more vertically are linking bands. The intersection of these two orientations may express offset.

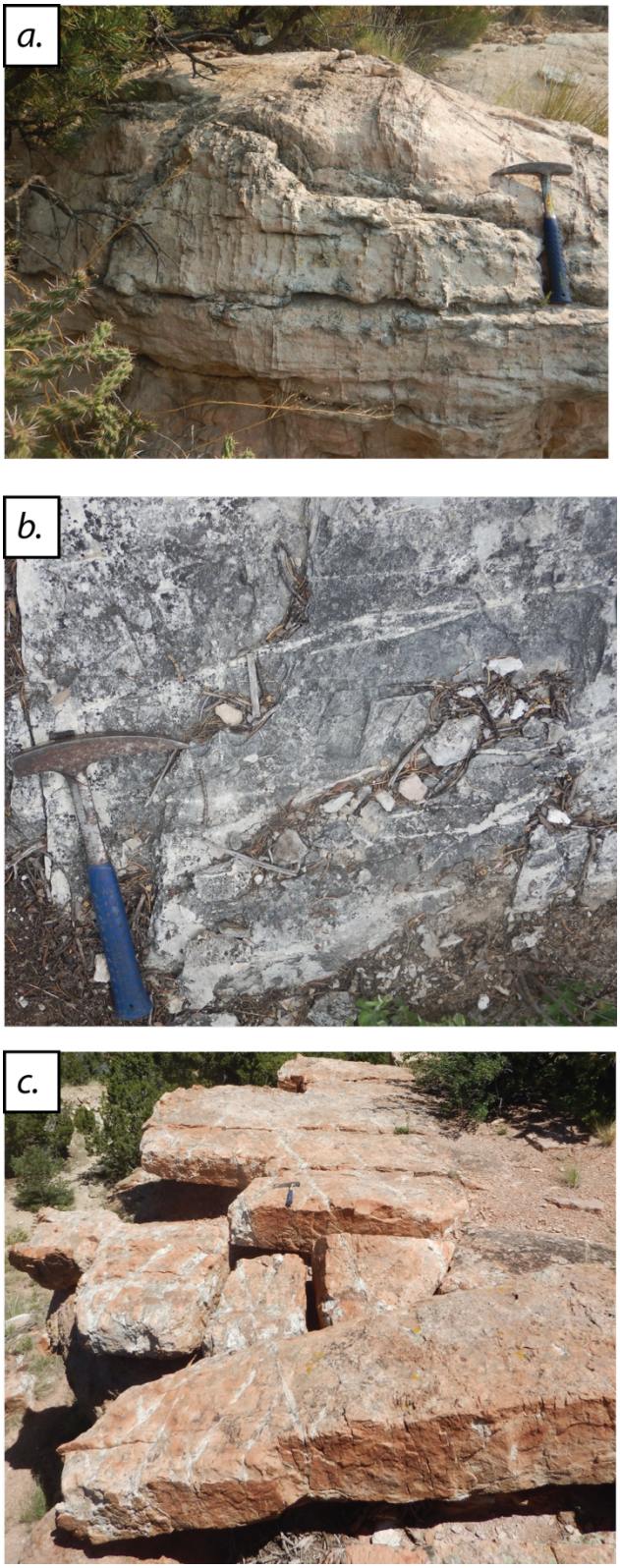

Figure 9. Deformation bands observed in the Harding Formation at **(a)** South Twin Mountain, **(b)** Sheep Mountain, and **(c)** the Mixing Bowl field areas.

Figure 10. Deformation bands observed in an assemblage of strands known as a band cluster in Cretaceous Dakota Group Sandstones.

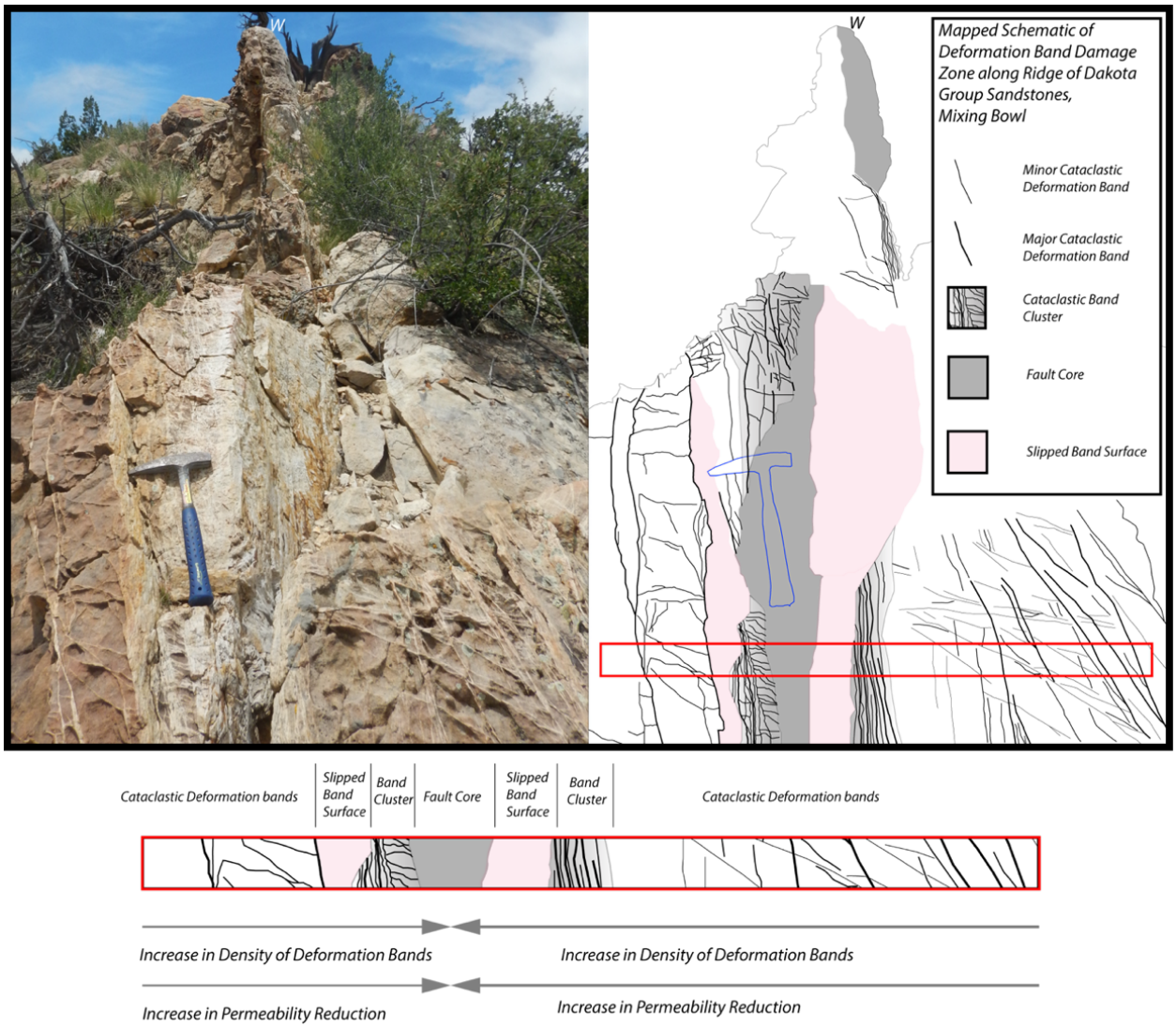

Figure 11. Mapped schematic of a fault zone in the Dakota Group Sandstones, Mixing Bowl. The damage zone comprises of single bands, band clusters, a fault core, as well as slipped bands along that fault core. Deformation bands increase in density as location in respect to the main fault core increases. Analogous with an increase in deformation band density towards the fault core, the porosity and permeability decreases (e.g., Fowles and Burley, 1994; Fisher and Knipe, 1998; Ogilvie and Glover, 2001; Fossen and Bale, 2007; Torabi et al., 2013).

Figure 12. Zone of high deformation band density in the Cretaceous Dakota Group Sandstones. Notice the multiple sets of different deformation bands orientations as well as the offset expressed throughout. Offset along bands represent the formation of ladder structures. Drafting dots in the middle of the image have a diameter of two centimeters.

Figure 13. Deformation bands show offset between bands in the Lytle Sandstone. Half-arrows indicate the sense-of-slip along the northeast-southwest oriented deformation band.

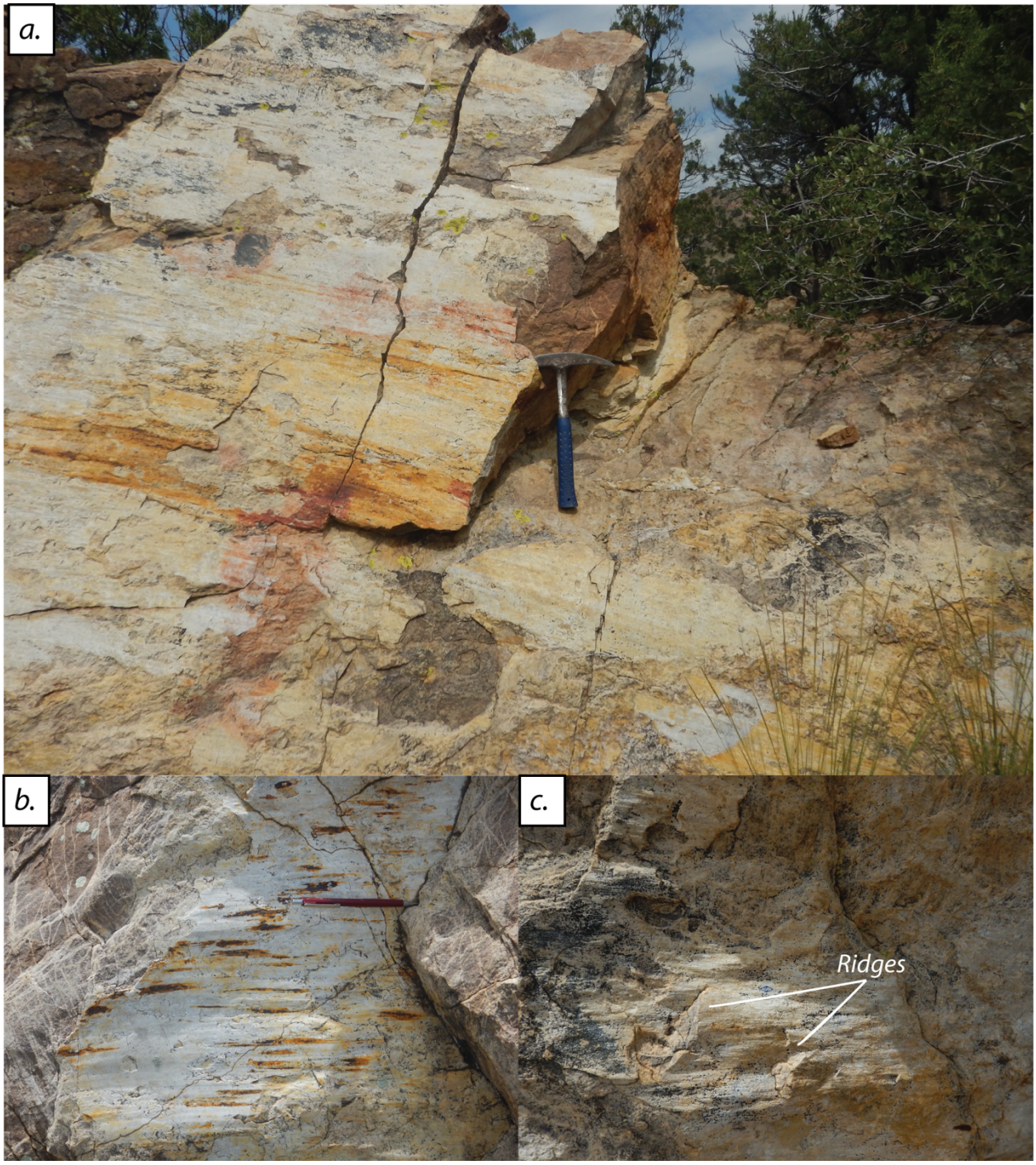

Figure 14. Slip surfaces and kinematic indicators of slip in the Dakota Group Sandstones. **(a)** A large slip surface displaying sub-horizontal slickenlines. (**b)** A deformation band slip surface displaying horizontally oriented slickenlines. **(c)** Horizontal slickenlines displaying millimeter-high ridges indicate slip direction to the left.

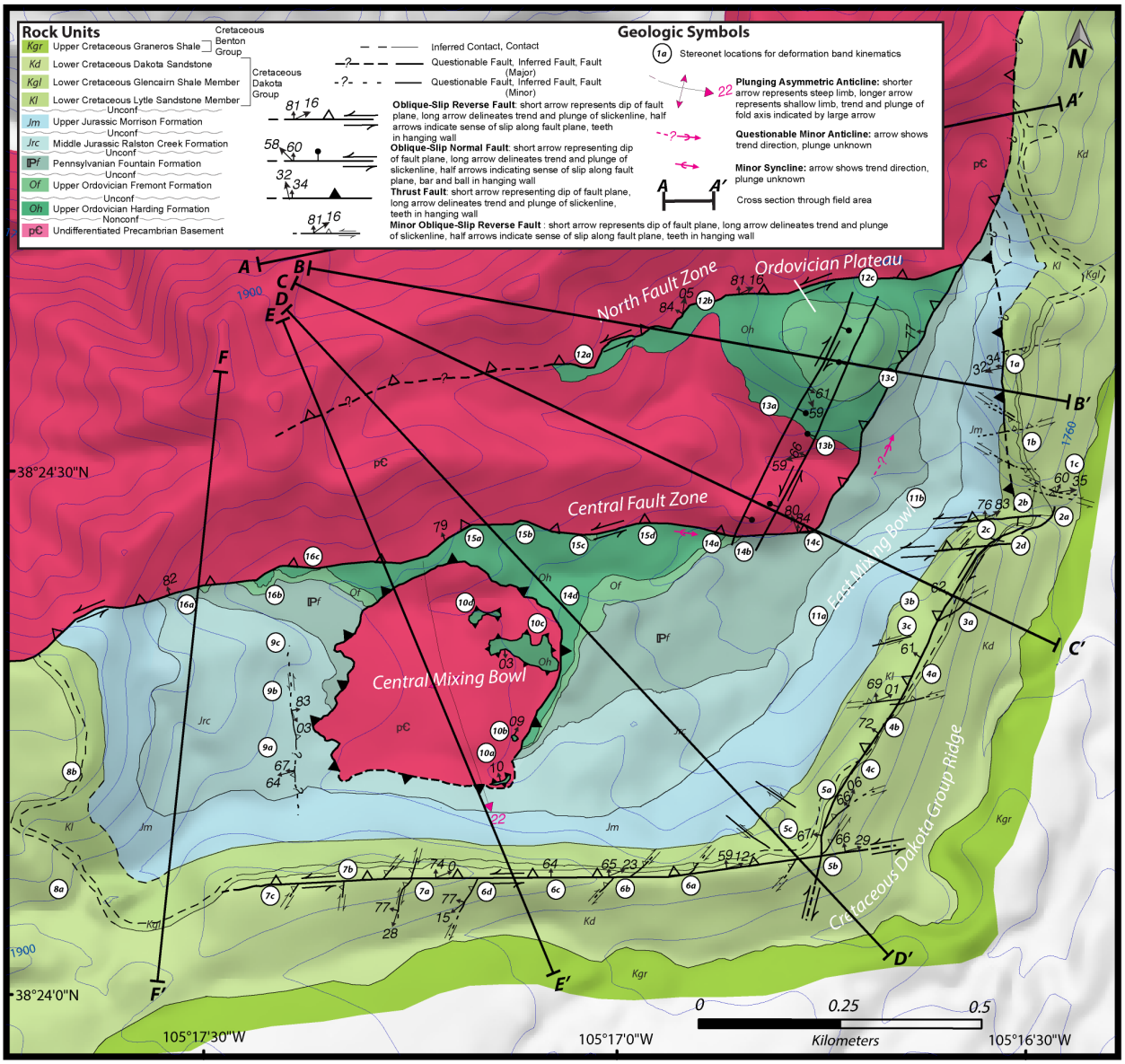

Figure. 15 Structure map of the Mixing Bowl field area. Units, faults, and stereonet substations are overlaid onto a 10 m resolution DEM. Each white circle indicates the location of each stereonet substation.

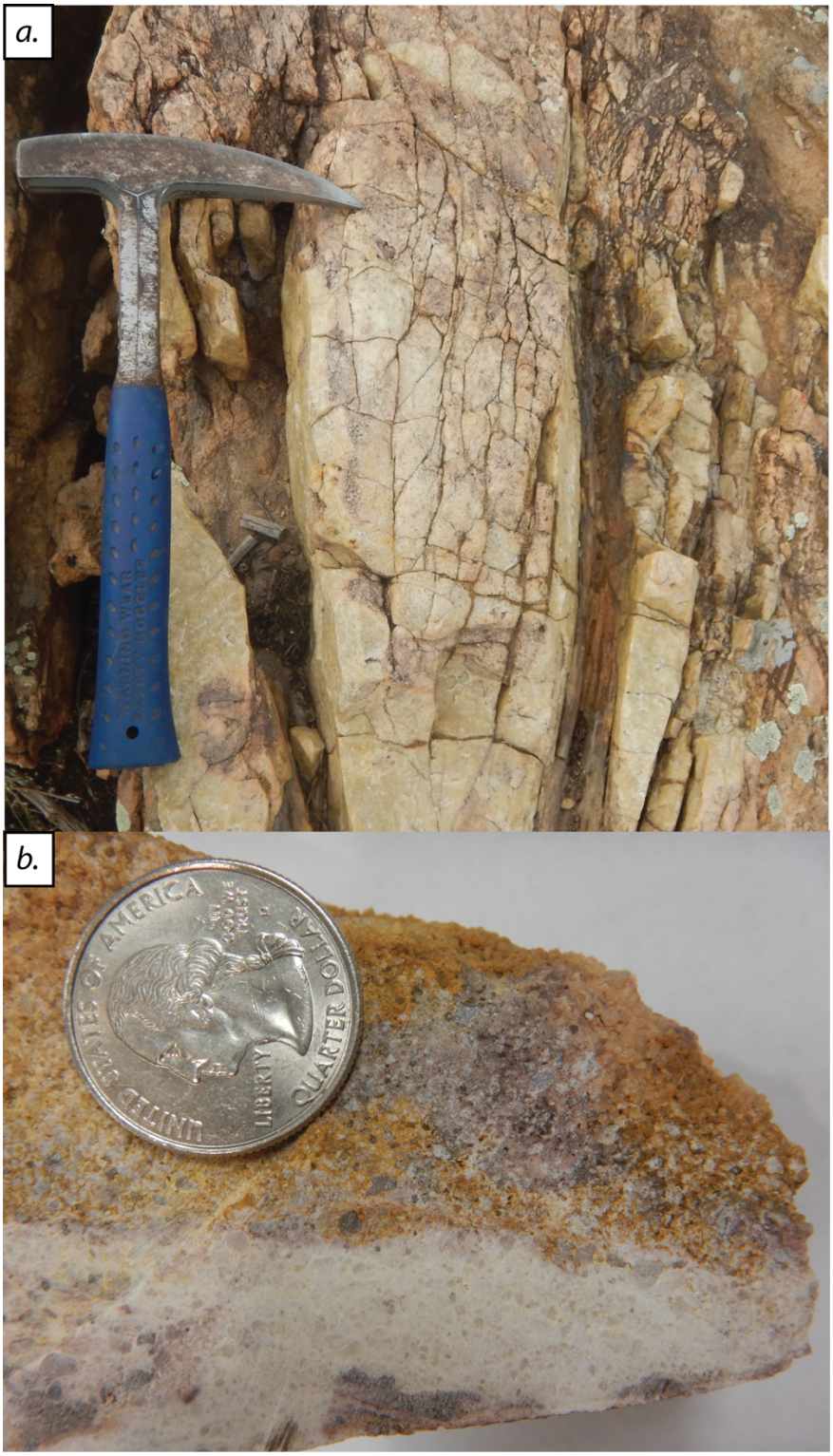

Figure 16. Heavily cemented Harding Sandstones from the central portion of the Mixing Bowl. **(a)** Outcrop photo of the heavily cemented sandstones. **(b)** Collected rock sample (S2). Note the rapid transition from porous Harding Sandstone to well-cemented, fine-grained Harding Sandstone.

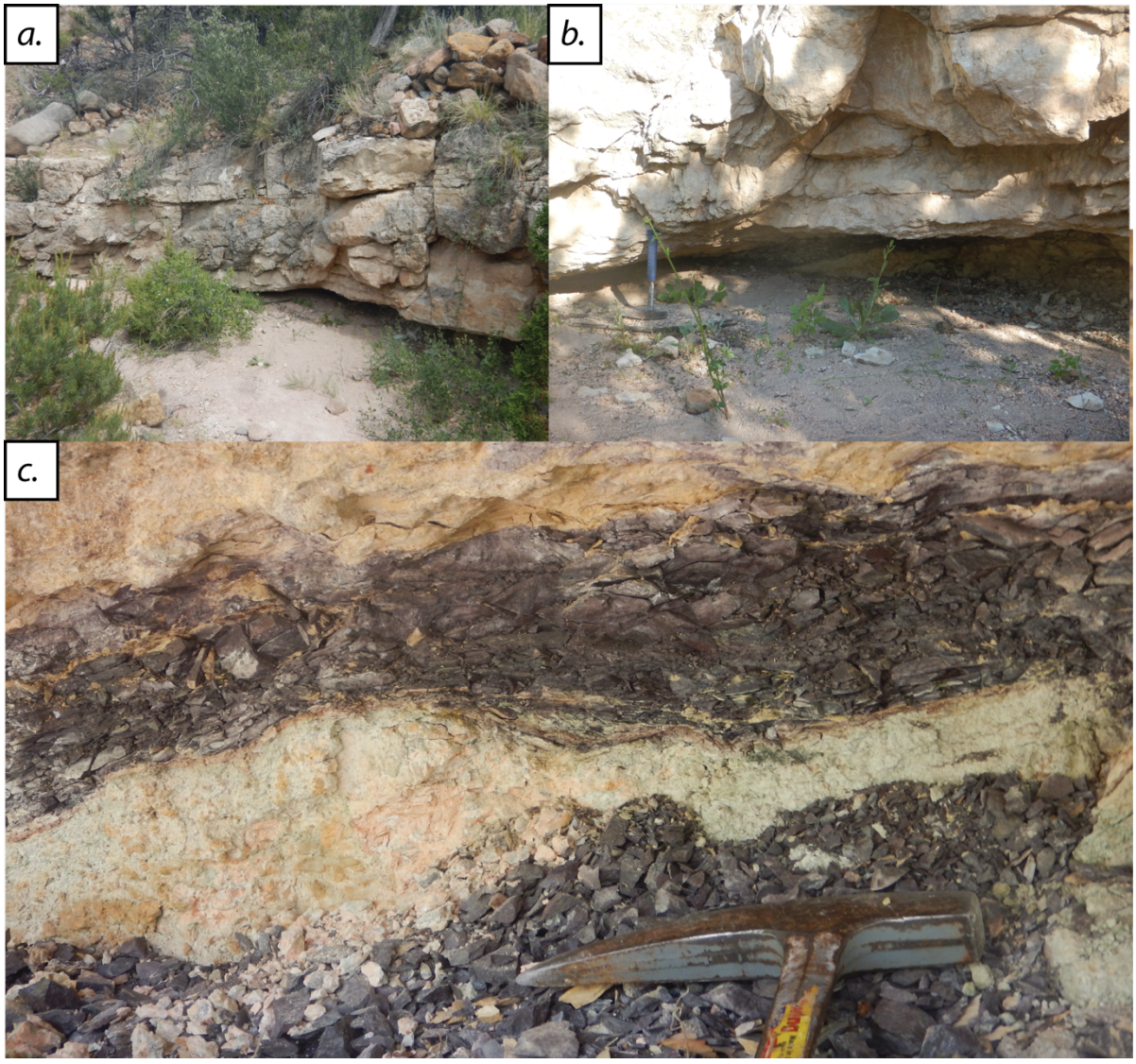

Figure 17. Horizontal brecciated fault rock observed in the central portion of the Mixing Bowl. **(a,b)** The Harding Formation directly overlies the sheared and brecciated fault zone. **(c)** The breccia consists of a purple layer on top of a green to white layer. Note the fractured pieces.

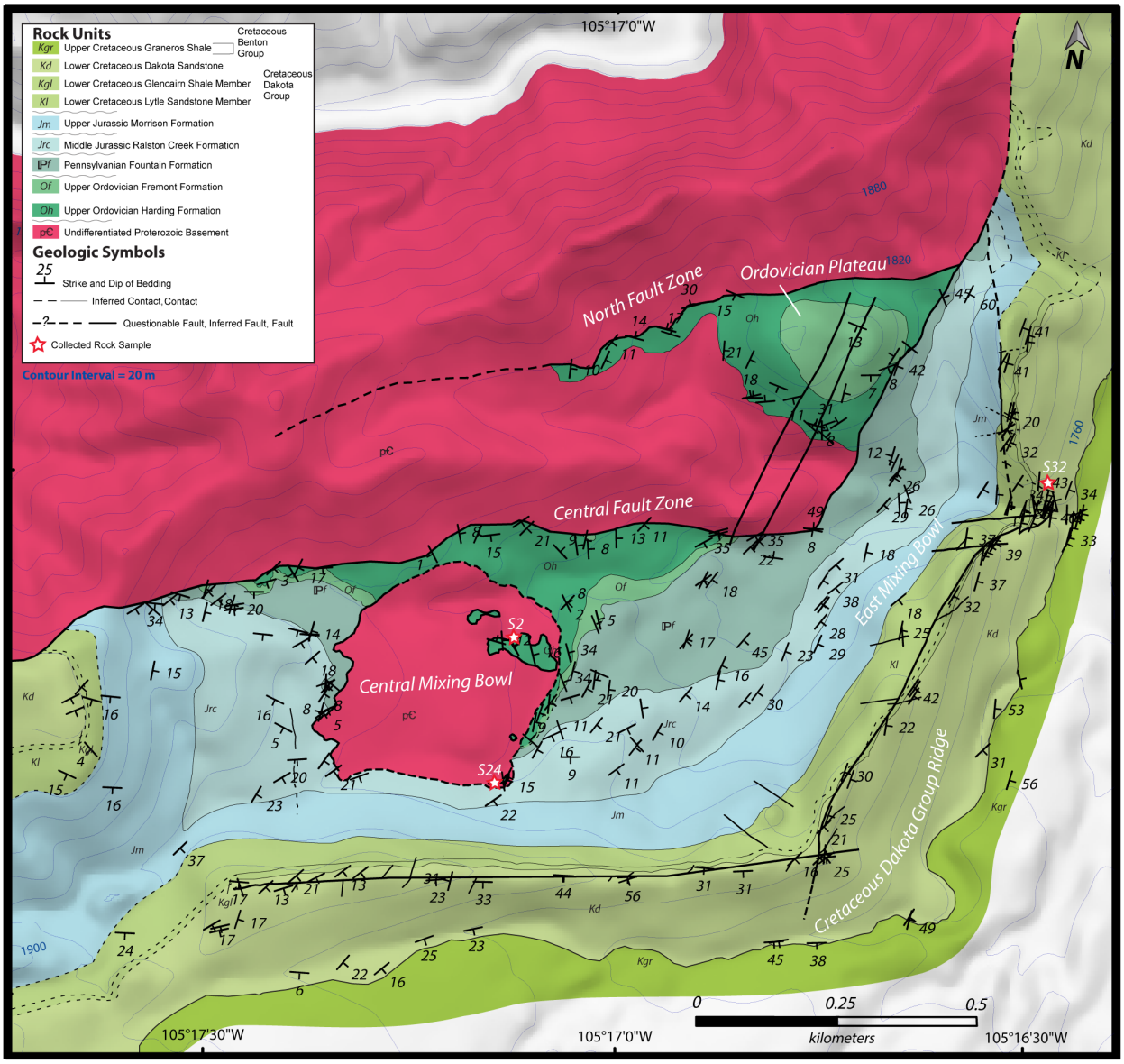

Figure 18. Bedding map of the Mixing Bowl field area. Units, faults, and stereonet substations are overlaid onto a 10 m resolution DEM. Collected samples: S2, S24, and S32 are fault rocks described in the field in *Section 4.1,* and in thin section in *Section 4.2c.*

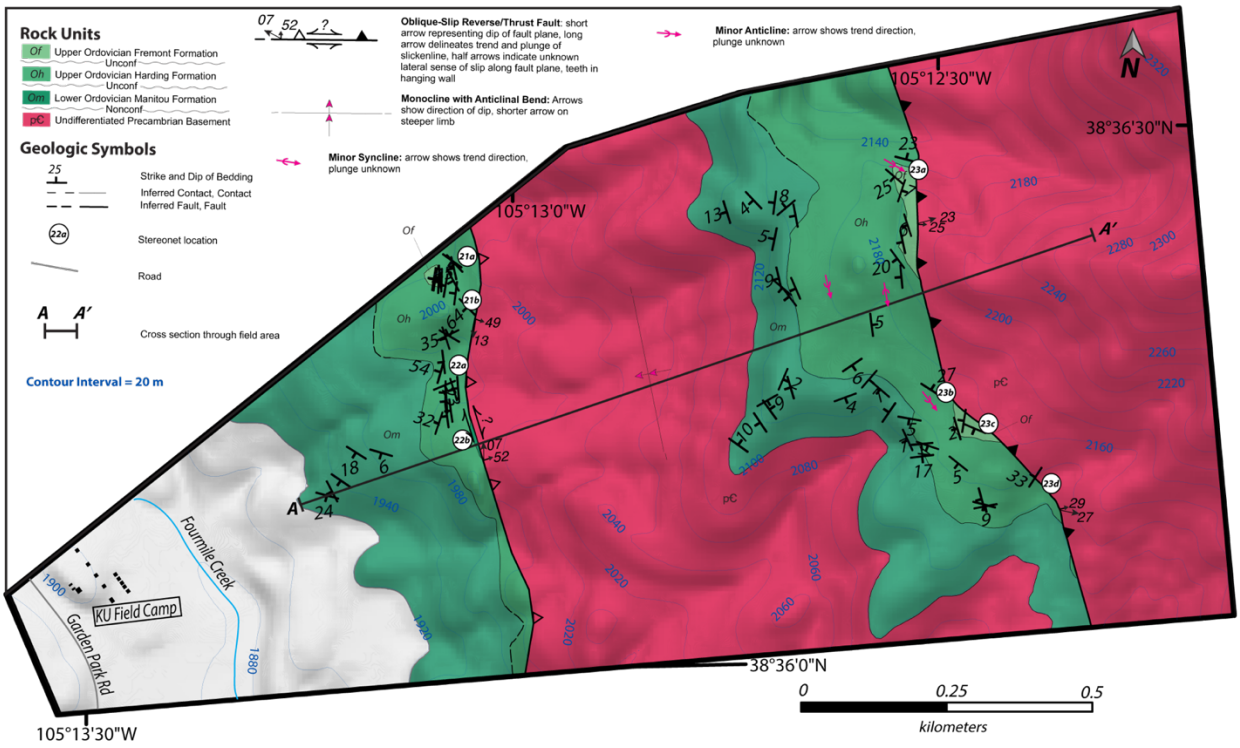

Figure 19. Geologic map of Sheep Mountain field area. Units, faults, and stereonet substations are overlaid onto a 10 m resolution DEM. Each white circle indicates the location of each stereonet substation.

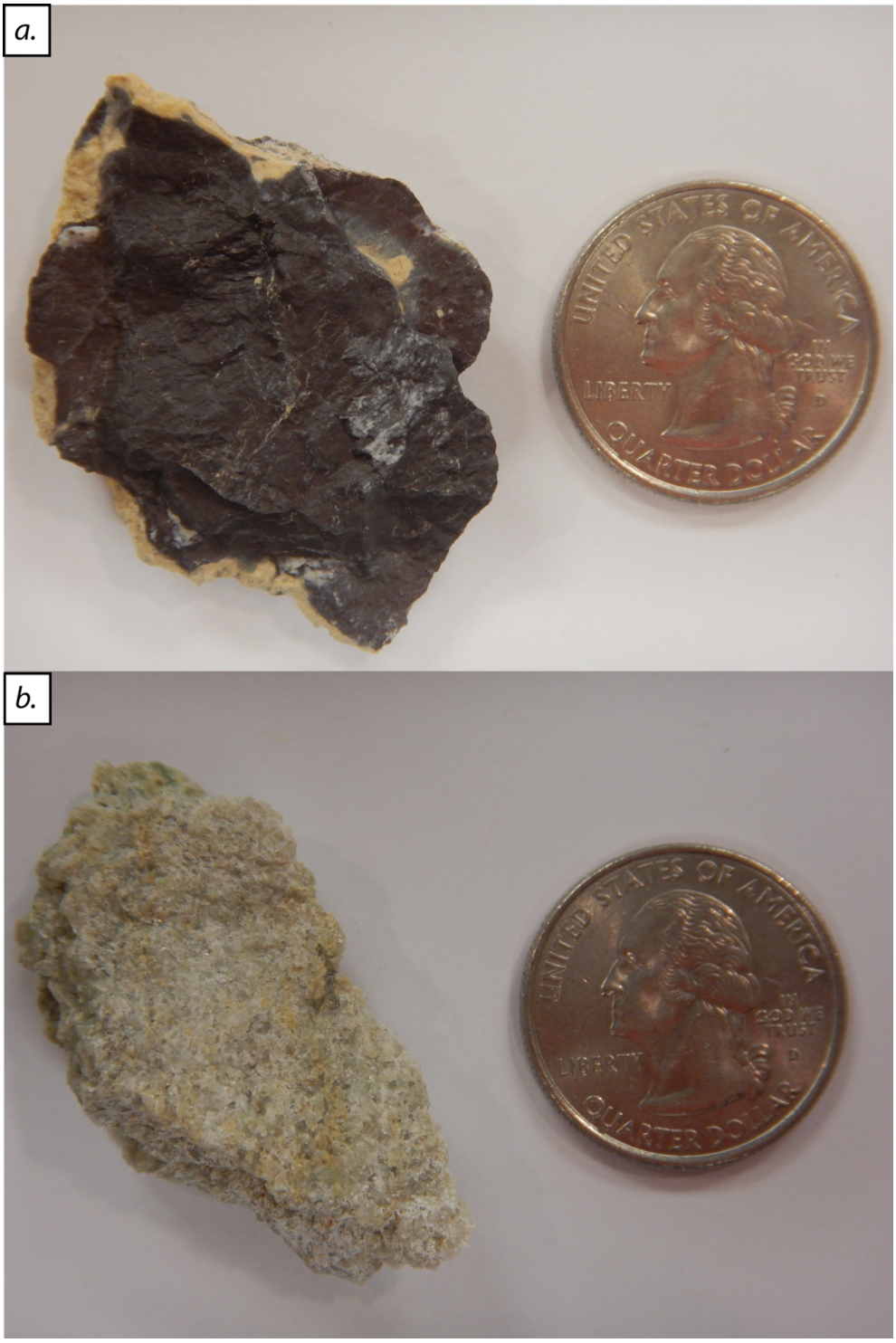

Figure 20. Horizontal brecciated fault rocks observed in the central portion of the Mixing Bowl. **(a)** The purple rock from the upper brecciated layer displays crystalline to fine-grain size. **(b)** The white to green rock from the lower brecciated layer shows medium to coarse-grained brecciated fragments.

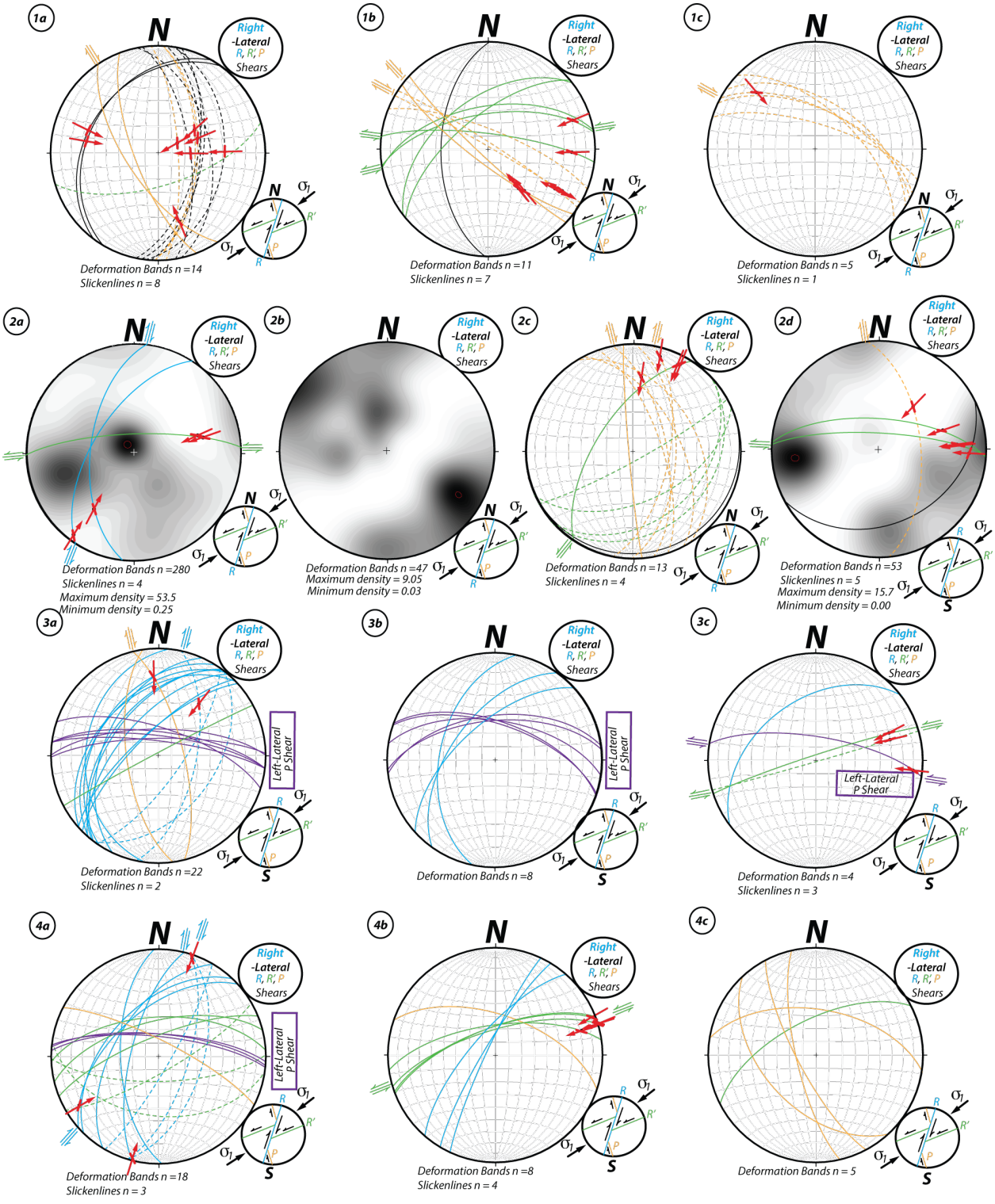

Figure 21. Stereonet stations 1 to 4. Master deformation band planes are solid and antithetic planes are dashed. Red arrows indicate slickenline formation and slip direction. Half arrows are added along the primitive circle to display sense-of-slip. Substations 2a, 2b, and 2d are density plots containing contour lines describing the density of poles. The black spots contain the most

poles and the white spots contain the least amount of poles. Each density plot contains different maximum and minimum density contours because they have different amounts of poles in each. A red circle is overlaid onto the density plot to indicate the location of the maximum density contours. If the deformation bands match a Riedel shear band orientation, they are color coded in conjunction with the suite of Riedel shear bands in the smaller circle to the bottom right of each stereonet.

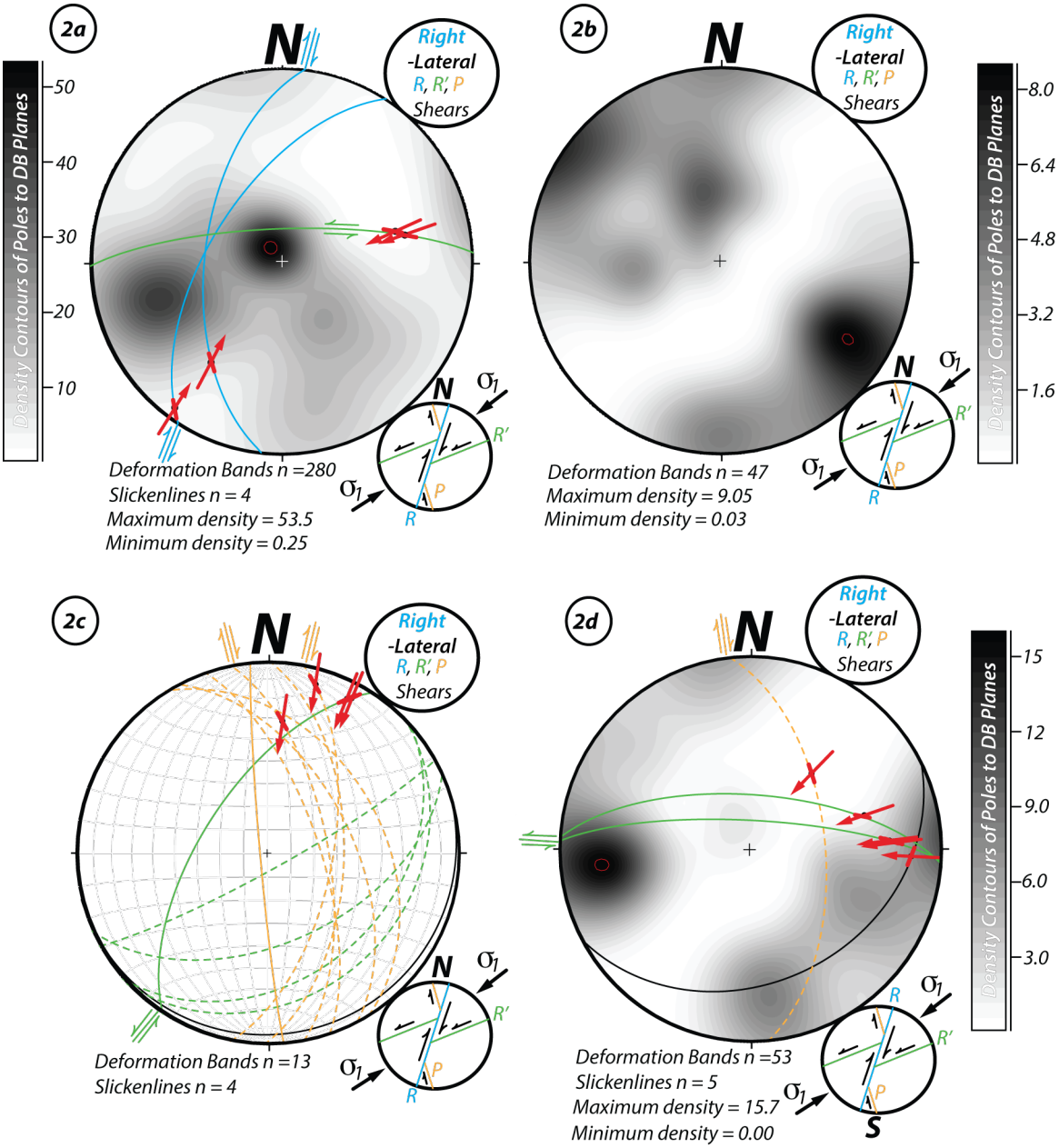

Figure 22. Density plots for stereonet station 2. Refer back to **Figure 21.** for information on the deformation band planes and slickenline lineations plotted on the stereonets. **Figure 21.** also provides information on the density plots for substation 2a, 2b, and 2d.

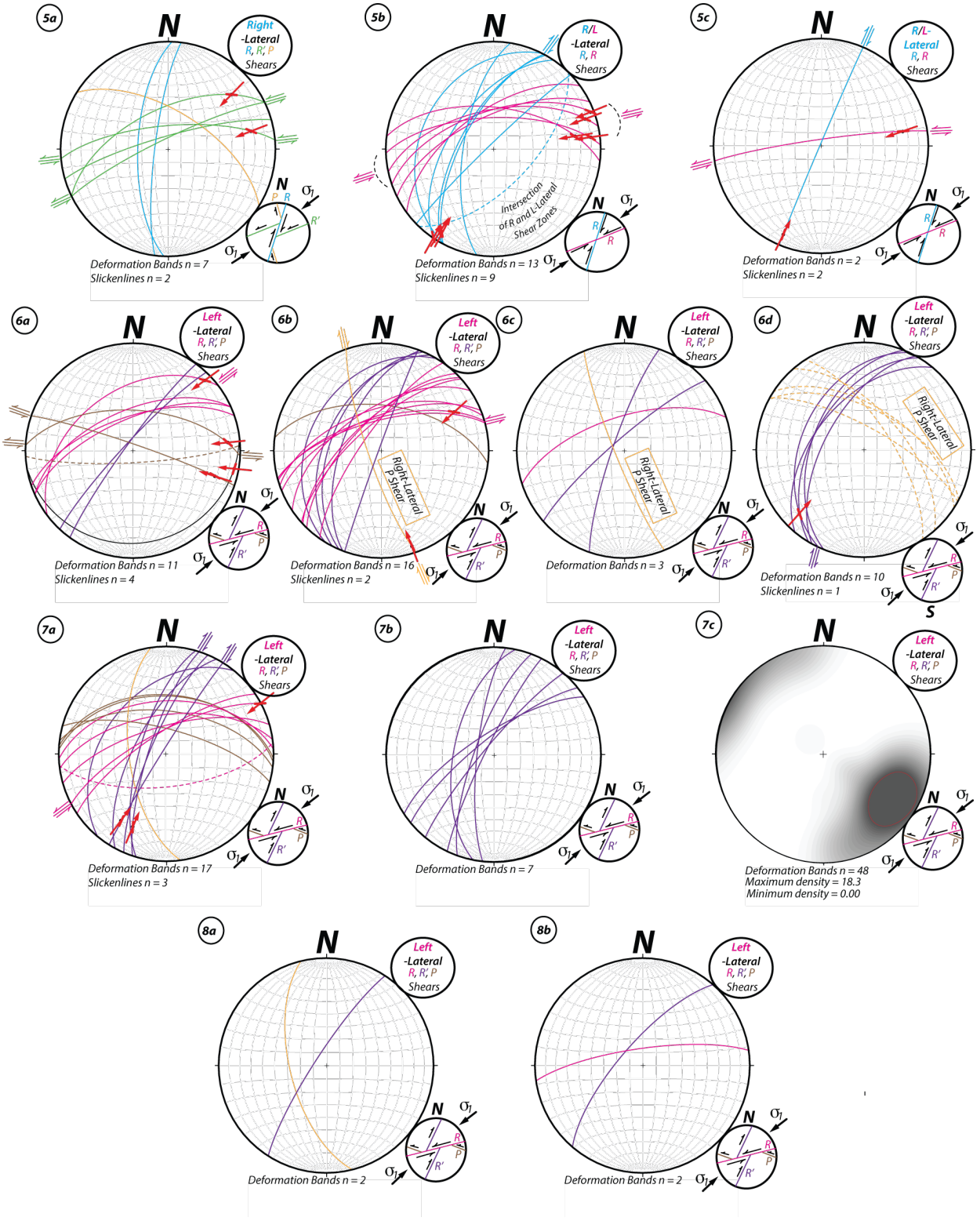

Figure 23. Stereonet stations 5 to 8. Refer back to **Figure 21.** for information on the deformation band planes and slickenline lineations plotted on the stereonets. **Figure 21.** also provides information on the density plot for substation 7c.

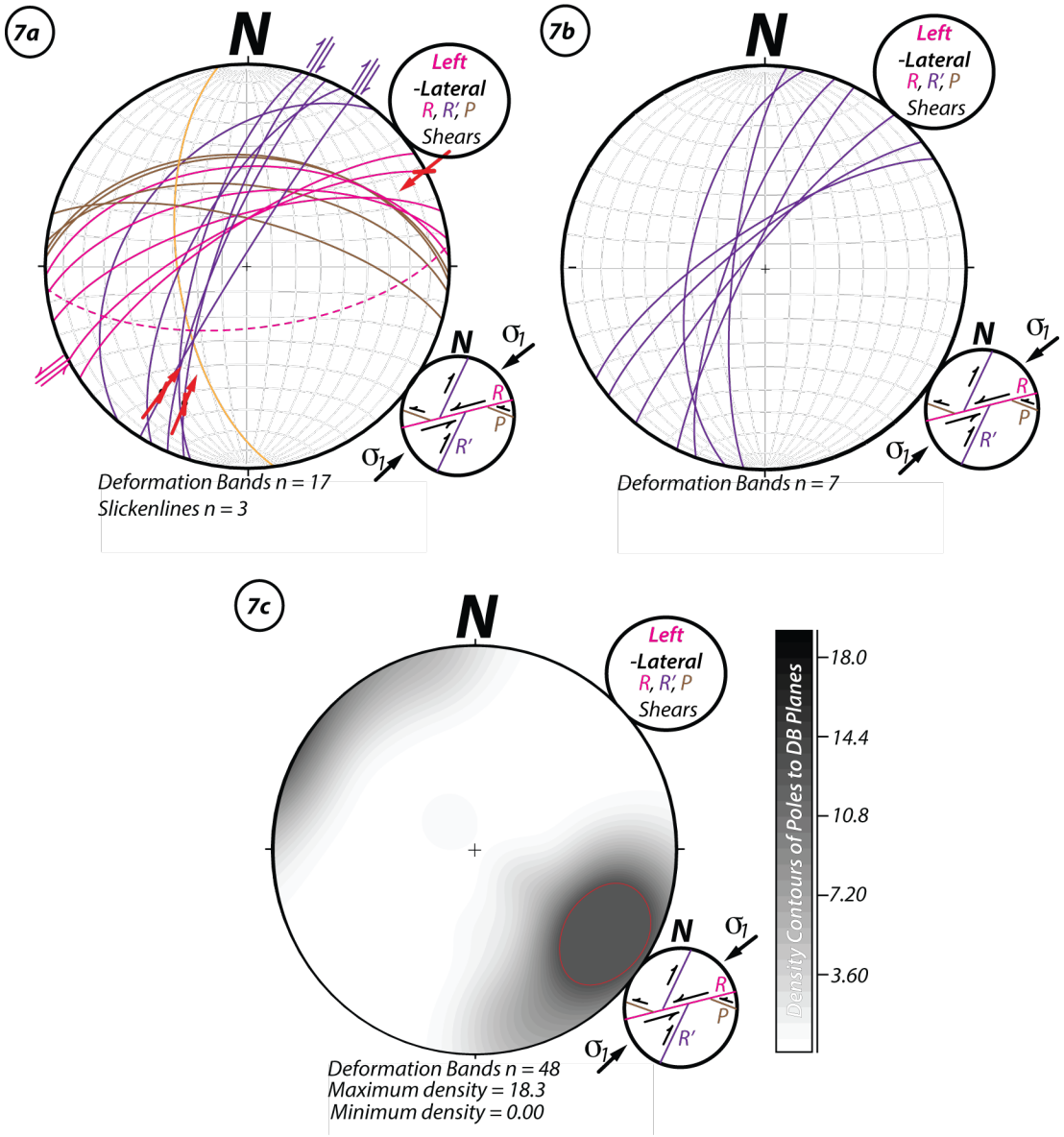

Figure 24. Density plot for stereonet substation 7c. Refer back to **Figure 21.** for information on the deformation band planes and slickenline lineations plotted on the stereonets. **Figure 21.** also provides information on the density plot for substation 7c.

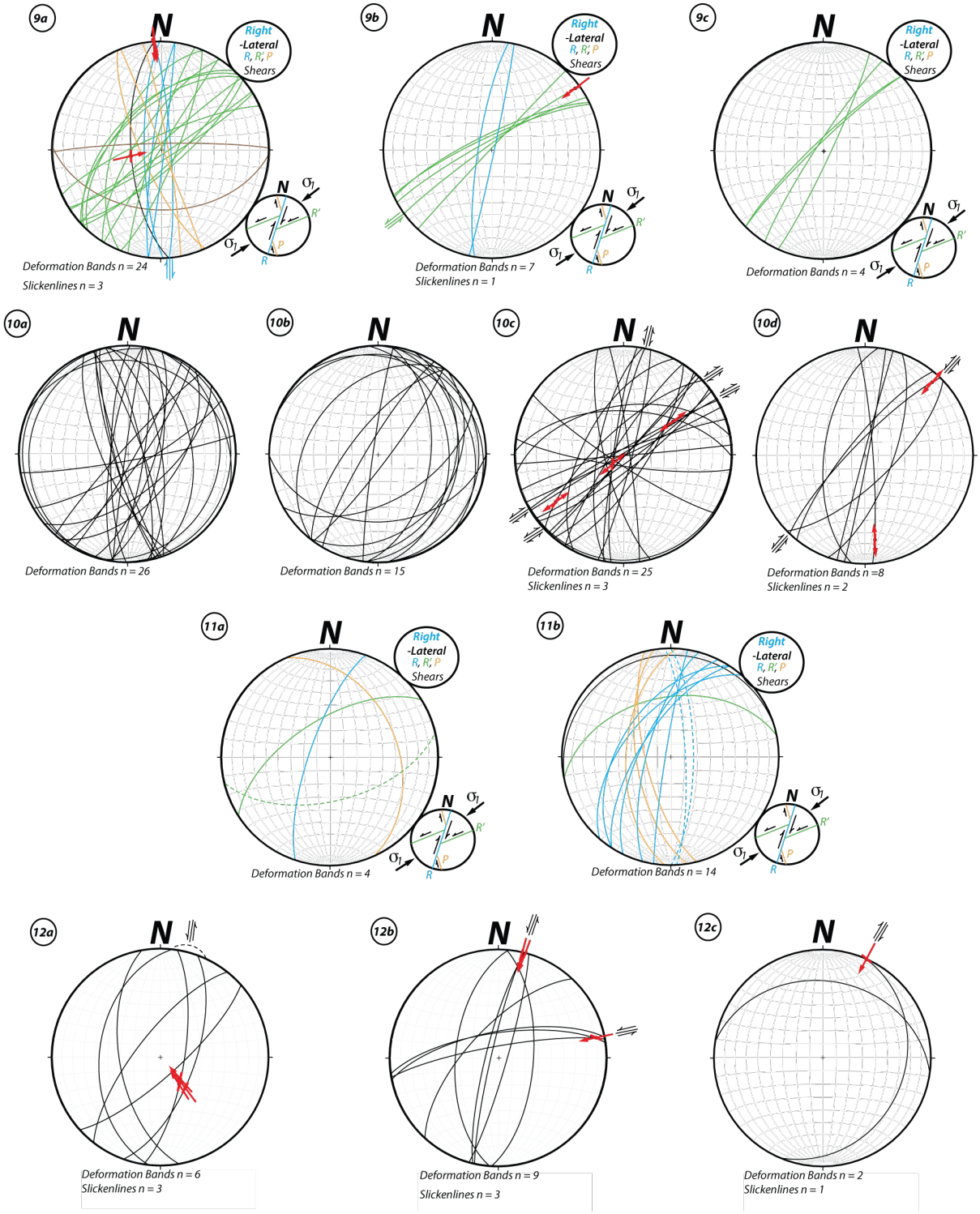

Figure 25. Stereonet stations 9 to 12. Refer back to **Figure 21.** for information on the deformation band planes and slickenline lineations plotted on the stereonets.

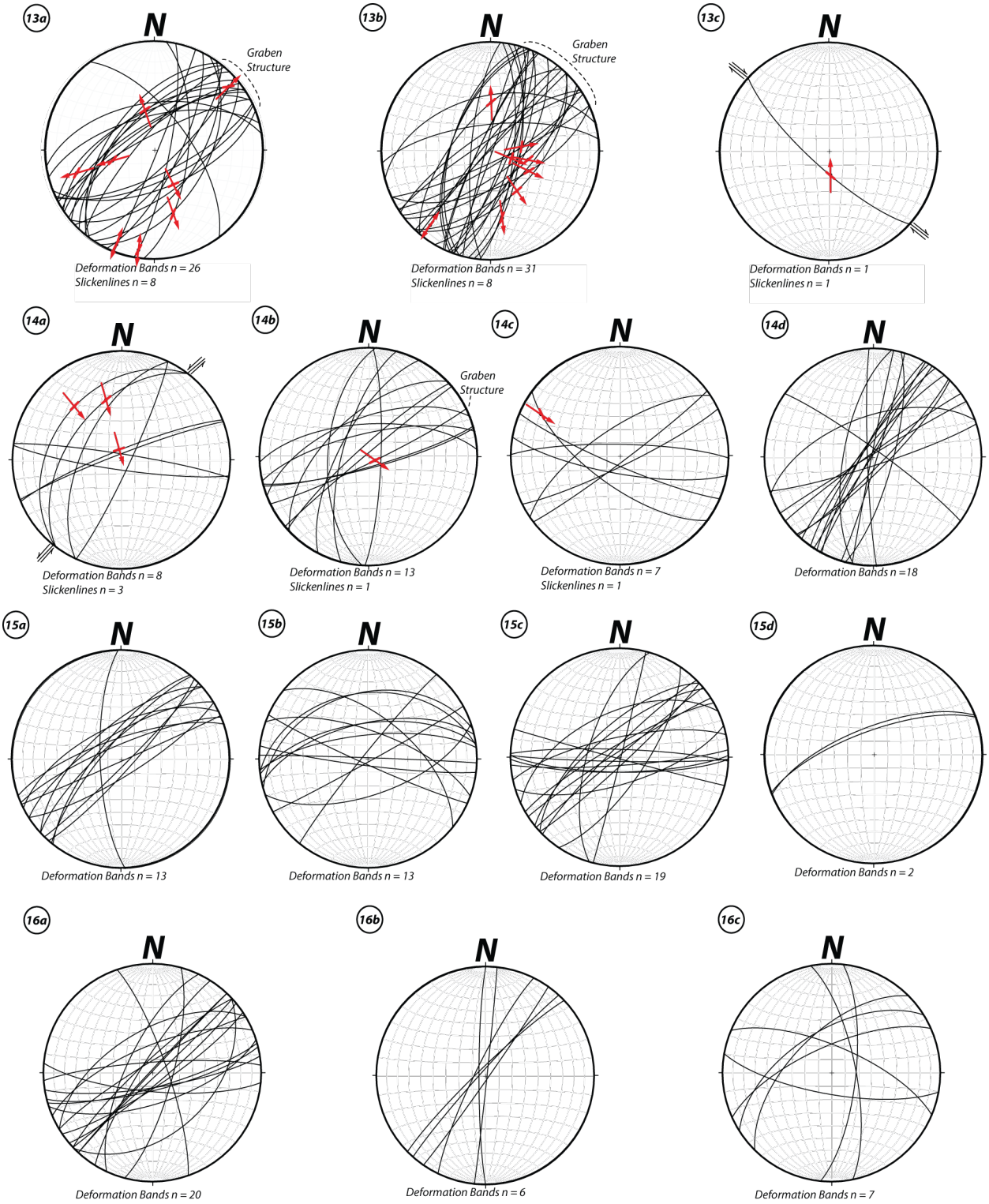

Figure 26. Stereonet stations 13 to 16. Refer back to **Figure 21.** for information on the deformation band planes and slickenline lineations plotted on the stereonets.

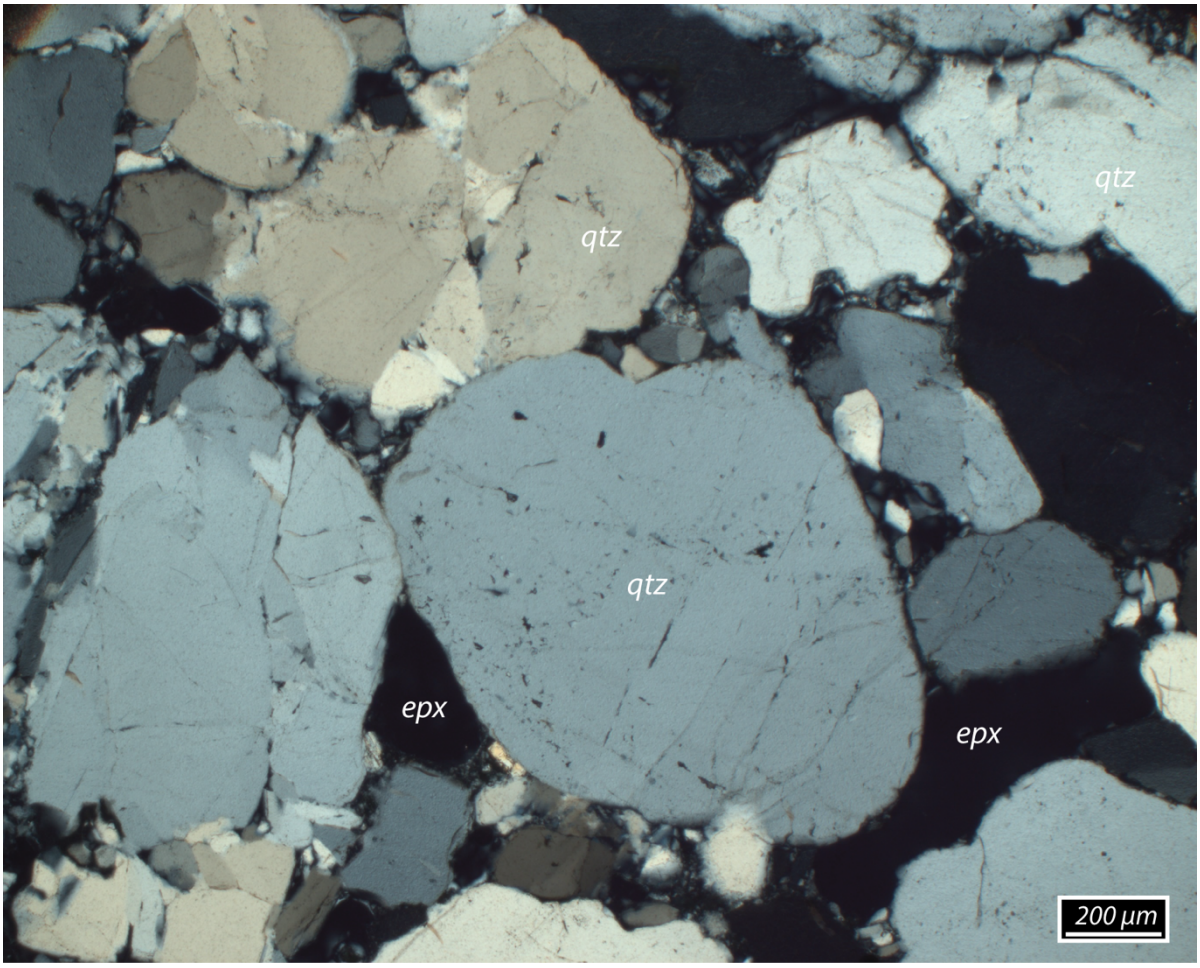

Figure 27.1. Thin section of porous Harding Sandstone from the central portion of the Mixing Bowl. The section is composed of poorly sorted quartz grains and epoxy, indicating its porous nature. The quartz grains are sub-round to round with medium to low sphericity (Wadell, 1932). Intragranular fractures and microcracks are observable.

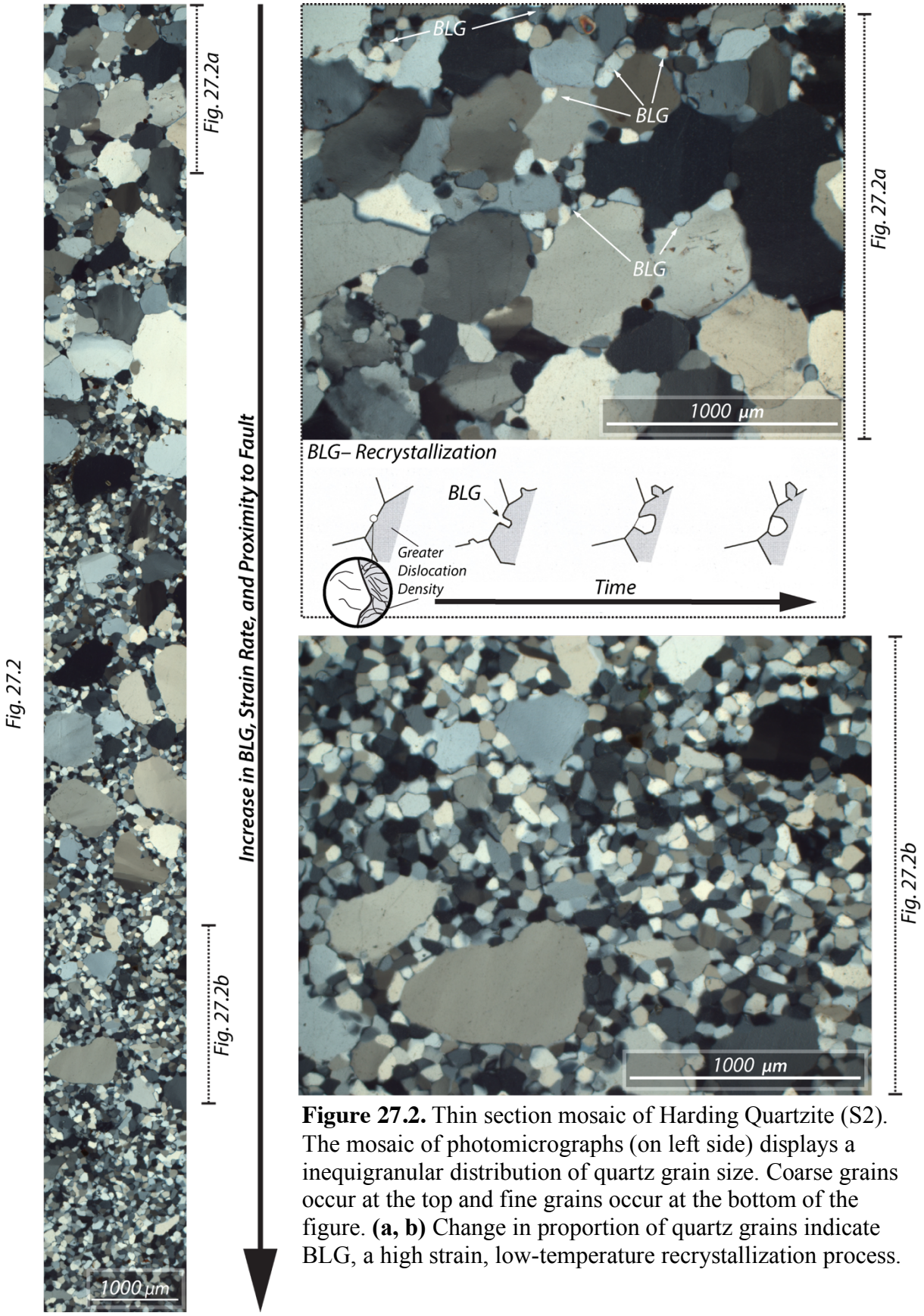

Figure 27.2. Thin section mosaic of Harding Quartzite (S2). The mosaic of photomicrographs (on left side) displays a inequigranular distribution of quartz grain size. Coarse grains occur at the top and fine grains occur at the bottom of the figure. **(a, b)** Change in proportion of quartz grains indicate BLG, a high strain, low-temperature recrystallization process.

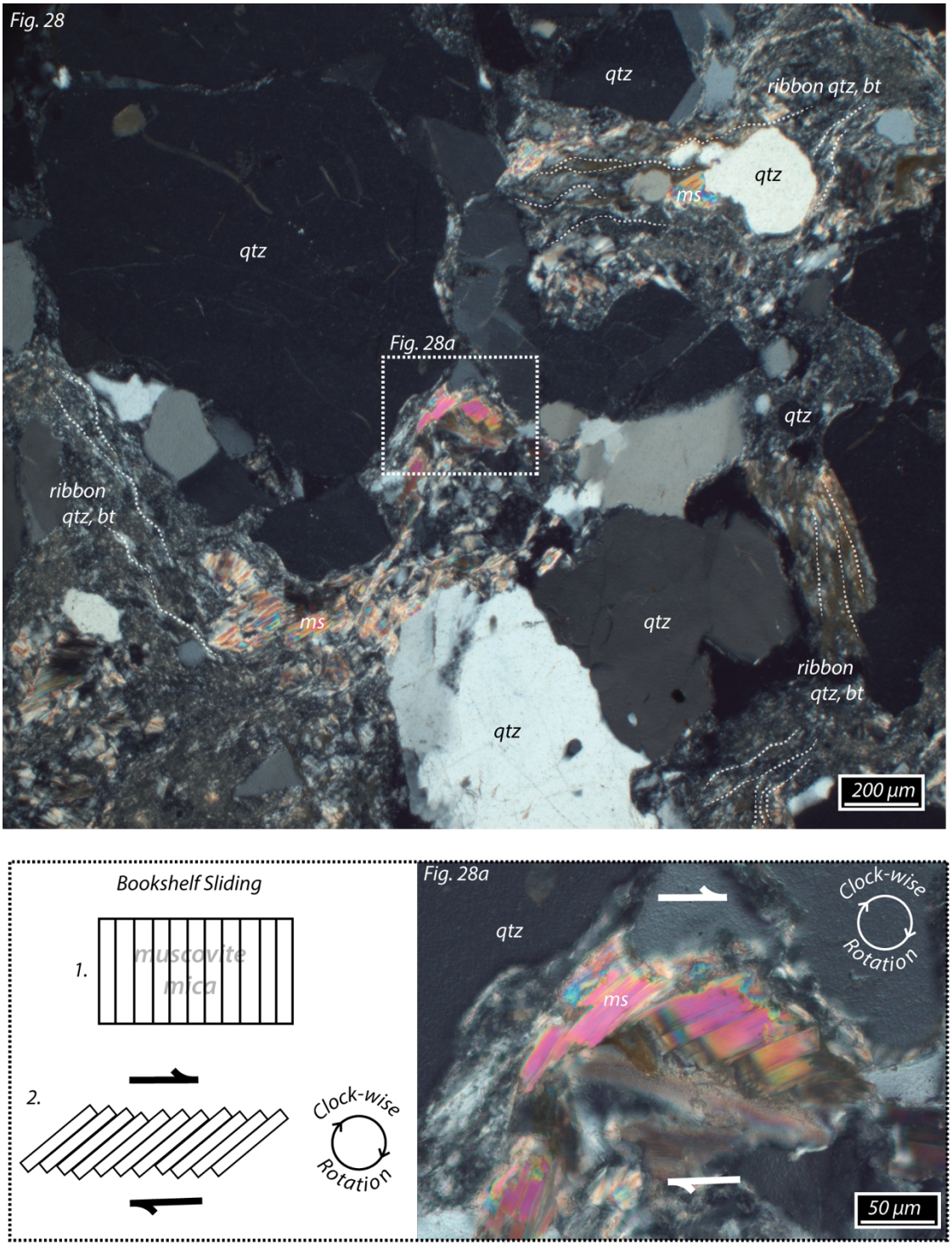

Figure 28. Thin section of brecciated fault rock from the horizontal fault zone in the central portion of the Mixing Bowl (S24). Ribbon quartz and biotite are interrupted by large quartz grains. **(a)** Muscovite displays bookshelf sliding (Lovering, 1928) as it rotates clock-wise due to a top-to-the-right sense of shear.

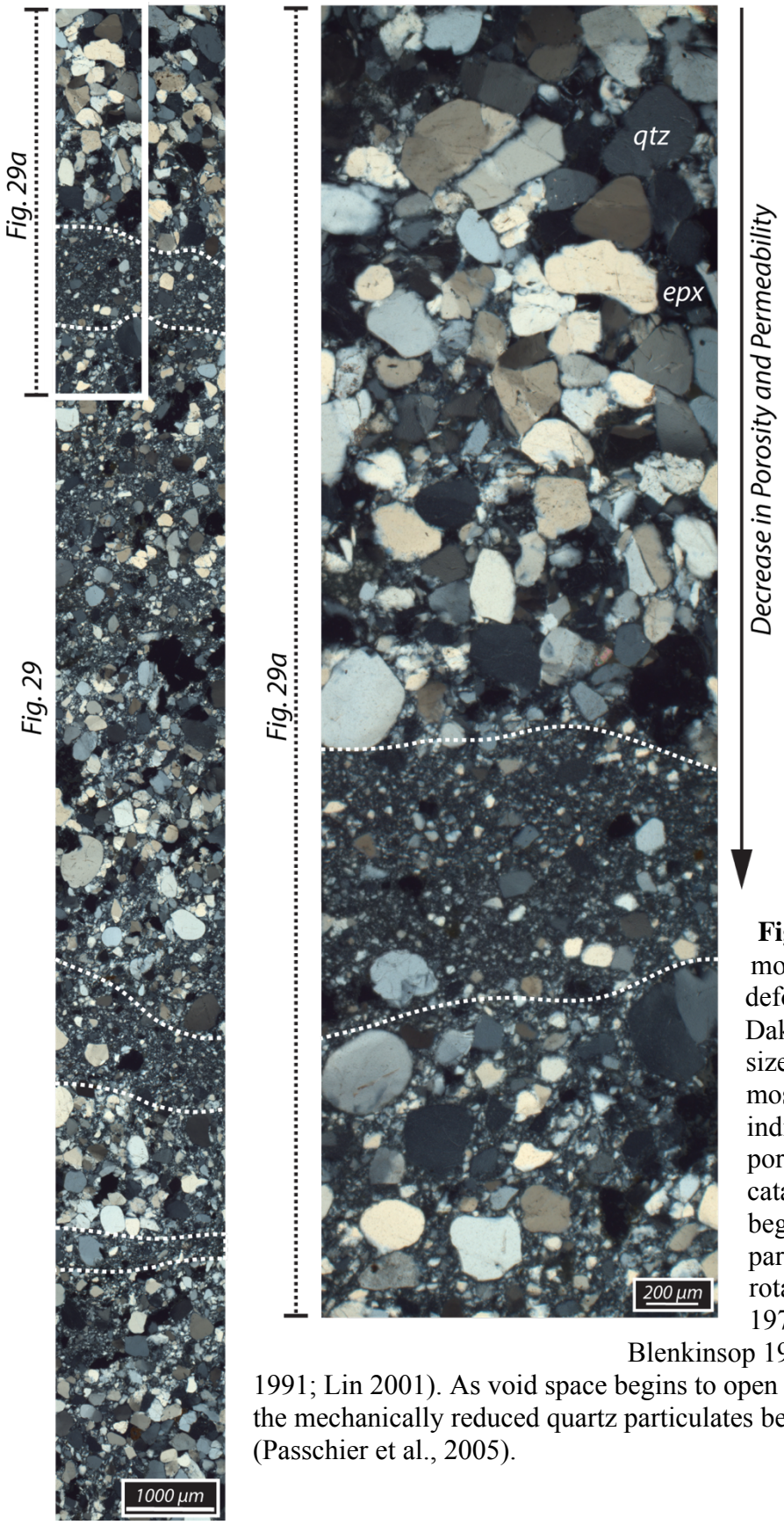

Figure 29. Thin section mosaic of cataclastic deformation bands in the Dakota Sandstone (S32). Grain size varies across the vertical mosaic. White dashed lines indicate boundaries between porous sandstone and cataclastic flow. **(a)** Grains begin to break into smaller particles as they slide and rotate past each other (Sibson 1977b; Evans 1988; Blenkinsop 1991b; Rutter and Hazidah 1991; Lin 2001). As void space begins to open up during cataclastic flow, the mechanically reduced quartz particulates begin to fill the open space (Passchier et al., 2005).

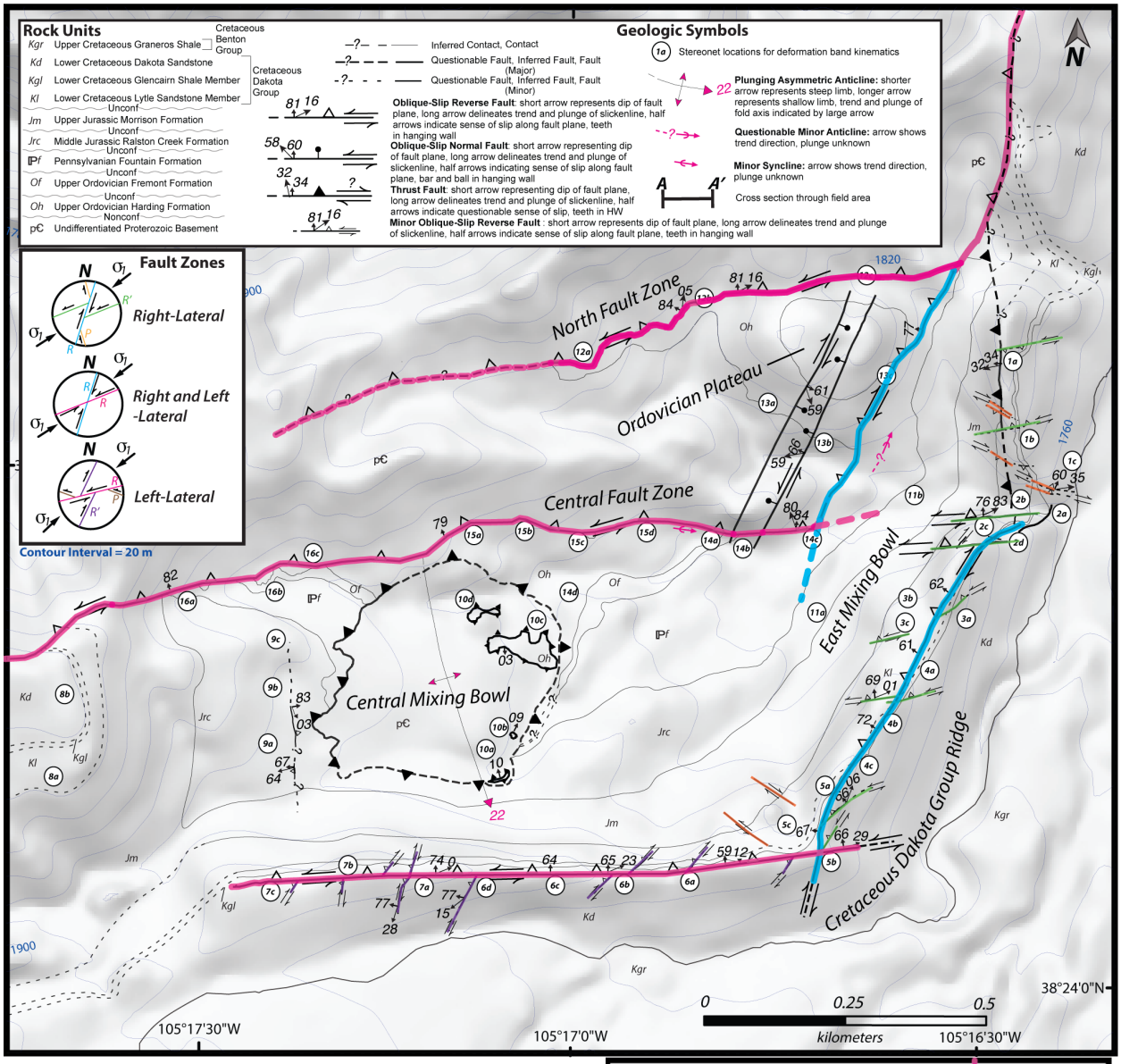

Fig. 30 Kinematic map of the Mixing Bowl field area. Faults and contacts are draped over a 10 m resolution DEM. Major and minor faults are color coded if they match Riedel shear band orientations as illustrated to the left of the Mixing Bowl. The oblique - slip kinematics along the faults indicate that the Mixing Bowl field area expresses a horsetail contractional splay.

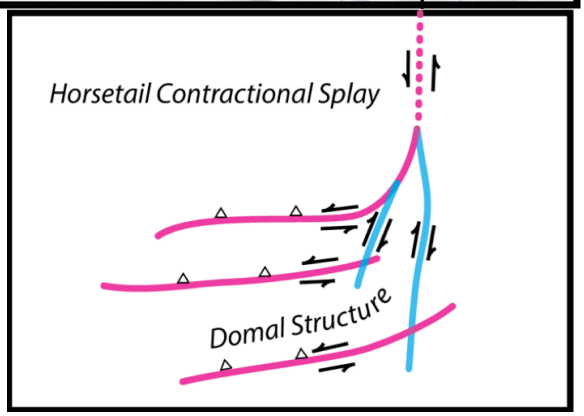

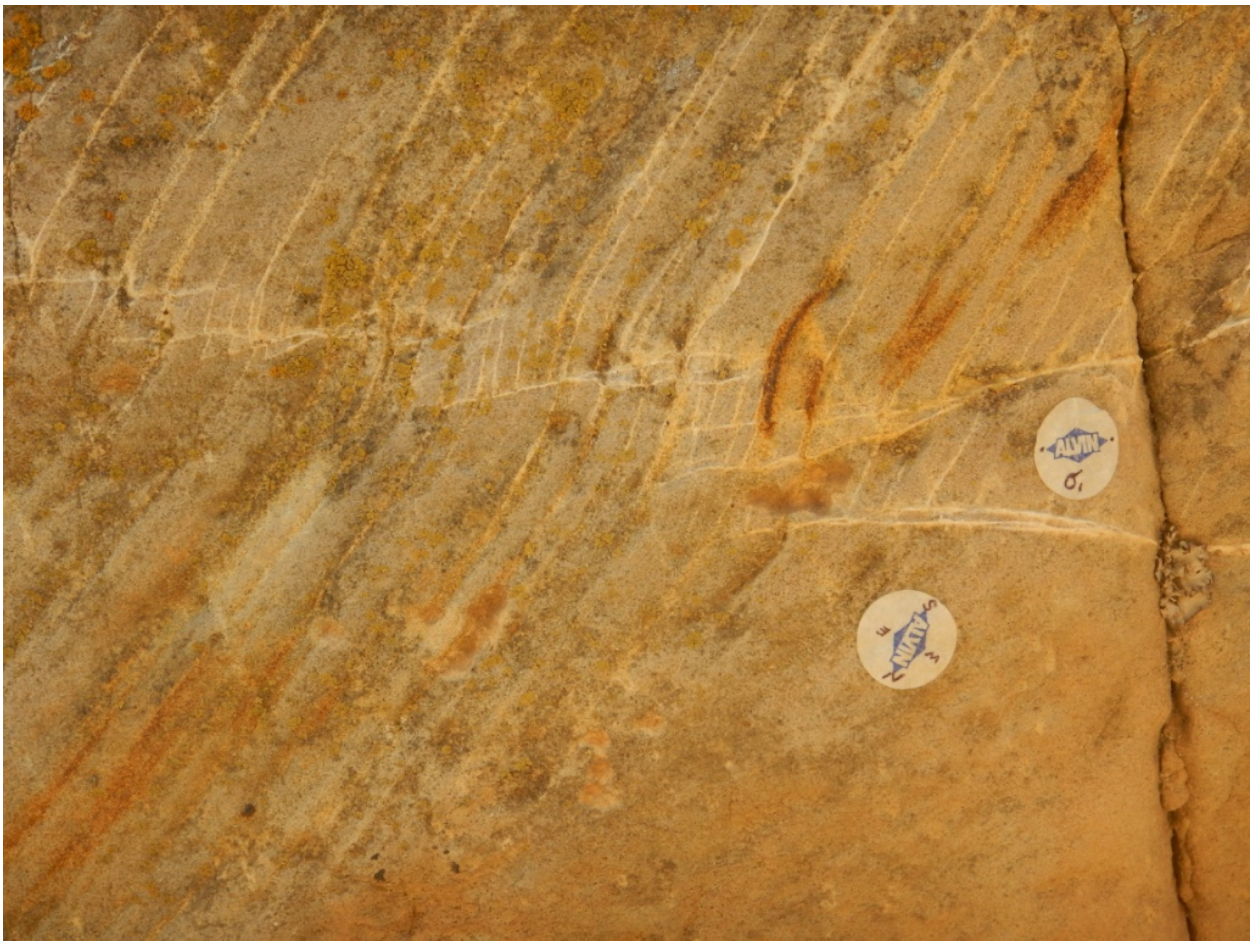

Fig. 31. Horizontal deformation bands in the Dakota Sandstone. The horizontal deformation bands are offsetting the vertical deformation bands. The horizontal bands are acting as bounding bands, where vertical bands are acting as linking bands.

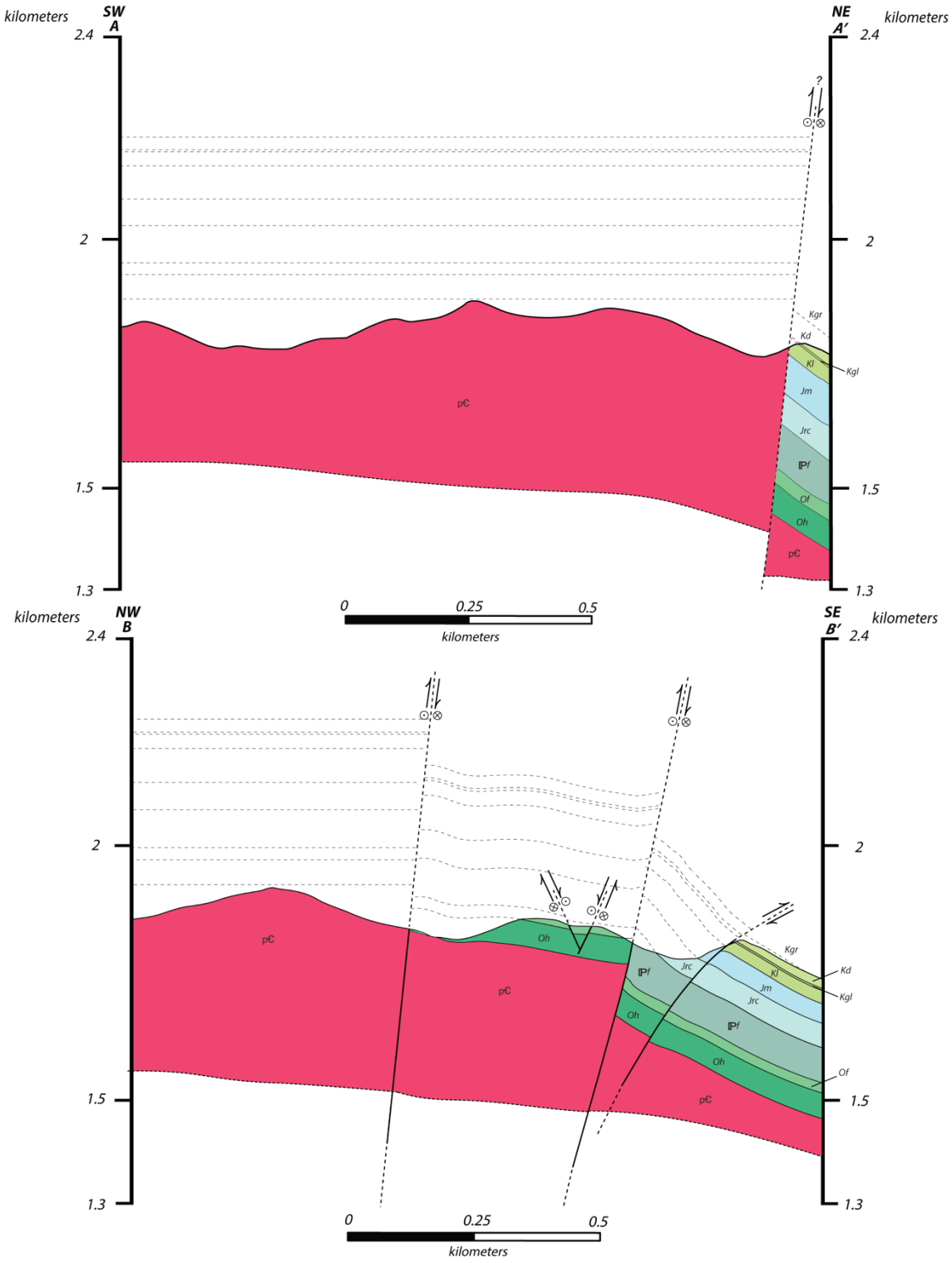

Figure 32. Cross sections A-A'and B-B'. Note the single fault in A-A' seems to split and form three separate faults in B-B'.

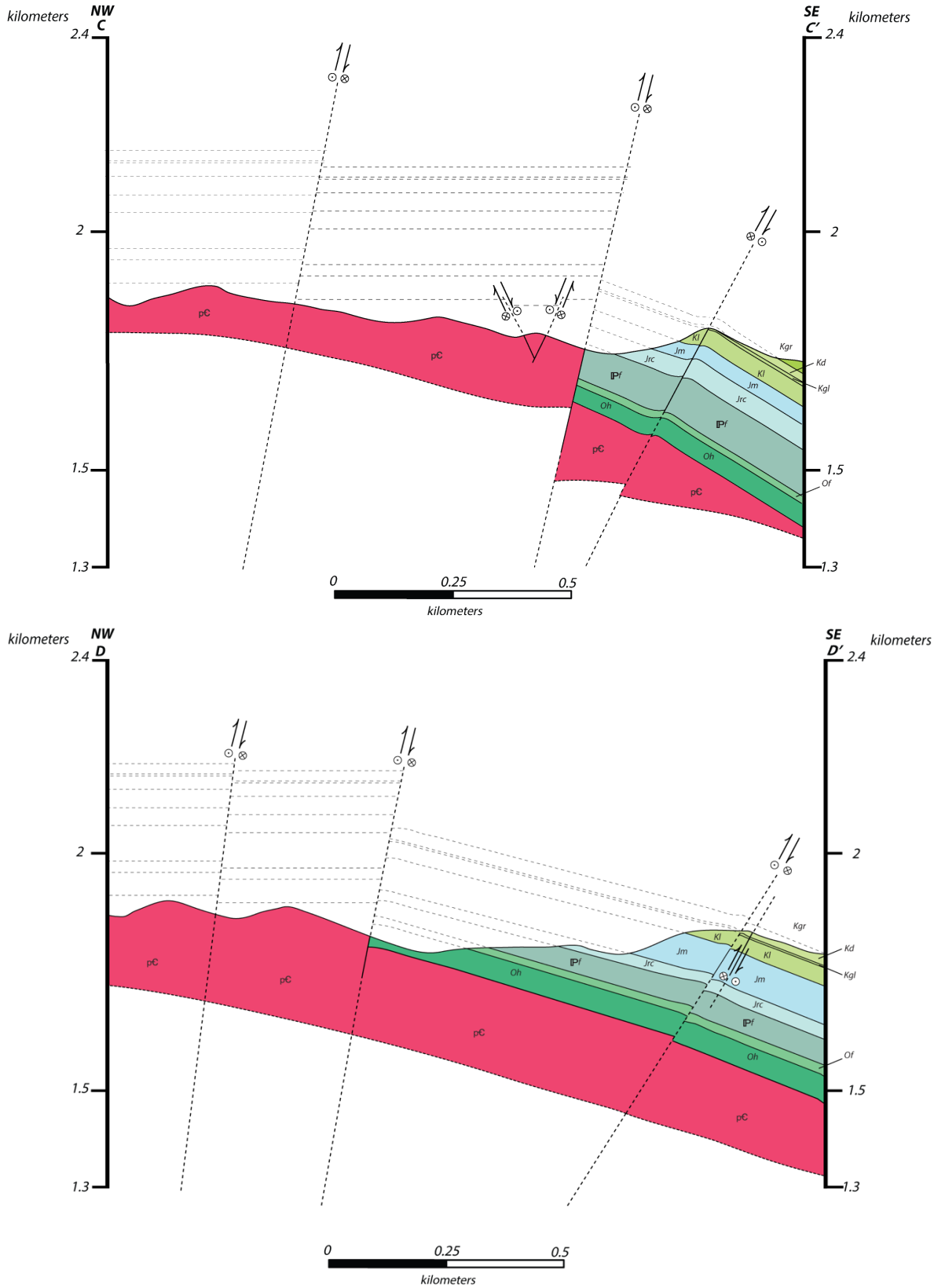

Figure 33. Cross sections C-C' and D-D'. The extent between the Central Fault Zone and the ridge significantly widens between C-C' and D-D' but bedding orientations stay constant.

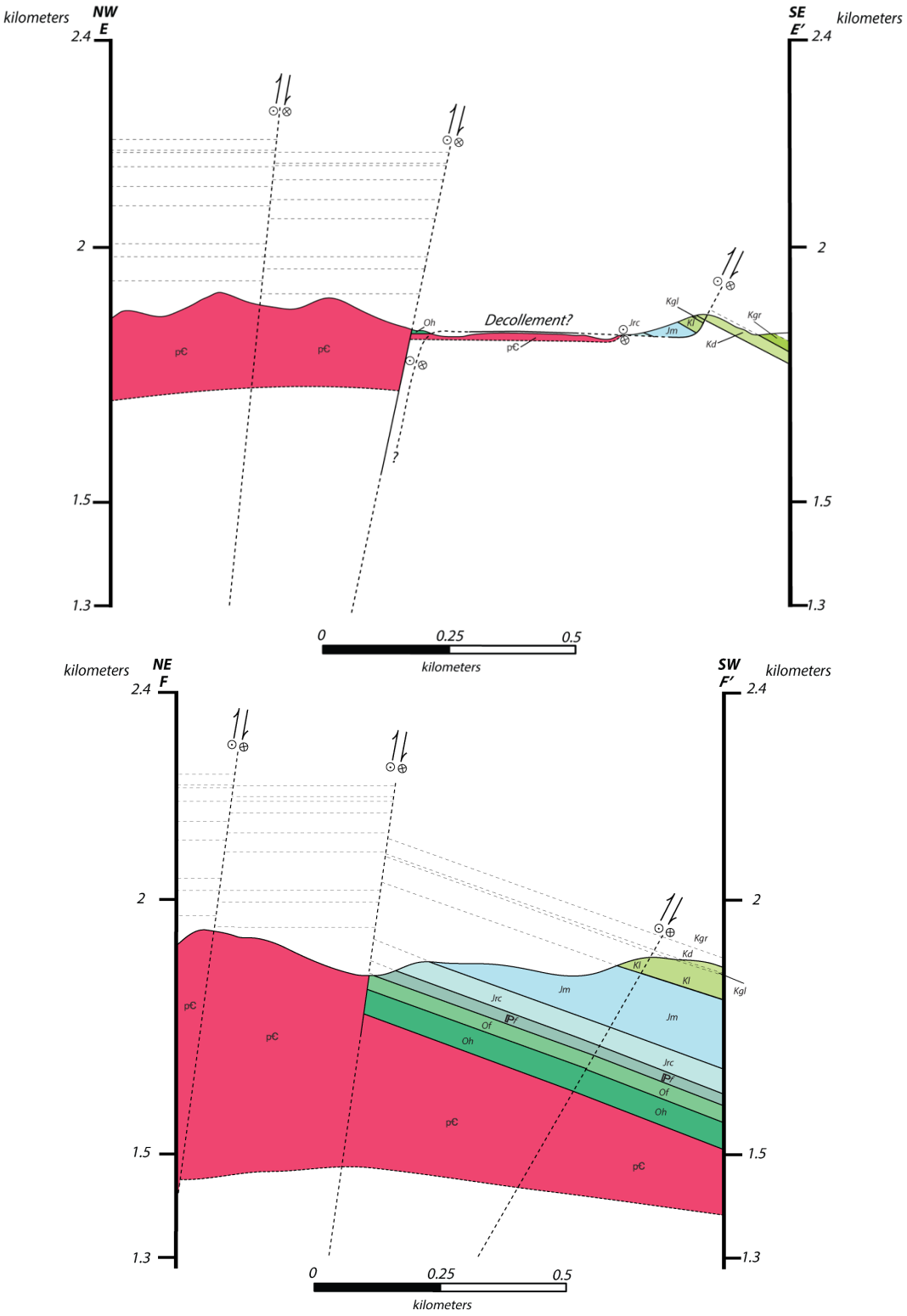

Figure 34. Cross Sections E-E' and F-F'. E-E' displays the inferred route of the horizontal fault zone observed in the middle of the Mixing Bowl. Note that the faults have been sub-vertical since cross section A-A'.

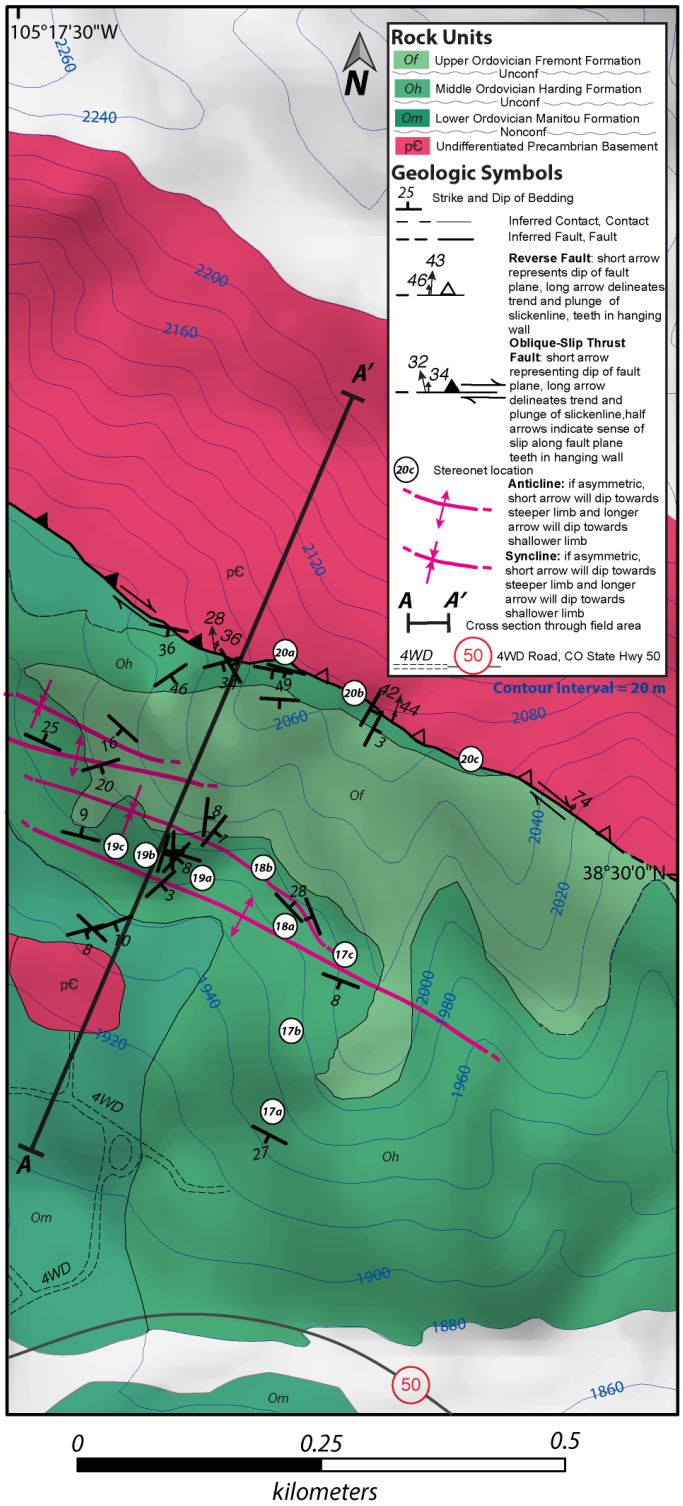

Figure 35. Geologic map of South Twin Mountain field area. Units, faults, and stereonet substations are overlaid onto a 10 m resolution DEM. Each white circle indicates the location of each stereonet substation.

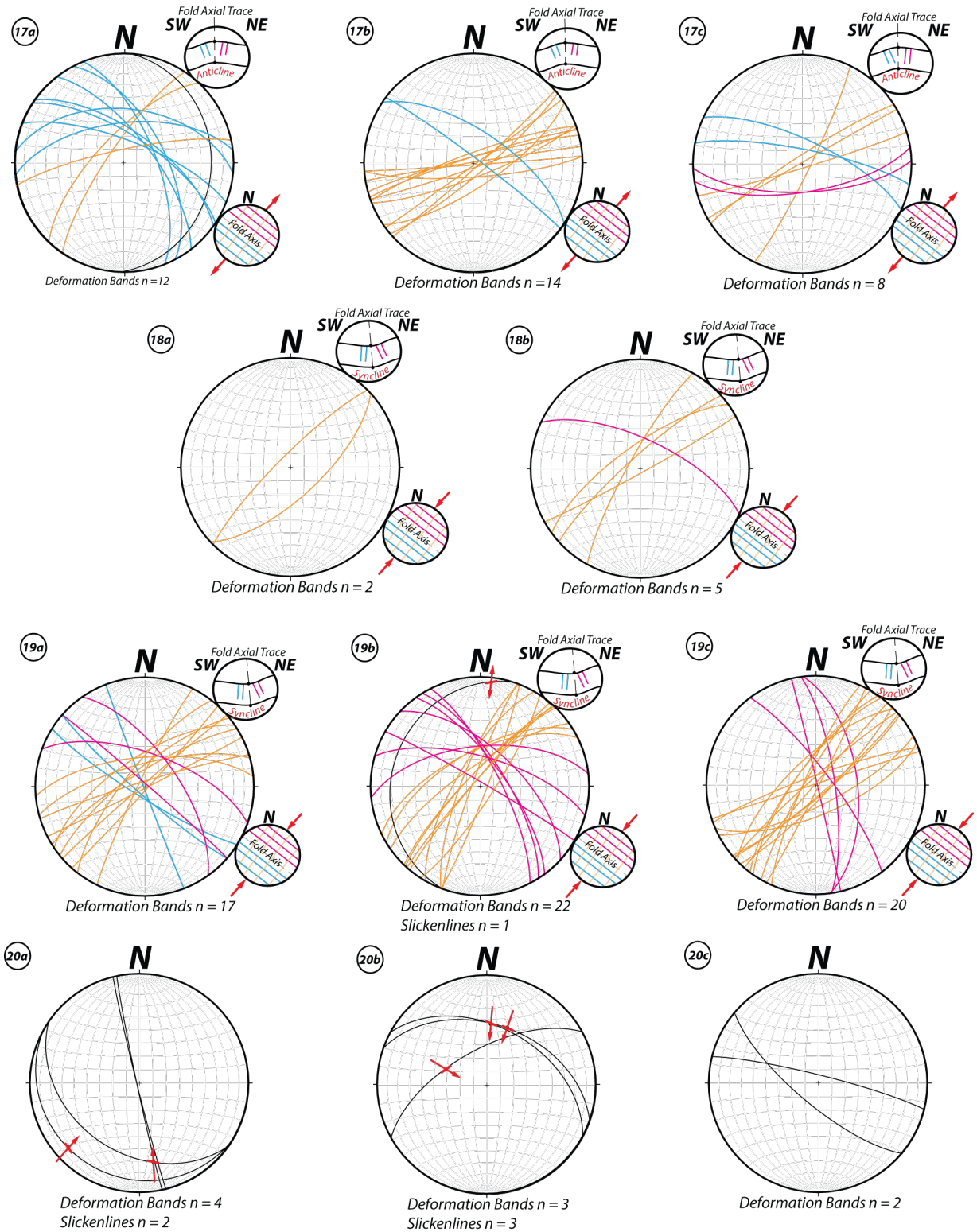

Figure 36. Stereonet stations 17 to 20. Deformation bands that occur in the southwest limb of synclines or anticlines are colored blue. Deformation bands that occur in northeast limbs of synclines or anticlines are colored pink. Deformation bands oriented orthogonally to the northeast- and southwest- dipping bands are colored orange. Red arrows indicate slickenline formation and slip direction.

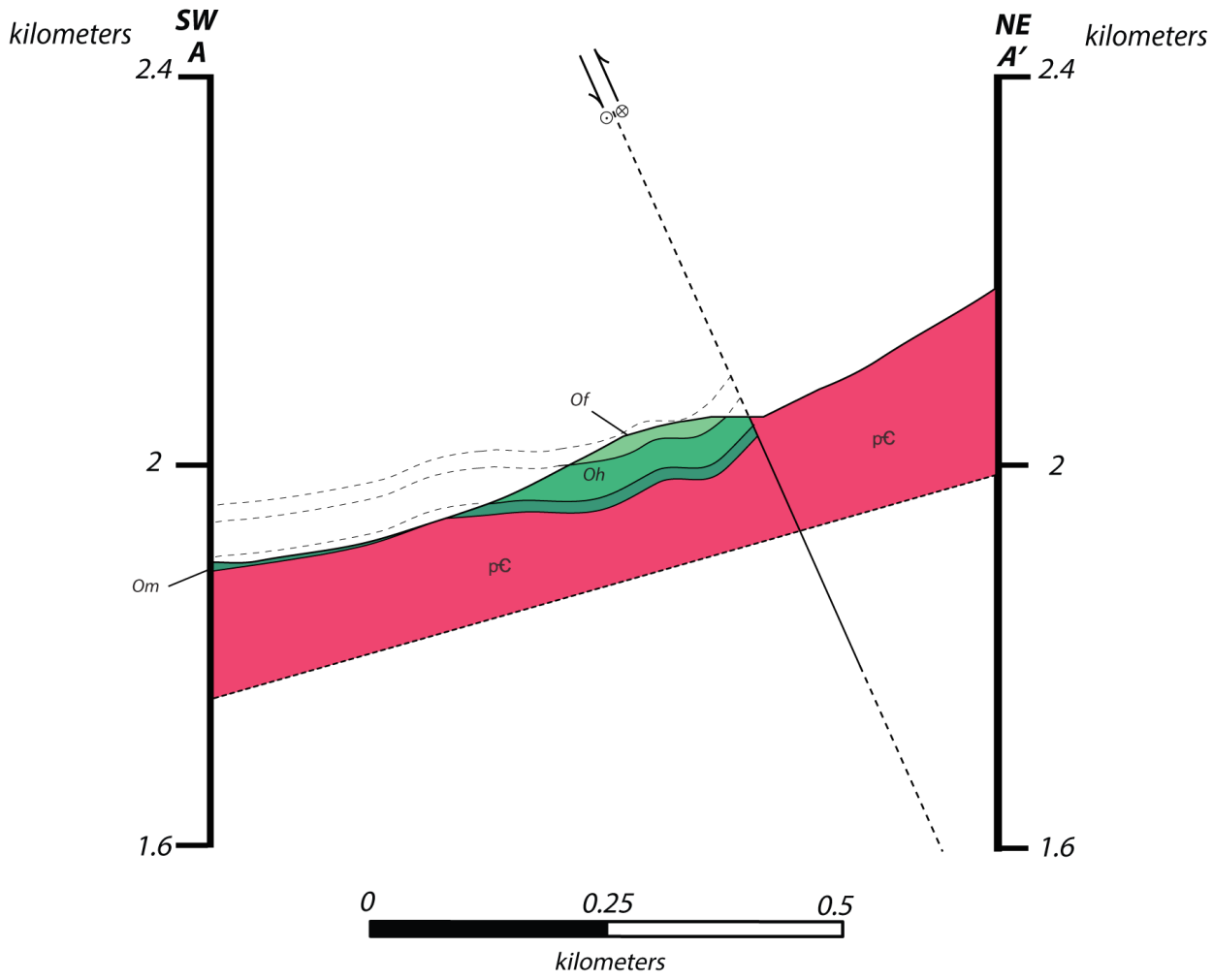

Figure 37. Cross section through the South Twin Mountain field area. The en-echelon anticlines and synclines in the footwall become cut off by the overthrusted Proterozoic basement rock.

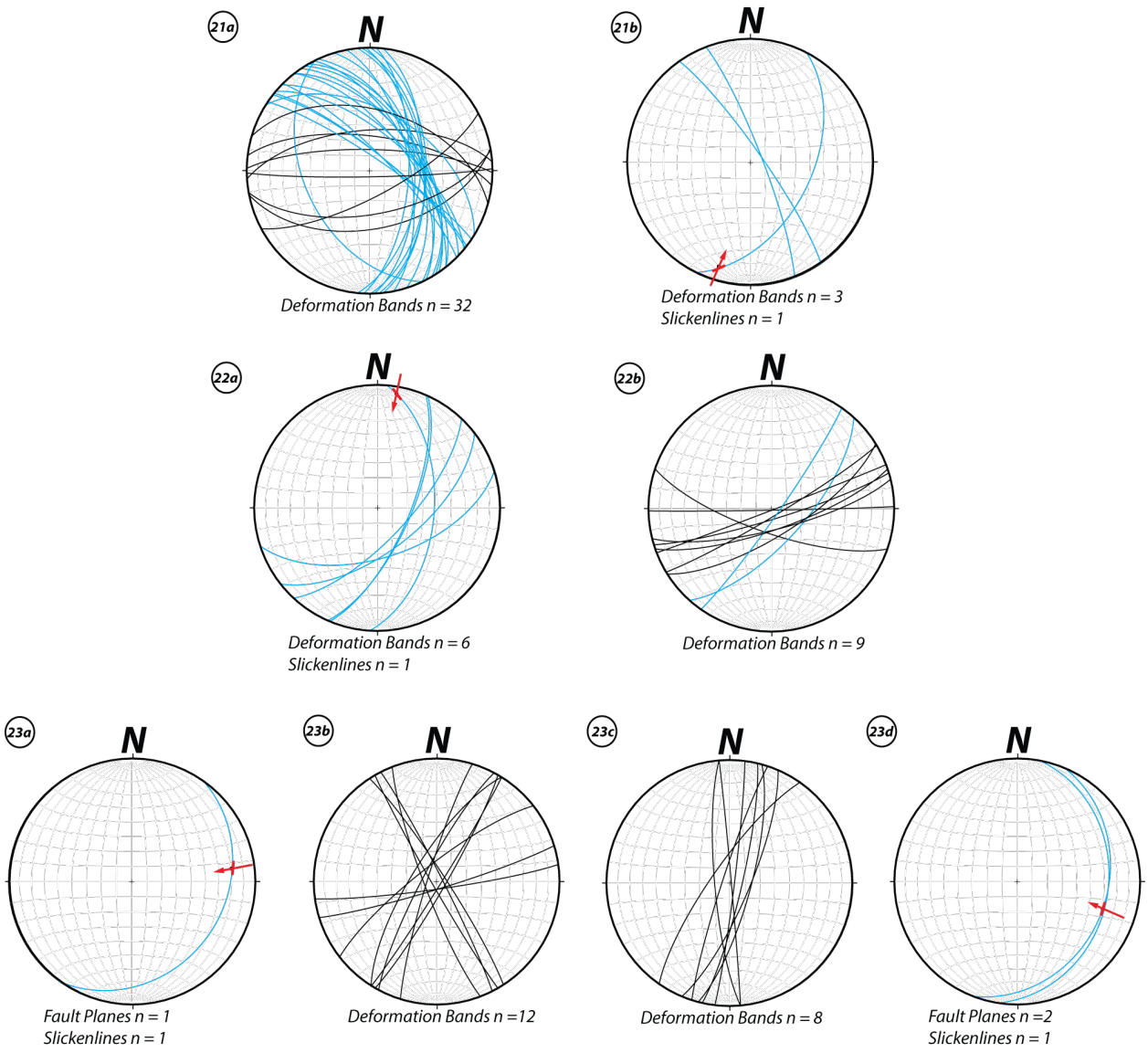

Figure 38. Stereonet stations 21 to 23. Deformation bands that reflect the orientation of the fault contact are colored blue. Red arrows indicate slickenline formation and slip direction.

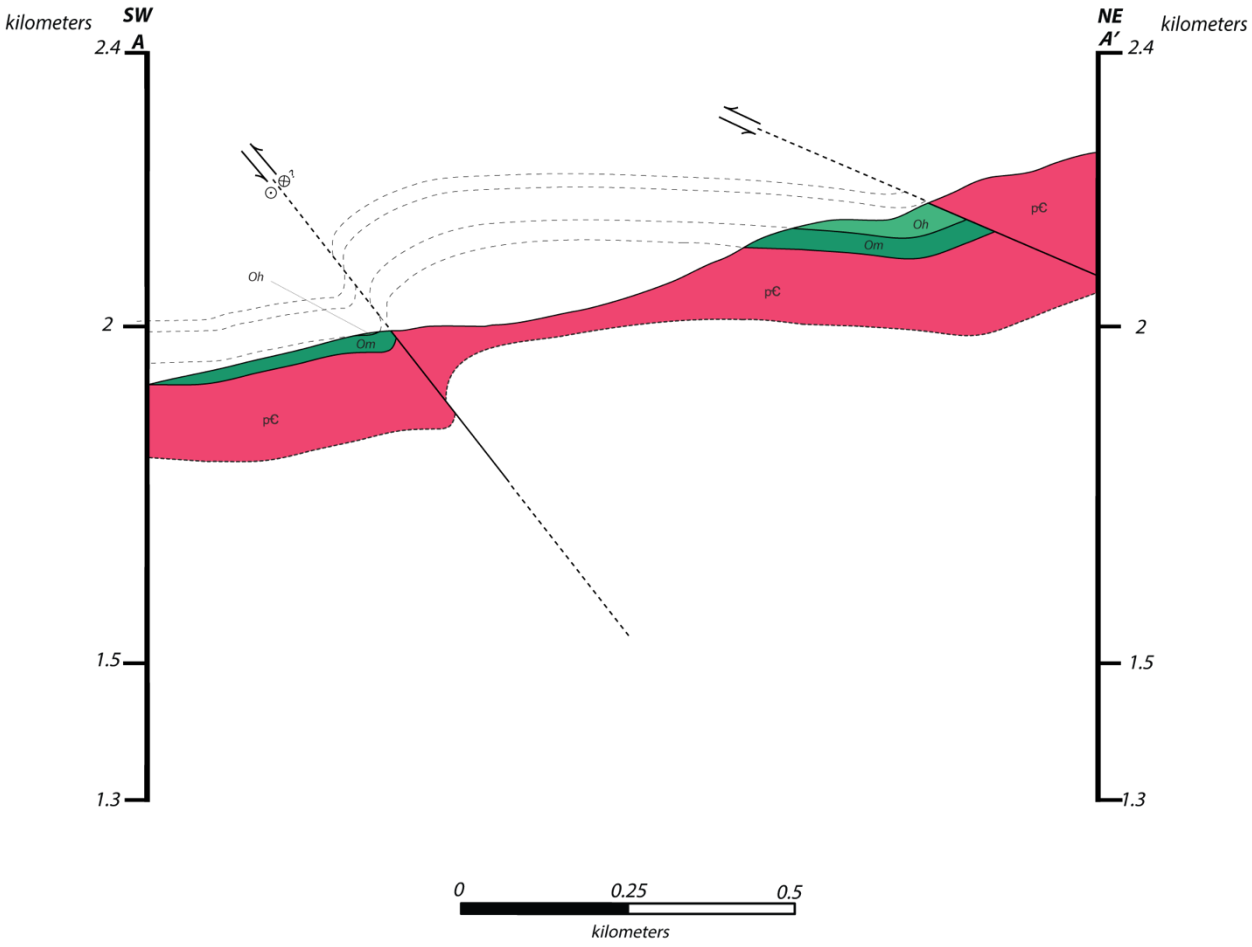

Figure 39. Cross section through the Sheep Mountain field area. The two parallel fault zones indicate overthrusting of Proterozoic rock. The eastern fault displays pure thrusting; where the western fault indicates a lateral component of slip to the overall thrusting. Ambiguity along slickenlines does not permit the lateral direction of slip. The two parallel fault form a monocline with an anticlinal bend.

Table 1. Tabulated results of station observations of deformation bands in the Mixing Bowl field area.

Station	Number of Deformation Bands	Deformation Band Dip Directions	Deformation Band Dip Magnitudes	Number of Slickenlines	Slickenline Trend Directions	Slickenline Plunge Magnitudes	Observed Kinematic Offset
1	30	All directions	34°–88°	16	NW, NE, SE, SW	18°–74°	Left- and right-lateral reverse-slip, thrust dip-slip
2	393	All directions	02°–89°	9	NE, SW	7°–39°	Left- and right-lateral reverse-slip, left- and right-lateral strike-slip, low-angle dip-slip
3	34	NE, NW,SE, SW	33°–89°	5	NE, SE	06°–41°	Left- and right-lateral reverse-slip, left-lateral strike-slip
4	31	All directions	41°–83°	7	NE, SE	0°–15°	Left- and right-lateral reverse-slip, left- and right-lateral strike-slip

Continuation of Table 1. Tabulated results of station observations of deformation bands in the Mixing Bowl field area.

Station	Number of Deformation Bands	Deformation Band Dip Directions	Deformation Band Dip Magnitudes	Number of Slickenlines	Slickenline Trend Directions	Slickenline Plunge Magnitudes	Observed Kinematic Offset
5	22	N, NE, NW, SE	32°–89°	13	NE, SW	04°–29°	Left- and right-lateral reverse-slip, left- and right-lateral strike-slip
6	40	NE, NW, SW	15°–88°	7	E, NE, SW	7°–23°	Left- and right-lateral reverse-slip, left- and right-lateral strike-slip
7	72	All directions	21°–89°	3	NE, SW	0°–28°	Left- and right-lateral reverse-slip, left- and right-lateral strike-slip
8	4	S, NW	62–81°	NA	NA	NA	Left-lateral strike-slip

Continuation of Table 1. Tabulated results of station observations of deformation bands in the Mixing Bowl field area.

Station	Number of Deformation Bands	Deformation Band Dip Directions	Deformation Band Dip Magnitudes	Number of Slickenlines	Slickenline Trend Directions	Slickenline Plunge Magnitudes	Observed Kinematic Offset
9	35	All directions except E	44°–89°	4	N, W, SW	3°–63°	Left- and right-lateral strike-slip, reverse dip-slip
10	74	All directions	03°–89°	5	S, NE, SW	24°–80°	NA
11	18	NE, NW, SE, SW	07°–86°	NA	NA	NA	NA
12	17	N, NW, SE	64°–84°	7	NE, SE	01°–72°	Right-lateral reverse-slip, left- and right-lateral strike-slip
13	58	NW, SE	48°–89°	17	All directions	08°–77°	Right-lateral reverse-slip, left- and right-lateral normal-slip, normal dip-slip

Continuation of Table 1. Tabulated results of station observations of deformation bands in the Mixing Bowl field area.

Station	Number of Deformation Bands	Deformation Band Dip Directions	Deformation Band Dip Magnitudes	Number of Slickenlines	Slickenline Trend Directions	Slickenline Plunge Magnitudes	Observed Kinematic Offset
14	46	All directions	35°–89°	5	NW, SW	32°–88°	Left-lateral reverse-slip, reverse dip-slip, left-lateral normal-slip
15, 16	80	All directions	39°–89°	NA	NA	NA	NA

Table 2. Tabulated results of station observations of deformation bands in the South Twin Mountain field area.

Station	Number of Deformation Bands	Deformation Band Dip Directions	Deformation Band Dip Magnitudes	Number of Slickenlines	Slickenline Trend Directions	Slickenline Plunge Magnitudes	Observed Kinematic Offset
17	34	All directions except the SW	21°–89°	NA	NA	NA	NA
18	7	NE, NW, SE	68°–87°	NA	NA	NA	NA
19	59	All directions	59°–89°	1	NE	03°	Strike-slip (slip direction unknown)
20	9	NE, NW, SE, SW	41°–83°	5	NE, SE	0°–15°	Right-lateral reverse-slip, thrust dip-slip

Table 3. Tabulated results of station observations of deformation bands in the Sheep Mountain field area.

Station	Number of Deformation Bands	Deformation Band Dip Directions	Deformation Band Dip Magnitudes	Number of Slickenlines	Slickenline Trend Directions	Slickenline Plunge Magnitudes	Observed Kinematic Offset
21	35	All directions	46°–86°	1	SW	13°	Left-lateral reverse-slip
22	15	SE, SW	52°–89°	1	NE	07°	Right-lateral strike-slip
23	23	All directions	25°–84°	2	NE, SE	25–29°	Thrust dip-slip

CHAPTER 5

Discussion

Deformation in the CCE (Fig.1) is well-exposed, widely observable, and when accommodated in Ordovician to Cretaceous porous sandstones, it is recorded by deformation bands. These deformation bands provide discernible kinematic indications for fault zone evolution. Vertical to sub-vertical orientations of deformation bands are predominant throughout the observed field sites. Observable band offset and the formation of slickenlines along slipped deformation band planes further substantiate and permit kinematic interpretations of the fault zones. The consistency of horizontal to sub-horizontal slickenline plunges along vertical to sub-vertical oriented deformation bands indicates the dominance of oblique-slip and especially strike-slip fault kinematics.

In zones of deformation consisting of a strike-slip motion, conjugate faults known as Riedel shear structures commonly develop (Cloos and Riedel, 1928; Fig. 41). Riedel shear structures are linkages of shear bands that form in areas of simple shear during the early stages of faulting. Geometrically, Riedel shear structures include conjugate shear bands organized in en-echelon arrays and noted as R (synthetic R shear bands) and R' (antithetic R shear bands) (Fig. 41). R shear bands are synthetic to the slip direction, developing right-stepping en-echelon elongated zones of brittle deformation along left-lateral shear zones and left-stepping en-echelon elongated zones of brittle deformation along right-lateral shear zones (Fig. 41). R' shear bands are antithetic and usually link coincident R shear bands (Fig. 41). Both R and R' shear bands

form at specific angles to the direction shearing. P shear bands are a secondary conjugate set of structures that form after the R and R' shear bands, and like the R shear bands are also synthetic to the main direction of shear (Riedel, 1929; Tchalenko, 1968; Modified from Katz et al., 2004; Fig. 41).

Riedel shear bands are observed in the Mixing Bowl field area (Fig. 12; Fig. 30). The well-exposed deformation bands along the ridge where slickenlines and offset between bands are readily indicated permit the classification of Riedel shear band orientations. The Cretaceous Dakota Group Ridge is made up of two separate strike-slip zones of deformation (Fig. 30). These two fault zones intersect at station 5 (Fig. 23.5), highlighting the bend in the Cretaceous Dakota Group Ridge (Fig. 30). The eastern portion of the ridge contains a northeast-southwest trending right-lateral reverse-slip fault (Fig. 21). This zone of deformation can also be characterized as a right-lateral transpressional fault zone. The damage zone associated with this transpressional fault consists of deformation bands that strike north-northeast to south-southwest (blue planes in stereonets) (Fig. 21; Fig. 30), and are interpreted to be right-lateral R shear bands. The deformation bands that strike east-northeast to west-southwest (green planes in stereonets) (Fig. 21; Fig. 30) are R' shear bands. These R' shear bands display left-lateral offset along the slipped deformation bands. The other Riedel shear band orientation is the P shear band, and it strikes north-northwest to south-southeast (orange planes in stereonets) (Fig. 21; Fig. 30) and has right-lateral slip.

Opposite to the eastern segment of the ridge, the western segment of the ridge consists of an east-northeast to west-southwest left-lateral reverse-slip fault or a left-lateral transpressional fault zone. The deformation band damage zone along this segment of the ridge contains east-northeast to west-southwest (pink planes in stereonets) (Fig. 23; Fig. 30) left-lateral R shear

bands. The deformation bands that strike north-northeast to south-southwest (purple planes in stereonets) (Fig. 23; Fig. 30) express R' shear bands that have right-lateral offset along slipped deformation bands. The third conjugate fault to form in a Riedel shear band set is the P shear. For the western segment, the P shear strikes north-northwest to south-southeast (brown planes in stereonets) (Fig. 23; Fig. 30) and like the R shear band is synthetic to the slip direction, indicating left-lateral offset along slipped deformation bands. The deformation band damage zones along the Cretaceous Dakota Group Ridge provide kinematic indicators for identifying Riedel shear band sets. Oblique-slip faults identified along the Central Fault Zone (pink) (Fig. 30), North Fault Zone (pink) (Fig. 30), and east of the Ordovician Plateau (blue) (Fig. 30), do not display multiple Riedel shear band orientations, but they are interpreted to be included in separate sets of en-echelon faults in conjunction with the Cretaceous Dakota Group Ridge faults (Fig. 30).

Conjugate Riedel shear bands indicate the maximum compressive stress direction through the identification of the acute bisector between the two fault planes (Cloos and Riedel, 1928; Fig. 40). For example, the acute bisector between the two shear planes indicates a northeast-southwest maximum compressive stress direction (Fig. 30). At the intersection along the Cretaceous Dakota Group Ridge, the acute bisector between the right-lateral transpressional fault zone and the left-lateral transpressional fault zone also indicates a northeast-southwest maximum compressive stress direction. The acute bisectors between the fault located east of the Ordovician Plateau, and the Central Fault Zone and the North Fault Zone are interpreted to express a northeast-southwest direction of maximum compressive stress. The maximum compressive stress directions observed in the Mixing Bowl as part of this research match those inferred for the Laramide orogeny in the CCE (Jurista, 1996).

Further identification of larger transpressional geologic structures indicates that the Mixing Bowl Field Area is a contractional horsetail splay (Fig. 3; Fig. 30) forming from the Wet Mountain Thrust System. The Wet Mountain Thrust System is located toward the western extent of the CCE, trends toward the north-northwest with a crustal shortening direction towards the northeast, and has a left-lateral, oblique-slip style of faulting (Scott et al., 1978; Jurista, 1996). The north-northwest trend of the Wet Mountain Thrust system, in conjunction with a left-lateral component of strike-slip kinematics, is oriented obliquely to the northeast crustal shortening direction has been described to indicate pre-existing weaknesses (Jurista, 1996, Erslev, 2004). The Wet Mountain Thrust system has been suggested to have been active and accommodate slip while the Wet Mountains were first uplifted during the Ancestral Rocky Mountain orogeny. The Wet Mountain Thrust system is believed to have been reactivated during the Laramide orogeny. (Jurista, 1996). The identification of pre-existing weaknesses and possible reactivation of faults validates observations and interpretations of an observable contractional horsetail splay in Mixing Bowl field area. The left-lateral, contractional horsetail splay would form due to pre-existing weaknesses in the rock where fault displacement would continue to be accommodated along approximate northwest-southeast trending splays throughout the Laramide orogeny (Fig. 30). Though the deformation bands seen along the Cretaceous Dakota Group Ridge are well-defined and are best exposed in the Mixing Bowl, the arrays of deformation bands indicate an immature fault zone that marks the end of fault displacement along the contractional horsetail splay. Cross sections (Figs. 32-34) as well as the structure map of the Mixing Bowl field area (Fig. 15) indicate the small amount fault displacement vertically and laterally through the ridge in comparison to the Central and North Fault Zone where Proterozoic rock has been well overthrusted.

The South Twin Mountain field area displays deformation band orientations related to the accommodation of folding through slip along deformation bands occurring in the footwall as well as the appearance of deformation band orientations characterizing the right-lateral transpressional movement along the fault zone between Proterozoic rocks and the Ordovician rocks (Fig. 35). The orientations and the northwest-southeast trend of the fold and transpressional fault regime indicate the Laramide shortening direction as well. The Sheep Mountain field area displays en-echelon, northwest-southeast trending reverse and thrust faults that characterize a monocline with an anticlinal bend (Fig. 19). Again, these faults match the direction of Laramide shortening when comparing the fault trends with the uplifted basement arches in the area, the Wet Mountains and the Front Range. The lower fault in this field area contains a component of strike-slip further defining its kinematics as a transpressional fault regime, but the lack of slickenlines creates ambiguity in detecting slip direction along the fault surface. Overall, deformation band damage zones consistently display oblique-slip kinematics in all three field areas.

Deformation bands in the CCE were not observed to indicate any Ancestral Rocky Mountain orogenic deformation. The Ordovician Harding Formation lacked any deformation bands that may have been overprinted by possibly younger Laramide-related deformation bands. In the Sheep Mountain field area, deformation band orientations inconsistent with Laramide orientations (Fig. 36.21a) were observed. However, unconformities display little to no difference in strata orientation above and below the contacts in all three field areas (see *Section 4.2a, 4.3a, and 4.4a*). The low dip magnitude of unconformities indicate that most of the deformation associated with the Ancestral Rocky Mountains may have been more distal from the embayment, or blind at depth where the faulting was solely restricted to thick-skinned deformation as

previously interpreted (Handschy and Dyer, 1987; Blakey and Knepp, 1989; Dickinson and Lawton, 2003; Baley and Ranney, 2003). Thick-skinned deformation describes uplift that only affects basement rocks through deep-seated thrust faults rather than shallower thrusts protruding up through Paleozoic sediments.

The outcrop of Proterozoic basement rock in the middle of the Mixing Bowl (Fig. 15), which is in direct structural contact with Ordovician to Jurassic sedimentary units, describes a horizontal fault zone that is mostly blind but is observed in the field as a geologic window. The presence of the horizontal fault is evident by field observations and analyses as well as expressions of microstructural deformation mechanisms found in rocks directly correlated to the Proterozoic outcrop. Microstructural mechanisms such as the bookshelf sliding seen in the muscovite, and the interruption of ribbon quartz and biotite by larger quartz grains, which are interpreted to come from the Harding Formation, indicate the presence of a fault breccia (Fig. 28). Secondly, the detection of low-temperature recrystallization of Harding Sandstones within the geologic window describes similar fault kinematics to the main horizontal fault observed as branches of minor sub-horizontal to horizontal faults splitting off the horizontal fault where the shearing has translated solely into the younger Ordovician Harding formation (Fig. 15). Lastly, horizontal deformation band orientations are largely identified and characterized in stereonet station 2 (Fig. 15; Fig. 21) where access through the ridge allows for regularly blind deformation band orientations to be observed. Sub-horizontal to horizontal deformation bands are observed throughout the Mixing Bowl and indicate the wide extent of shallow faulting. Horizontal deformation bands show evidence of offsetting vertical deformation bands related to oblique-slip tectonics throughout station 2. The occurrence of this offset is temporally important because this would indicate that a horizontal faulting event may post-date the formation of the contractional

horsetail splay. In terms of the structural architecture of oblique-slip structures, the more coherent explanation for this horizontal shear zone is that it acts as a translation of blind slip occurring below the surface outcrops of observed fault damage zones. For example, it is possible that as the contractional horsetail splay continues to displace between the Central Fault Zone and the Cretaceous Dakota Group Ridge, it protrudes out and above current topography (Fig. 34) and becomes blind again before becoming vertical and exhuming as the immature fault zones along the ridge. Further studies need to constrain the structural significance of the Proterozoic basement rock outcrop in the central portion of the Mixing Bowl with the nearby vertical faults.

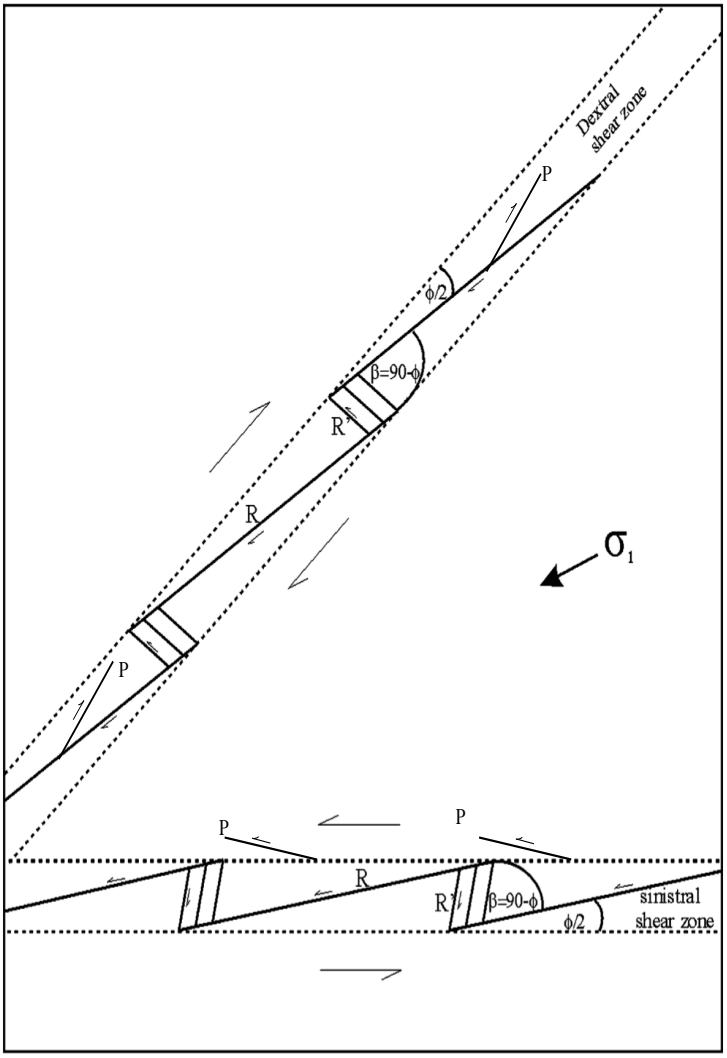

Figure 40. Suite of Riedel shear band orientations within a conjugate shear zone.
R shear bands are synthetic to the slip direction, developing right-stepping en-echelon elongated zones of brittle deformation along left-lateral shear zones and left-stepping en-echelon elongated zones of brittle deformation along right-lateral shear zones. R' shear bands are antithetic, and usually join coincident R shear bands. σ_1, the maximum compressive principle stress, is noted from the intersection of the conjugate shear zones. ϕ, is the angle of internal friction of the host rock. R shear bands generate angles of approximately $\phi/2$ to the direction of shearing and R' shear bands create a $90 - \phi/2$ angle to the direction shearing. Both the R shear band and R' shear band form an acute angle at $\beta = 90 - \phi$. P Shears are subsidiary conjugate structures that form after the R and R' shear band and, like the R shear band, is also synthetic to the main direction of shear. (Figure after Riedel, 1929; Tchalenko, 1968; Modified from Katz et al., 2004).

CHAPTER 6

Conclusions

This thesis examines the kinematics of fault damage zones in the Cañon City Embayment (CCE), Colorado, through a detailed study of deformation bands originating from large-scale orogenic processes. Three field areas were studied: the Mixing Bowl, South Twin Mountain, and Sheep Mountain. To characterize the deformation in these areas, 688 bedding orientations from Ordovician to Cretaceous sedimentary units were recorded, with 1131 deformation band orientations were collected from Ordovician, Pennsylvanian, Jurassic, and Cretaceous porous sandstones. Slipped bands displaying slickenlines, which are direct indicators of slip direction, were characterized by 112 lineation measurements. The integration of this field data into kinematic analyses conducted in stereonets, subsequent cross section construction, as well as a description of microstructural expressions of fault rocks in the Mixing Bowl field area, allow for a detailed understanding of these deformation structures from the micro- to macro-scale.

The main conclusions of this study are:

1. Deformation bands observed in the three field areas describe reverse faulting with major strike-slip components of both right- and left-lateral sense. Riedel shear band orientations describe a northeast-southwest crustal shortening direction in the Mixing Bowl field area, and both South Twin Mountain and Sheep Mountain field areas display northwest-southeast trending fault zones, all of which is consistent with previous Laramide shortening direction observations in the CCE.

2. The Mixing Bowl field area represents a left-lateral, contractional horsetail splay that formed and evolved along reactivated faults owing to pre-existing weaknesses from early uplift of the Wet Mountains during the Ancestral Rocky Mountain orogeny. The northeast-southwest trending splays, which become younger towards the southeast, were reactivated during the Laramide orogeny until displacement concluded along the Cretaceous Dakota Group ridge.
3. No deformation bands indicated deformation during the Ancestral Rocky Mountain orogeny, as evident by:
    a. no overprinting of deformation bands from younger Laramide-related orogenic processes, or substantially different deformation band orientations that could be related to the Ancestral Rocky Mountain orogeny.
    b. the lack of major angular unconformities between Ordovician units and younger Pennsylvanian to Jurassic units in each field area.
4. The Proterozoic exposure in the middle of the Mixing Bowl field area is not fully explained at the time of this writing. These contacts are structural and not depositional because of:
    a. the observation and description of the microstructural deformation seen in a fault breccia from the horizontal fault zone between the Proterozoic basement rock and Harding Formation in the central portion of the Mixing Bowl.
    b. the detection of low-temperature recrystallization of the Harding Sandstones, indicating a high strain environment, juxtaposed to Proterozoic basement rock within the zone described as a geologic window.

c. the large amount of horizontal deformation bands observable in stereonet station 2 with more horizontal to sub-horizontal deformation bands observed throughout the Mixing Bowl field area.

REFERENCES

Allulee, J.L., Holland, S.M., 2005. The sequence stratigraphic and environmental context of primitive vertebrates: Harding Sandstone, Upper Ordovician, Colorado, USA. Palaios 20, 518–533.

Anderson, E.M., 1905. The dynamics of faulting. Transactions of the Edinburgh Geological Society 8, 387–402.

Antonellini, M.A., Aydin, A., Orr, L., 1999. Outcrop-aided characterization of a faulted hydrocarbon reservoir: Arroyo Grande oil field, California, USA. In: Haneberg, W.C., Mozley, P.S., Moore, J.C., Goodwin, L.B. (Eds.), Faults and Subsurface Fluid Flow in the Shallow Crust. American Geophysical Union Geophysical Monograph 113, 7–26.

Aydin, A., Johnson, A.M., 1978. Development of faults as zones of deformation bands and as slip surfaces in sandstone. Pure Applied Geophysics 116, 931–942.

Aydin A., Nur A., 1982. Evolution of stepover basins and their scale independence. Tectonics 1, 91–105.

Aydin, A., Reches, Z.E., 1982. Number and orientation of fault sets in the field and in experiments. Geology 10, 107–112.

Aydin A., Nur A., 1985. The types and role of stepovers in strike-slip tectonics. In: Biddle, K.T., Christie-Blick, N. (Eds.), Strike-slip deformation, basin formation, and sedimentation. Society of Economic Palaeontologists and Mineralogists Special Publication 37, 35–45.

Aydin, A., Borja, R.I., Eichhubl, P., 2006. Geological and mathematical framework for failure modes in granular rock. Journal of Structural Geology 28, 83–98.

Ballas, G., Soliva, R., Sizun, J. P., Benedicto, A., Cavailhes, T., Raynaud, S., 2012. The importance of the degree of cataclasis in shear bands for fluid flow in porous sandstone. American Association of Petroleum Geologists Bulletin 96, 2167–2186.

Baily, J.E., Hirsch, P.B., 1962. The recrystallization process in some polycrystalline metals. Proceedings of the Royal Society of London A 267, 11–30.

Beck, M.E. Jr., 1983. On the mechanism of tectonic transport in zones of oblique subduction. Tectonophysics 93, 1–11.

Blakey, R.C., Knepp, R., 1989. Pennsylvanian and Permian geology of Arizona. In: Jenney, J.P. and Reynolds, S.J. (Eds.), Geologic evolution of Arizona. Arizona Geological Society Digest 17, 313–347.

Blenkinsop, T.G., Sibson, R.H., 1991. Aseismic fracturing and cataclasis involving reaction softening within core material from the Cajon Pass drillhole. Journal of Geophysical Research 97, 5135–5144.

Boyer, R.E., 1962. Petrology and structure of the southern Wet Mountains, Colorado. Geological Society of America Bulletin 73, 1047–1070.

Brown, S.R., Scholz, C.H., 1985. Broad bandwidth study of the topography of natural rock surfaces. Journal of Geophysical Research 90, 2575–2582.

Bryan, P. and Gordon, R.G., 1990. Rotation of the Colorado Plateau: An updated analysis of paleomagnetic poles. Geophysical Research Letters 17, 1501–1504.

Candela, T., Renard, F., Bouchon, M., Brouste, A., Marsan, D., Schmittbuhl, J., and Voisin, C., 2009. Characterization of fault roughness at various scales: Implications of three-dimensional high resolution topography measurements. Pure and Applied Geophysics 166, 1817–1851.

Candela, T., Renard, F., Klinger Y., Mair, K., Schmittbuhl, J., and Brodsky, E.E., 2012. Roughness of fault surfaces over nine decades of length scales. Journal of Geophysical Research, 117.

Christie-Blick N., Biddle K.T., 1985. Strike-slip deformation, basin formation, and sedimentation. Society of Economic Palaeontologists and Mineralogists Special Publication 37, 1–34.

Cloos, H., 1928. Experimente zur inneren Tektonic. Centralblatt für Mineralogie Abteilung B, 609–621.

Copeland, P., Currie, C.A., Lawton, T.F., Murphy, M.A., 2017. Location, location, location: The variable lifespan of the Laramide orogeny. Geology 45, 422–422.

Crawford, B.R., 1998. Experimental fault sealing: shear band permeability dependency on cataclastic fault gouge characteristics. In: Coward, M.P., Daltaban, T.S., Johnson, H. (Eds.), Structural Geology in Reservoir Characterization. Geological Society, London, Special Publications 127, 27–48.

Crowell J.C., 1974. Origin of late Cenozoic basins of southern California. In: Dickinson W. R. (Ed.), Tectonics and Sedimentation. Society of Economic Palaeontologists and Mineralogists 22, 190–204.

Cruikshank, K.M., Zhao, G., Johnson, A.M., 1991. Analysis of minor fractures associated with joints and faulted joints. Journal of Structural Geology 13, 865–886.

Cunningham,W., Mann, P., 2007. Tectonics of strike-slip restraining and releasing bends, Geological Society, London, Special Publications 290, 1–12.

Darton, N.H., 1920. Geothermal data of the United States, including many original determinations of underground temperature. United States Geological Survey Bulletin No. 701, 97.

Davis, G.H., 1999. Structural geology of the Colorado Plateau region of southern Utah with special emphasis on deformation bands. Geological Society of America Special Paper 342, 1–157.

Davis, G.H., Bump, A.P., Garcia, P.E., Ahlghren, S.G., 2000. Conjugate Riedel deformation band shear zones. Journal of Structural Geology 22, 169–90.

DeVoto, R.H., 1980. Pennsylvanian stratigraphy and history of Colorado. In: Kent, H. C., Porter, K. W. (Eds.), Colorado Geology: Rocky Mountain Association of Geologists-1980 Synopsium, 71–102.

Dewey J.F., Holdsworth R.E., Strachan R. A., 1998. Transpression and transtension zones. In: Holdsworth R. E., Strachan R. A., Dewey J. F. (Eds.), Continental Transpressional and Transtensional Tectonics. Geological Society, London, Special Publications 135, 1–14.

Dickinson, W.R., Snyder, W.S., 1978. Plate tectonics of the Laramide Orogeny. In: Matthews, V. (Ed.), Laramide folding associated with basement block faulting in the western United States. Geological Society of America Memoir 151, 355–366.

Dickinson W.R., Lawton T.F., 2003. Sequential intercontinental suturing as the ultimate control for Pennsylvanian Ancestral Rocky Mountains deformation. Geology 31, 609–612.

Doblas, M. 1998. Slickenside kinematics indicators. Tectonophysics 295, 187–197.

Drury M.R., Humphreys F.J., White S.H., 1985. Large strain deformation studies using polycrystalline magnesium as a rock analogue. Part II: dynamic recrystallization mechanisms at high temperatures. Physics of the Earth and Planetary Interiors 40, 208–222.

Epis, R.C., Chapin, C.E., 1975. Stratigraphic nomenclature of the Thirtynine Mile volcanic field, central Colorado. United States Geological Survey Bulletin No. 1395-C, 23.

Erslev, E.A., Rogers, J.L., Harvey, M., 1988. The northeastern Front Range revisited: Compression and crustal wedging in a classic locality for vertical tectonics. Field trip guidebook for the 1988 Geological Society of America Annual Meeting, 141–150.

Erslev, E.A., Rogers, J.L., 1993. Basement cover geometry of Laramide fault propagation folds. In: Schmidt, C. J., Chase, R., Erslev, E. A. (Eds.), Laramide basement deformation in the Rocky Mountain foreland of the western United States. Geological Society of America Special Paper 280, 339–358.

Erslev, E.A., Holdaway, S.M., O'Meara, S.A., Jurista, B., Selvig, B., 2004. Laramide minor faulting in the Colorado Front Range. New Mexico Bureau of Geology and Mineral Resources Bulletin 160, 181–203.

Erslev, E.A., Selvig, B., 1996. Thrusts, backthrusts and triangle zones—Laramide deformation in the northeastern margin of the Colorado Front Range. In: Bolyard, D.W., Sonnenberg, S. A. (Eds.), Geologic history of the Colorado Front. Rocky Mountain Association Geologists Field Trip Guide 7, 65–76.

Evans, J.P., 1988. Deformation mechanisms in granitic rocks at shallow crustal levels. Journal of Structural Geology 10, 437–443.

Fisher, Q.J., Knipe, R.J., 2001. The permeability of faults within siliciclastic petroleum reservoirs of the North Sea and Norwegian Continental Shelf. Marine and Petroleum Geology 18, 1063–1081.

Fossen, H., Bale, A., 2007. Deformation bands and their influence on fluid flow. American Association of Petroleum Geologists Bulletin 91, 1685–1700.

Fossen, H., Schultz, R.A., Shipton, Z.K., Mair, K., 2007. Deformation bands in sandstone: a review. Journal of the Geological Society London 164, 755–769.

Fowles, J., Burley, S., 1994. Textural and permeability characteristics of faulted, high porosity sandstones. Marine and Petroleum Geology 11, 608–623.

Fondriest, M., Smith, S.A.F., Candela, T., Nielsen, S.B., Mair, K., Di Toro, G., 2013. Mirror-like faults and power dissipation during earthquakes. Geology 41, 1175–1178.

Frederickson, E.A., Delay, J.M., Saylor, W.W., 1956. Ralston Formation of the Cañon City Embayment, Colorado. American Association of Petroleum Geologists Bulletin 40, 2120–2148.

Gibson, R.G.,1998. Physical character and fluid-flow properties of sandstone-derived fault zones. Geological Society, London, Special Publications 127, 83–97.

Hamilton, W., 1981. Plate-tectonic mechanism of Laramide deformation. Contributions to Geology 19, 87–92.

Handschy, J.W., Dyer, R., 1987. Polyphase deformation in Sierra del Cuervo, Chihuahua, Mexico: Evidence for Ancestral Rocky Mountain tectonics in the Ouachita foreland of northern Mexico. Geological Society of America Bulletin 99, 618–632.

Harper, T., Moftah, I., 1985. Skin effect and completion options in the Ras Budran reservoir. Society of Petroleum Engineers Middle East Oil Technical Conference and Exhibition, SPE Paper 13708, 211–226.

Healy, D., Blenkinsop, T.G., Timms, N.E., Meredith, P.G., Mitchell, T.M., Cooke, M.L., 2015. Polymodal faulting: Time for a new angle on shear failure. Journal of Structural Geology, 80, 57–71.

Heuret, A., Lallemand, S., 2005. Plate motions, slab dynamics and back-arc deformation. Physics of the Earth and Planetary Interiors 149, 31–51.

Jamison, W.R., Stearns, D.W., 1982. Tectonic deformation of Wingate Sandstone, Colorado National Monument. American Association of Petroleum Geologists Bulletin 66, 2584–2608.

Jarrard R.D., 1986. Terrane motion by strike-slip faulting of fore-arc slivers. Geology 14, 780–783.

Jurista, B.K., 1996. East-northeast Laramide compression and shortening of the Cañon City Embayment, south-central Colorado. Unpublished M.S. thesis, Colorado State University, Fort Collins.

Katz, Y., Weinberger, R., Aydin, A., 2004. Geometry and kinematic evolution of Riedel shear structures, Capitol Reef National Park, Utah. Journal of Structural Geology 26, 491–501.

Kluth, C.F., Coney, P.J., 1981. Plate tectonics of the Ancestral Rocky Mountains. Geology 9, 10–15.

Kluth, C.F., Nelson, S.N., 1988. Age of the Dawson Arkose, Southwestern Air Force Academy, Colorado, and implications for the uplift history of the Front Range. The Mountain Geologist 25, 29–35.

Knipe, R.J., Jones, G., Fisher, Q.J., 1998. Faulting, fault sealing and fluid flow in hydrocarbon reservoirs. Geological Society, London, Special Publications 147, 7–21.

Laubach, S.E, Eichhubl, P., Hilgers, C., Lander, R.H., 2010. Structural diagenesis. Journal of Structural Geology 32, 1866–1872.

Lee, J.-J., Bruhn, R., 1996. Structural anisotropy of normal fault surfaces, Journal of Structural Geology 18, 1043–1059.

Lees, J.M., 2017. Graphics for Spherical Distributions and Earthquake Focal Mechanisms (package RFOC). R package version 3.2.2.

Leonard, E.M., Langford, R.P., 1994. Post-Laramide deformation along the eastern margin of the Colorado Front Range–A case against significant faulting. The Mountain Geologist 31, 45–52.

Lin, A., 2001. S-C fabrics developed in cataclastic rocks from the Nojima fault zone, Japan and their implications for tectonic history. Journal of Structural Geology 23, 1167–1178.

Lipman, P.W., 1971. Iron–titanium oxide phenocrysts in compositionally zoned ash flow sheets from southern Nevada: Journal of Geology 79, 438–456.

Lovering, T. S., 1928. The fracturing of incompetent beds. Journal of Geology 36, 709–17.

Logan, J.M., 1966. Structure and petrology of the eastern margin of the Wet Mountains, Fremont County, Colorado. Ph.D. thesis, University of Oklahoma.

Lowell, J.D., 1983, Foreland deformation. In: Lowell, J.D, Gries, R.R. (Eds.), Rocky Mountain foreland basins and uplifts. Rocky Mountain Association of Geologists, Denver, Colorado, 1–8.

Lowell, J.D., 1974. Regional characteristics of porphyry copper deposits of the Southwest. Economic Geology 69, 601–17.

Mallory, W.W., 1972. Regional synthesis of the Pennsylvanian system. In Mallory, W.W., (Ed.), Geologic Atlas of the Rocky Mountain Region. Rocky Mountain Association of Geologists, Denver, Colorado, 111–142.

Marshak S., Nelson W., McBride J., 2003. Phanerozoic strike–slip faulting in the continental interior platform of the United States: examples from the Laramide orogen, mid–continent, and Ancestral Rocky Mountains. In: Storti, F., Holdsworth, R., Salvini, F. (Eds.), Intraplate Strike–slip Deformation Belts. Geological Society, London, Special Publications 210, 159–184.

Mateer, N.J., 1987. The Dakota Group of northeastern New Mexico and southern Colorado. New Mexico Geological Society, Guidebook 38, 223–236.

Means, W.D., Xia, Z.G., 1981. Deformation of crystalline materials in thin section. Geology 9, 538–543.

McClay, K., Bonora, M., 2001. Analog models of restraining stepovers in strike–slip fault systems. American Association of Petroleum Geologists Bulletin 85, 233–260.

Midland Valley Exploration Ltd., 2017. Move2017. 1 suite: Glasgow.

Moore, A.C., 1970. Descriptive terminology for the textures of rocks in granulite facies terrains. Lithos 3, 123–127.

Oldow, J.S., Bally, A.W., Ave Lallemant, H.G., and Leeman, W.P., 1989. Phanerozoic evolution of the North American Cordillera— United States and Canada. In: Bally, A.W., Palmer, A.R. (Eds.), The geology of North America, an overview. Geological Society of America 1A, 139–232.

Ogilvie, S.R., Orribo, J.M., Glover, P.W.J., 2001. The influence of deformation bands upon fluid flow using profile permeametry and positron emission tomography. Geophysical Research Letters 38, 61–64.

Olsson, W.A., Lorenz, J.C., Cooper, S.P., 2004. A mechanical model for multiply-oriented conjugate deformation bands. Journal of Structural Geology 26, 325–338.

Passchier, C.W., Trouw, R.A.J. 2005. Microtectonics. Springer, Berlin Heidelberg.

Peacock, D.C.P., Sanderson, D.J., 1991. Displacements, segment linkage and relay ramps in normal fault zones. Journal of Structural Geology 13, 721–733.

Peacock, D.C.P., Sanderson, D.J., 1992. Effects of layering and anisotropy on fault geometry. Journal of the Geological Society 149, 793–802.

Petit, J.P., Laville, E., 1987. Morphology and microstructures of hydroplastic slickensides in sandstones. In: Jones, M.E., Preston, R.M.F. (Eds.), Deformation of Sediments and Sedimentary Rocks. Geological Society, London, Special Publications 29, 107–121.

Pittman, E.D., 1981. Effect of fault-related granulation on porosity and permeability of quartz sandstones, Simpson Group (Ordovician), Oklahoma. American Association of Petroleum Geologists Bulletin 65, 2381–2387.

Power, W.L., Tullis, T.E., Brown, S.R., Boitnott, G.N., and Scholz, C.H., 1987. Roughness of natural fault surfaces. Geophysical Research Letters 14, 29–32.

R Core Team, 2015. R: A language and environment for statistical computing. R Foundation for Statistical Computing, Vienna, Austria.

Rascoe, B., Jr., and Baars, D. L., 1972. Permian System. In: W. W. Mallory, (Ed.), Geologic Atlas of the Rocky Mountain Region. Rocky Mountain Association of Geologists, Denver, Colorado, 143–165.

Renard, F., Voisin, C., Marsan, D., and Schmittbuhl, J., 2006. High resolution 3D laser scanner measurements of a strike-slip fault quantify its morphological anisotropy at all scales. Geophysical Research Letters, 33, L04305.

Riedel, W., 1929. Zur Mechanik geologischer Brucherscheinungen. Zentralblatt für Mineralogie, Geologie und Paleontologie Abteilung B, 354–368.

Rotevatn, A., Tveranger, J., Howell, J.A., Fossen, H., 2009. Dynamic investigation of the effect of a relay ramp on simulated fluid flow: geocellular modeling of the Delicate Arch Ramp, Utah. Petroleum Geoscience 15, 45–58.

Rutter, E.H., Hadizadeh, J., 1991. On the influence of porosity on the low-temperature brittle-ductile transition in siliciclastic rocks. Journal of Structural Geology 13, 609–614.

Sagy, A., Brodsky, E.E., 2009. Geometric and rheological asperities in an exposed fault zone: Journal of Geophysical Research 114, B02301.

Sagy, A., Brodsky, E.E., Axen, G.J., 2007. Evolution of fault-surface roughness with slip. Geology 35, 283–286.

Scott, G.R., Epis, R., 1977. Cañon City area: Colorado Scientific Society spring field trip, April 15, 1977. Unpublished Field Guide, 8.

Scott, G.R., Taylor, R.B., Epis, R.C. and Wobus, R.A., 1978. Geologic map of the Pueblo 1º x 2º quadrangle, south–central Colorado. U.S. Geological Survey Miscellaneous Investigations Series Map I-1022, scale 1: 250,000.

Sibson, R.H., 1977b. Fault rocks and fault mechanisms. Journal of the Geological Society of London 133, 191–213.

Sieh, K., Natawidjaja, D., 2000. Neotectonics of the Sumatran fault, Indonesia. Journal of Geophysical Research 105, 28 295–28 326.

Siman-Tov, S., Aharonov, E., Sagy, A., Emmanuel, S., 2013, Nanograins form carbonate fault mirrors: Geology 41, 703–706.

Shigematsu, N., 1999. Dynamic recrystallization in deformed plagioclase during progressive shear deformation. Tectonophysics 305, 437–452.

Sternlof, K., Karimi-Fard, M., Pollard, D.D., Durlofsky, L.J., 2006. Flow and transport effects of compaction bands in sandstone at scales relevant to aquifer and reservoir management. Water Resources Research 42, W07425.

Stipp, M., Stünitz, H., Heilbronner, R., Schmid, S.M., 2002. The eastern Tonale fault zone: a "natural laboratory" for crystal plastic deformation of quartz over a temperature range from 250 to 700 °C. Journal of Structural Geology 24, 1861–1884.

Sylvester, A.G., 1988. Strike-slip faults. Geological Society of America Bulletin 100, 1666–1703.

Taylor, R.B., Scott, G.R., Wobus, R.A., and Epis, R.C., 1975a. Reconnaissance geologic map of the Royal Gorge Quadrangle: Fremont and Custer Counties, Colorado. U.S. Geological Survey Miscellaneous Investigations Map I-869, scale 1: 62,500.

Taylor, R.B., Scott, G.R., 1973. Reconnaissance Geologic Map of the Wetmore Quadrangle, Custer and Pueblo Counties, Colorado. Miscellaneous Field Studies Map MF-548, Wetmore Quadrangle, Colorado. U.S. Geological Survey.

Tchalenko, J.S., 1968. The evolution of kink bands and the development of compression textures in sheared clays. Tectonophysics 6, 159–174.

Tchalenko J.S., 1970. Similarities between shear zones of different magnitudes. Geological Society America Bulletin 81,1625–1640.

Tchalenko, J.S., Ambraseys, N. N., 1970. Structural analysis of the Dasht–e–Bayaz (Iran) earthquake fractures, Geological Society of America Bulletin 81, 41–60.

Torabi, A., Fossen, H., Braathen, A., 2013. Insight into petrophysical properties of deformed sandstone reservoirs. American Association of Petroleum Geologist Bulletin 97, 619–637.

Tueckmantel, C., Fisher, Q.J., Manzocchi, T., Skachkov, S., Grattoni, C.A., 2012. Two-phase fluid flow properties of cataclastic fault rocks: implication for CO2 storage in saline aquifers. Geology 20, 39–42.

Tullis, J., Dell'Angelo, L., Yund R.A., 1990. Ductile shear zones from brittle precursors in feldspathic rocks: the role of dynamic recrystallization. In: Hobbs, B.E., Heard, H.C. (Eds.), Mineral and rock deformation: laboratory studies. American Geophysical Union, Geophysical Monograph 56, 67–81.

Tungatt, P.D., Humphreys, F.J., 1984. The plastic deformation and dynamic recrystallisation of polycrystalline sodium nitrate. Acta Metallurgica 32, 1625–1635.

Tweto, O., 1975b. Laramide orogeny in the southern Rocky Mountains. In: Curtis, B.F. (Ed.), Cenozoic history of the southern Rocky Mountains. Geological Society of America Memoir 144, 1–44.

Tweto, O., and Lovering, T.S., 1977, Geology of the Minturn 15' Quadrangle, Eagle and Sunnit Counties, Colorado. United States Geological Survey Professional Paper 956, 96.

Tweto, O., 1980. Tectonic history of Colorado. In: Kent, H.C., Porter, K.W., (Eds.), Colorado Geology. Rocky Mountain Association of Geologists, Denver, Colorado, 5–10.

Urai, J., Means, W.D., Lister G.S., 1986. Dynamic recrystallization of minerals. In: Heard, H.C., Hobbs, B.E. (Eds.), Mineral and rock deformation: laboratory studies, the Paterson volume. American Geophysical Union, Geophysical Monograph 36, 161–200.

Wadell, H., 1932. Volume, shape, and roundness of rock particles. Journal of Geology 40, 443–451.

Weimer, R.J., Dolson, J.C., Ethridge, F.G., and Warme, John, 1990. 2-Day Geology Field Trip, Sequence Stratigraphy—Lower K, Fort Collins, Boulder, Morrison Area. Rocky Mountain Association of Geologists, Denver, Colorado, 130.

Wilcox, R.E., Harding T.P., Seely D.R., 1973. Basic wrench tectonics. American Association of Petroleum Geologists 57, 74–96.

Wilson J.T., 1965. A new class of faults and their bearing on continental drift. Nature 207, 343–347.

Wobus, R.A., Epis, R.C., and Scott, G.R., 1979. Geologic map of the Cover Mountain quadrangle, Fremont, Park, and Teller Counties, Colorado. United States Geological Survey Map I-1179.

Wobus, R.A., Chase, R.B., Scott, G.R., and Taylor, R.B., 1985. Reconnaissance geologic map of the Cooper Mountain quadrangle, Fremont County, Colorado. United States Geological Survey Miscellaneous Investigations Map MF-1762, scale 1: 62,500.

Woodcock, N.H., 1986, The role of strike-slip fault systems at plate boundaries. Royal Society of London Philosophical Transactions, Series A, 317, 13–29.

Yeats R., Sieh K., Allen C., 1997. The Geology of Earthquakes. Oxford University Press. New York.

Zhang P., Burchfiel C., Chen S., Deng Q., 1989. Extinction of pull–apart basins. Geology 17, 814–817.

APPENDIX A

Field Site Photos

1. View of the northern portion of the Mixing Bow field area. View is oriented towards the northeast.

2. View of the southern portion of the Mixing Bowl field area. View is oriented towards the southeast.

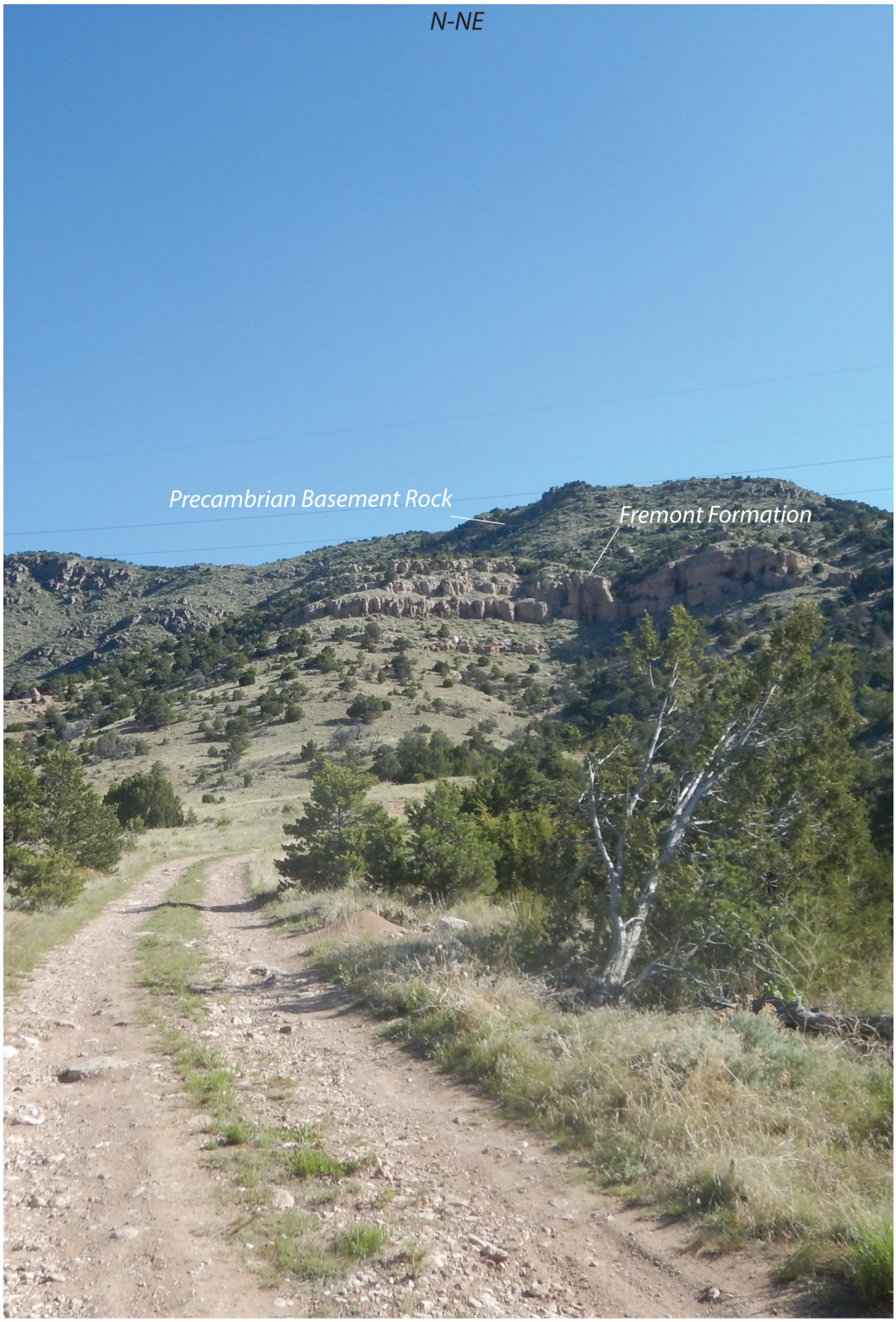

3. View of the South Twin Mountain field area from the 4WD road. Image is oriented towards the north-northeast.

4. View of the southeastern portion of the South Twin Mountain field area. Image is oriented towards the south-southeast and taken above the Fremont Formation.

5. Image of the depositional contact between the Fremont Formation and the Harding Formation in the Sheep Mountain field area. The location of the contact is marked by the hammer. Photo is oriented towards the west-southwest.

6. Image of the Manitou Formation oriented vertically in the western portion of the Sheep Mountain field area. Photo is oriented towards the north-northeast.

7. Image of the Manitou Formation where bedding is oriented horizontally within the eastern portion of the Sheep Mountain field area.

APPENDIX B

Template for R Programming Language for Constructing Stereonets

```
#R programming code for stereonet construction.
#Utilization of Package RFOC.
#RFOC–Graphics for Spherical Distributions and Earthquake Focal Mechanisms (Lees, 2013).
#This code was used to produce an equal area stereonet showing deformation band planes and
slickenline lineations.

#-------------------------------------------------------------------------------------
#-------------------------------------------------------------------------------------
#-------------------------------------------------------------------------------------

#Loading the package RFOC.
#library(RFOC)

#-------------------------------------------------------------------------------------

#Adding an equal area stereonet.
#net(col = 'col' , border = 'col')

##net() is the function to construct the equal area stereonet.
##col is the color of the great and small circles in the stereonet.
##border is the color of the primitive circle.

#-------------------------------------------------------------------------------------

#Adding a title to the stereonet.
#title(main = 'Stereonet Substation 1a')

##title() is a function that describes the stereonet.
##main gives a main title to the stereonet.

#-------------------------------------------------------------------------------------

#Adding north label to delineate the 0 or 360 degree mark on the primitive circle.
#text(x= 0 , y= 1.04, labels = 'N', font = 2)

##x,y are the numeric vectors of the coordinates where the text labels should be written.
##labels displays what should be written at those coordinates.
##font is the typeface for the label.

#-------------------------------------------------------------------------------------

#Adding a plus sign to the middle of the stereonet.
#text(x= 0 , y= 0, labels = '+', font = 2, col = 'black')

##col is the color of the label.
```

```
#-------------------------------------------------------------------------------

#Adding a deformation band plane.
#lowplane(az, dip)

##lowplane() is the function used to project a great circle on a focal sphere.
##az is the azimuth angle of the strike of the plane.
##dip is the dip angle of the plane.

#-------------------------------------------------------------------------------

#Adding a slickenline lineation.
#focpoint(az1, dip1, pch = 16)

##focpoint() is the function used to plot a point on the stereonet.
##az1 is the azimuth angle of the trend of the lineation.
##dip1 is the plunge angle of the measured lineation.
##pch is the plot character or symbol for the point on the stereonet.


#-------------------------------------------------------------------------------
#-------------------------------------------------------------------------------

#Below is an example of the code utilized for Stereonet Substation 1a.
#'for (i in 1:length(strike)) {lowplane(strike[i], dip[i])}' is a loop.

library(RFOC)

#Stereonet Substation 1a.
net(col = 'whitesmoke' , border = 'black')
title(main = 'Stereonet Substation 1a')
text(x= 0 , y= 1.04, labels = 'N', font = 2)
text(x= 0 , y= 0, labels = '+', font = 2, col = 'black')

strike <- c(217, 211, 007, 348, 009, 004, 002, 012, 002, 073, 351, 146, 159, 356)
dip <- c(34, 35, 39, 50, 56, 58, 60, 60, 62, 65, 66, 66, 72, 75)
for (i in 1:length(strike)) {lowplane(strike[i], dip[i])}

trend <- c(288, 279, 162, 089, 069, 053, 091, 064)
plunge <- c(32, 33, 32, 39, 58, 56, 66, 74)
for (i in 1:length(trend)) {focpoint(trend[i], plunge[i], pch = 16)}

#-------------------------------------------------------------------------------
#-------------------------------------------------------------------------------
#-------------------------------------------------------------------------------
#The output is below.
```

Stereonet Substation 1a

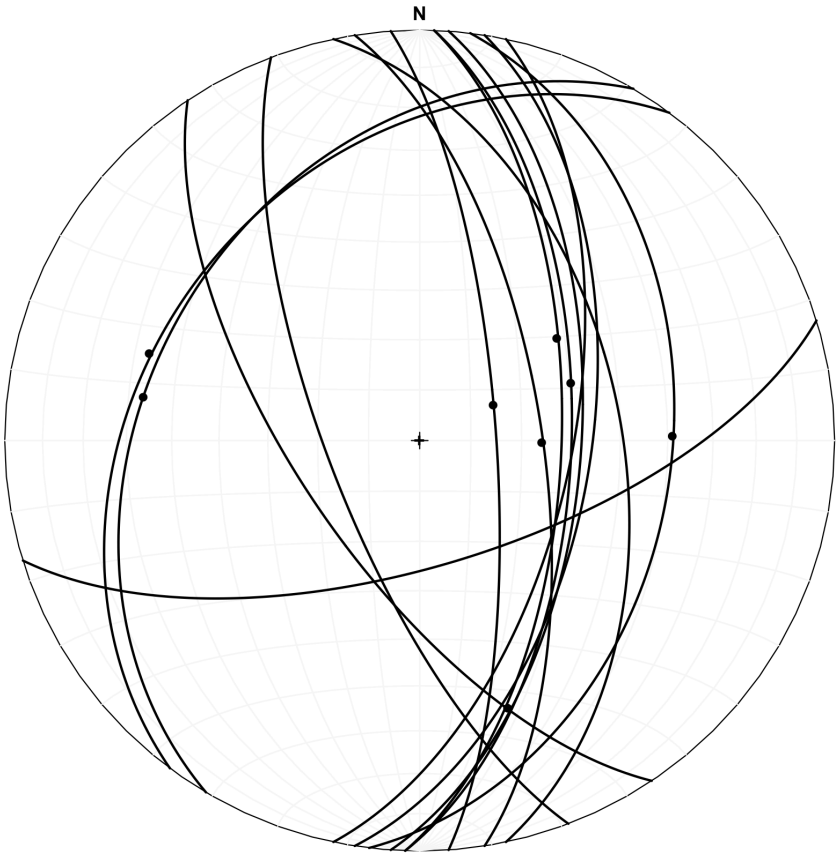

APPENDIX C

GPS Locations for Field Images

Figure Number/Appendix Image	GPS Coordinates
5a	38º 24.434’N 105º 16.498’W
5b	38º 24.452’N 105º 16.505’W
5c	38º 24’ 22N 105º 17’ 08”W
5d	38º 36’30”N 105º 12’ 34”W
5e	38º 24’13”N 105º 17’ 07”W
6	38º 24.459’N 105º 16.478’W
7a	38º 24.22’N 105º 16.839’W
7b	38º 24’15”N 105º 17’ 24”W
8	38º 24.430’N 105º 16.550’W
9a	38º 30.010’N 105º 17.386’W
9b	38º 36.345’N 105º 13.060’W
9c	38º 24.367’N 105º 17.057’W
10	38º 24.262’N 105º 16.656’W
11	38º 24.431’N 105º 16.526’W
12	38º 24.133’N 105º 16.753’W
13	38º 24.441’N 105º 16.572’W
14a	38º 24’ 22”N 105º 16’ 35”W
14b	38º 24.431’N 105º 16.526’W
14c	38º 24.431’N 105º 16.526’W
16a	38º 24’ 22”N 105º 17’ 08”W
17	38º 24’13”N 105º 17’ 07”W
Appendix A Image 1	38º 24.326’N 105º 17.646’W
Appendix A Image 2	38º 24.326’N 105º 17.646’W
Appendix A Image 3	38º 29.798’N 105º 17.445’W
Appendix A Image 4	38º30’03”N 105º 17’ 21”W
Appendix A Image 5	38º 36’ 20”N 105º 13’ 06”W
Appendix A Image 6	38º 36’16”N 105º 13’ 02”W
Appendix A Image 7	38º 36’ 14”N 105º 12’ 42”W